

Supervisor: Prof. Dr. Cornelia Kasper

Department of Biotechnology

University of Natural Resources and Life Sciences, Vienna

Strategies in adipo-derived mesenchymal stem cell expansion

Institute of Biotechnology

University of Natural Resources and Life Sciences, Vienna

Zur Erlangung des Grades

Master of Science/ Diplomingenieurin

M.Sc./ Dipl.-Ing.ⁱⁿ

Genehmigte Master Arbeit

Von

Monira Awad B.Sc.

Sapere aude!

Horaz 20 v. Chr.; (Epist. 1, 2, 40f)

Erklärung

Ich versichere, dass ich diese Masterarbeit selbstständig und nur unter Verwendung der angegebenen Hilfsmittel und Quellen durchgeführt habe.

Wien, im Oktober 2014

Kurzfassung

Schlüsselwörter: Mesenchymale Stammzellen, Fettgewebe, Langzeitkulturen, Hypoxie, Sauerstoffkonzentration, Bioreaktorkultivierung statische Kultivierung, Dynamische Kultivierung.

Mesenchymale Stammzellen (MSC) werden als einer der vielversprechendsten Zelltypen für klinische Anwendung und insbesondere im Bereich der Gewebezüchtung erachtet. Der erste Erfolg mit einer Isolierung von MSC ist mehr als 30 Jahren her und begann mit mesenchymalen Stammzellen aus dem Knochenmark (bone marrow mesenchymal stem cell, BM-MSC). Anschließend wurde aus einer Vielzahl von Geweben wie auch aus dem Fettgewebe isoliert. Darüber hinaus haben sich MSC im Hinblick auf zwei wesentliche Aspekte zu einem unverzichtbaren Bestandteil in der regenerativen Medizin bewiesen. Zum einen sind sie in der Lage, ihre Multipotenz in der Zellkultur aufrechtzuerhalten und zum anderen können MSC zu verschiedenen Zelltypen wie Adipozyten, Chondrozyten und Osteoblasten differenzieren. Fettgewebe (adipose tissue, AD) wird als eine der wichtigsten Stammzellenquellen gesehen, da Zellen aus dem Fettgewebe sehr schnell und einfach zu gewinnen sind. Es sollte auch berücksichtigt werden, dass AD-MSC nur kurze Verdopplungszeiten haben, die eine Voraussetzung für die Gewebezüchtung ist, weil *ex vivo* expandierte Stammzellen enorm hohe Zellausbeuten erreichen müssen um in der therapeutischen Anwendung nützlich sein zu können.

Beim Arbeiten mit mesenchymalen Stammzellen ist klar zu betonen, dass es im Hinblick der ethischen Grundmoral keine Beschränkungen bis dato im gesetzlichen Rahmen gibt, was im Gegensatz zu den höchst umstrittenen embryonalen Stammzellen ganz anders der Fall ist. Stammzellen geben Hoffnung auf neuartige Behandlungsstrategien und dennoch wird ihr Einsatz in der Forschung stark diskutiert. Unterschiedliche Länder haben sich dazu entschlossen die embryonale Stammzellforschung in einer sehr unterschiedlichen Art und Weise zu reglementieren. Die embryonale Stammzellforschung verursacht zahlreiche moralische Dilemmas. Sie zwingt uns zwischen zwei fundamentalen Prinzipien zu entscheiden. Zum einem die Pflicht Leid zu verhindern oder zu verringern und zum andern die Pflicht menschliches Leben zu respektieren. Im Fall der embryonalen Stammzellforschung scheint es unmöglich beiden Prinzipien zu folgen, was mit dem Einsatz von mesenchymalen Stammzellen möglich ist. Auf Grund der hohen medizinischen Relevanz von AD-MSC, ist es wichtig *ex vivo* Kultivierungsstrategien zu entwickeln, die eine optimale Zellausbeute erlauben. Dabei ist sowohl die erreichbare Zellmenge als auch die Qualität der gezüchteten Zellen entscheidend. Ziel dieser Arbeit war es einen Beitrag zur Optimierung von AD-MSC Expansionsstrategien zu leisten. Dazu wurde diese Studie in zwei Teile getrennt um erstens die Qualität und zweitens die Ausbeute von *ex vivo* expandierten AD-MSC zu studieren und des Weiteren zu optimieren. Im ersten Teil dieser Forschung wurden grundlegende Aspekte

statischer Expansionsstrategien untersucht: Die Auswirkung unterschiedlicher Verdauungsenzyme und der Einsatz von thermoresponsiblen Oberflächen auf das Expansionsverhalten von AD-MSC wurde mit konventioneller Expansion verglichen. Außerdem wurde der Einfluss der Sauerstoffkonzentration auf das Expansionsverhalten von AD-MSC untersucht. Dazu wurden Langzeitkulturen unter hypoxischen (5% O₂) und normoxischen (21% O₂) Bedingungen kultiviert und das Wachstumsverhalten beider Kulturen verglichen. Zusätzlich wurden MSC-Oberflächenmarker bestimmt und die Zellen in Adipozyten, Chondrozyten und Osteoblasten differenziert um nachzuweisen, dass es sich bei dem Zellmaterial um mesenchymale Stammzellen handelt. Der Einfluss von unterschiedlichen Verdauungsenzymen bei der Zellablösung von AD-MSC zeigten keine signifikanten Unterschiede in Bezug auf die charakterisierten Zelloberflächenmarker. Darüber hinaus resultierte eine Zunahme der Gesamtzellzahl bei Verwendung von thermoresponsiblen Oberflächen verglichen zu herkömmlichen TCPS. Des Weiteren erhöhte sich die Expansionsrate von AD-MSC unter hypoxischen Bedingungen im Vergleich zu atmosphärischen Standardbedingungen. Außerdem resultierte eine effizientere Proliferationskapazität von AD-MSC unter hypoxischen verglichen zu normoxischen Bedingungen über mehr als 20 Passagen, das sich in der maximal erreichten Zellausbeute und den verbrauchten Metaboliten bestätigte. Zudem bewies die Kultivierung von AD-MSC unter Hypoxie besseres adipogenes Differenzierungspotenzial.

Der zweite Teil dieser Forschung konzentrierte sich auf Expansionsmöglichkeiten von AD-MSC in dynamischen Prozessen, zum einem in einem Z[®]RP 2000 H Bioreaktor unter hypoxischen Bedingung (5% O₂) und zum anderen in einem 3D-Einweg-Bioreaktor-system, dem TubeSpin[®] Bioreaktor unter atmosphärischen (21% O₂) Bedingungen. Auf der einen Seite wird unter hypoxischen Bedingungen eine physiologische Umgebung die der körpereigenen nahe kommt durch den geringen Sauerstoffgehalt geschaffen und auf der anderen Seite, wird diese körperähnliche Umgebung durch die Verwendung von Bioreaktoren verstärkt, da dadurch die Dynamik des menschlichen Körpers *ex vivo* nachgestellt wird.

Vorteile der dynamischen Kultivierung in Bioreaktoren sind zudem auch die automatisierte Steuerung der Prozesse, welche kausativ damit das Risiko von Kontaminationen senkt. Noch dazu wird durch den kontinuierlichen Medium Austausch die homöostatische *in-vivo*-Mikroumgebung des Körpers nachgestellt. Signalmoleküle und Zytokine beeinflussen dabei sehr wesentlich das Zellwachstum in dynamischen Prozessen. Aufgrund dieser Einflussfaktoren sowie der Kultivierung von AD-MSC unter hypoxischen Bedingungen ist in dem Z[®]RP Bioreaktor 2000 H eine 7,4-fach erhöhte Expansionsrate von AD-MSC bezogen auf das Inokulum nach 5 Tagen erreicht worden. Mit nur einem Expansionssystem können daher enorm hohe Zellzahlen generiert werden. Über 50 Standard-Zellkulturflaschen wären nötig um die gleiche Zellausbeute zu gewährleisten. Bei der dynamischen Kultivierung in dem Suspension TubeSpin[®] Bioreaktor ist auch erfolgreich ein Wachstum von AD-MSC über 96 Stunden in Suspension als 3D-Zell-Aggregate festgestellt worden, die sowohl morphologisch wie auch mit der noch vorhandenen metabolischen Aktivität überzeugten.

Abstract

Keywords: Mesenchymal stem cells, adipose tissue, long term cultivation, hypoxia, oxygen tension, bioreactor cultivation, static cultivation, dynamic cultivation.

Mesenchymal stem cells (MSC) are known to be one of the most promising cell types for clinical application, especially in the field of tissue engineering. The first success in the isolation of MSC took place over 30 years ago and started with bone marrow derived mesenchymal stem cells (BM-MSC) and has subsequently been isolated from a variety of viable tissues such as adipose tissue. The availability of MSC has established these cells as an indispensable and powerful tool in regenerative medicine.

They are able to expand while maintaining their multipotency in cell culture and are capable of differentiating into different cell types such as adipocytes, chondrocytes and osteoblasts. Adipose (AD) tissue has been shown to be a very successful MSC source since cells from adipose tissue are able to be quickly and easily received. AD-MSC also guarantee short population-times, an essential requirement for tissue engineering. *Ex vivo* expanded AD-MSC have to achieve high population numbers in order to be useful in therapeutic applications. Additionally, by discussing problems due to ethical responsibility, AD-MSC are not involved, because up until now there were no restrictions for their use in contrast to the highly controversial embryonic stem cells.

These cells give confident hope for new treatment strategies, but yet their use in research is highly debated. Different countries have decided to regulate embryonic stem cell research in a very different manner. The embryonic stem cell research causes different moral dilemmas. It forces human beings to choose between two moral principles. On the one hand it is our duty to reduce/prevent suffering and on the other hand our duty to respect human life.

In the case of ESC research, it seems impossible to follow these two principals at the same time, what seems to be possible with the use of MSC.

Due to the high medical relevance of AD-MSC, it is important to develop *ex vivo* cultivation strategies that allow optimal cell yield. At this point, both the number of cells which can be achieved and the quality of the cultured cells is critical. The aim of this work was to accomplish a contribution to the optimization of AD-MSC expansion strategies.

For this purpose this study was separated into two parts in order to optimize the quality as well as the yield of *ex vivo* expanded AD-MSC. The first strategy explores the different effects of digestive enzymes and thermoresponsible surfaces (UpCellTM surfaces) to investigate the proliferation capacities on a static culture.

Furthermore, several advantages and disadvantages of long-term cultivation of AD-MSC under hypoxic (5% O₂) and normoxic (21% O₂) conditions were investigated. This involves the expansion capacity, the differentiation potential towards cell types (adipocytes, chondrocytes and osteoblasts) and the investigation of characteristic stem cell surface markers to guarantee the existence of such AD-MSC, based on static expansion.

Different digestive enzymes for cell detachment showed the enzymatic influences on surface markers of AD-MSC. The cell equivalence of AD-MSC after the impact of all used digestive enzymes showed no significant differences. Moreover, the proliferation capacity demonstrated an increase of the total cell number higher by using a thermoresponsible surface rather than conventional surfaces. Furthermore, the effect of hypoxia on AD-MSC culture improves additionally. Cell expansion under hypoxic condition for over 20 passages was more efficient than under normoxic condition. This is reflected in the maximum of cell yield and exploited metabolites. AD-MSC cultivated under hypoxia showed better retention of their adipogenic differentiation potential.

The second strategy focuses on the dynamic expansion of AD-MSC in a Z[®]RP 2000 H bioreactor under hypoxic condition (5% oxygen tension) and in a disposable TubeSpin[®] bioreactor system under the normoxic (21% O₂) condition. Both expansions are based on dynamic processes. Hypoxic condition was used because of the ability of AD-MSC to survive in a milieu after transplantation and that the functions relating to the local tissue requirements can be investigated. Dynamic cultivation provides automated control and process and lowers risk of contamination. In addition, the partial medium exchange supports the homeostatic *ex-vivo* microenvironment by producing signal molecules and cytokines, which affects the cell growth positively.

Furthermore, the expansion of AD-MSC in the Z[®]RP 2000 H bioreactor resulted in a 7.4-fold increase of the expansion-rate compared to the inoculum after a cultivation time of 5 days. That means that by using only one expansion system, the same cell yield can be achieved, where normally more than 50 TCPS would be necessary to ensure the same cell yield.

The dynamic cultivation in the suspension TubeSpin[®] bioreactor demonstrated that AD-MSC were possible to expand also in suspension for over 96 hours as 3D-cell-aggregates. The morphology as well as the metabolic activity of the created 3D cell-clusters was also satisfying.

1 Index of contents

Kurzfassung	1
Abstract.....	3
1 Index of contents	5
List of abbreviations and definitions	11
2 Introduction	15
2.1 Researched goals.....	16
3 Theoretical background	19
3.1 Cellular metabolism.....	19
3.2 Glycolysis and the catabolism of hexoses	19
3.3 Fates of pyruvate.....	20
3.4 Glycolysis is under tight regulation	22
3.5 The role of aerobic glycolysis on proliferating cells	23
3.6 <i>In vivo</i> oxygen concentration.....	24
3.7 Oxygen concentration and its impact on MSC	25
3.8 Glucose catabolism is similar in cancerous tissue and MSC under hypoxia.....	26
3.9 A lack of oxygen leads to the formation of ROS.....	29
3.10 Damaged glucose assimilation by Insulin-dependent diabetes mellitus	29
3.11 Glycolysis at limiting concentration of oxygen (hypoxia).....	30
3.12 Regulatory enzymes act as metabolic valves	31
3.13 Adipose tissue	32
3.14 Glutamine or glucose, which nutrient is more efficient in terms of growth, metabolism and growth inhibitors?	33

3.15	Lipolysis	34
3.16	Immunosuppressive properties of MSC.....	35
3.17	The linking pathway between growth control and glucose metabolism	36
3.18	Future prospects	37
4	Results	39
	Static cultivation	39
4.1	Stem cell characterization	39
4.1.1	Long-term AD-MSK cultivation under varying oxygen tensions	39
4.1.2	Metabolic activity of AD-MSK under varying oxygen tensions.....	43
4.1.3	Differentiation potential of AD-MSK under varying oxygen tensions	47
4.1.4	Metabolic activity of AD-MSK during differentiation under varying oxygen tensions.....	50
4.2	Alternative expansion strategies	56
4.2.1	Short-term cell expansion with alternative surfaces.....	56
4.2.2	Morphological examination.....	59
4.2.3	The expansion of AD-MSK on Thermo Scientific Nunc™ UpCell surface under varying oxygen tensions	61
4.3	Influence of different digestive enzymes for passaging on AD-MSK.....	62
4.3.1	Comparison of different enzymatic means of dissociation adherent monolayers of AD-MSK	62
4.3.2	Influence on cell growth and surface markers via flow cytometric analysis of surface antigen expression.....	65
	Dynamic cultivation	70
4.4	Expansion of AD-MSK in the Z®RP 2000 H bioreactor	70

4.4.1	Cell growth in the Z [®] RP 2000 H bioreactor under hypoxia.....	70
4.4.2	Morphological examination.....	73
4.4.3	Glucose consumption	73
4.4.4	Metabolic activity assessment (MTT assay)	74
4.4.5	Surface immuno-phenotype characterization of AD-MSc after expansion in the Z [®] RP 2000 H bioreactor.....	75
4.5	Expansion of AD-MSc in the TubeSpin [®] bioreactor.....	78
4.5.1	Morphological examination.....	79
4.5.2	Metabolic activity assessment (MTT assay)	81
4.5.3	Cell proliferation assessment.....	82
5	Conclusions and outlook	87
6	References	91
6.1	References.....	91
6.2	References (web)	102
7	Materials	105
7.1	Materials	105
7.2	Equipment.....	105
7.3	Chemicals.....	107
7.4	Differentiation Media	108
7.5	Solutions and buffers	108
7.6	Kits.....	108
8	Methods	109
8.1	Biological material.....	109

8.2	Isolation of AD-MSC.....	109
8.3	Cell thawing.....	109
8.4	Enzymatic detachment.....	110
8.5	Cumulative cell population doubling.....	110
8.6	Population doubling level.....	111
8.7	Proliferation: The exponential part of the cell growth curve.....	111
8.7.1	Examination of cell proliferation.....	111
8.7.2	The CuBiAn [®] XC biochemistry analyser.....	112
8.8	Cell differentiation.....	112
8.8.1	Fibronectin coated plates.....	113
8.8.2	Fixation of the cell layer.....	113
8.8.3	Staining procedures.....	113
8.8.4	Metabolites measurement during cell differentiation.....	115
8.9	Comparison of different enzymatic means of dissociation adherent monolayers of AD-MSC.....	115
8.9.1	Cell viability assessment.....	115
8.9.2	Preparation of compensation samples of the flow cytometer.....	116
8.9.3	Immuno-fluorescent staining.....	117
8.10	Short-term cell expansion with alternative surfaces.....	118
8.10.1	Thermo Scientific Nunc UpCell [™] surfaces under normoxic condition.....	118
	<i>In vitro</i> cell culture.....	118
8.10.2	Detachment of cells by using temperature reduction.....	119
8.10.3	Thermo Scientific NuncUpCell [™] surface under hypoxic condition.....	120

8.11	Cell expansion in the Z [®] RP 2000 H bioreactor	120
8.11.1	Nova BioProfile analyser.....	122
8.11.2	Metabolic activity assessment (MTT assay)	122
8.12	Dynamic cell expansion in the TubeSpin [®] bioreactor	124
	Creation of 3D-cell-aggregates	125
8.12.1	Prior-cultivation (static) in TCPS	125
8.12.2	Spheroid generation.....	125
8.12.3	Second cultivation in U-bottom 96 well plates	125
8.12.4	Morphological examination of created 3D-cell-aggregates	126
8.12.5	Expansion in the TubeSpin [®] bioreactor	126
8.12.6	Cell proliferation assay of AD-MSK in the suspension TubeSpin [®] bioreactor	127
8.12.7	Metabolic activity assessment (MTT assay)	128
8.13	Statistical analysis	128
9	Supplementary materials	130
	Flow cytometric analysis of different digestive enzymes	130
9.1	Accutase.....	131
9.2	Trypsin S.....	132
9.3	TrpLE [™] Express	133
10	Acknowledgements	134
11	Curriculum Vitae	136

List of abbreviations and definitions

μm	Micrometre
2D	Two-dimensional
3D	Three-dimensional
a.u.	Arbitrary units
AD	Adipose-derived
AD-MSC	Adipose tissue derived mesenchymal stem cell
ADP	Adenosine diphosphate
Akt 1	V-akt murine thymoma viral oncogene homolog 1
AMP	Adenosine monophosphate
AMPK	AMP-activated protein kinase
Ang-2	Angiopoietin-2
ATP	Adenosine 5'-triphosphate
BM-MSC	Bone marrow derived mesenchymal stem cells
C°	Degree
cAMP	Cyclic AMP
CD	Cluster of differentiation
c-Myc	Myelocytomatosis viral oncogene homolog
CO ₂	Carbon dioxide
COX4-1	Cytochrome c oxidase subunit 4 isoform 1
COX4-2	Cytochrome c oxidase subunit 4 isoform 2
DC	Dendritic cells
ddH ₂ O	Double-distilled water
DNA	Deoxyribonucleic acid
ECM	Extracellular matrix
ESC	Embryonal stem cells
FADH ₂	Flavin adenine dinucleotide
FCS	Fetal calf serum
FSC	Forward scatter
G-1-P	Glucose-1-phosphate
G-6-P	Glucose-6-phosphate
GDH	Glutamate dehydrogenase
GLUT1	Glucose transporter 1

GLUT2	Glucose transporter 2
GLUT3	Glucose transporter 3
GLUT4	Glucose transporter 4
GM	Gentamicin
G-proteins	Guanosine nucleotide-binding proteins
GTPase	Enzyme of a large hydrolase family
H ₂ O	Water
HFN	Human fibronectin
HIF	Hypoxia-inducible factor
HIF-1	Hypoxia-inducible transcription factor 1
HIF-1 α	Subunit of HIF-1
HIF-2 α	Subunit of HIF-1
hMSC	Human mesenchymal stem cells
HRE	Hypoxia response elements
HS	Human serum
HSL	Hormone-sensitive lipase
Hypoxia	Low oxygen level
IRS	Insulin receptor substrate
ISCT	International Society for Cellular Therapy
KEGG	Kyoto Encyclopedia of Gens and Genomes
LDH	Lactate dehydrogenase
LKB1	Liver kinase B1 (protein kinase)
MAPK	Mitogen activated protein kinase
MHC- II	Class II Major Histocompatibility complex
Min	Minutes
MN	Mean
MSC	Mesenchymal stem cells
mTOR	Mammalian target of rapamycin
NAD ⁺	Nicotinamide adenine dinucleotide (oxidized form)
NADH	Nicotinamide adenine dinucleotide (reduced form)
NADPH	Nicotinamide adenine dinucleotide phosphate
NH ₃	Ammonia
NKC	Natural killer cells
Normoxia	21% oxygen level (atmospheric O ₂ tension)

O ₂	Oxygen
p53	Tumour suppressor protein
PBS	Phosphate buffer saline
PD	Population doubling
PDL	Population doubling level
PFK-1	6-phosphofructokinase
PI3K	Phosphoinositide 3-kinase
PIK3CA	Phosphatidylinositol-4,5-bisphosphate 3-kinase, Catalytic subunit alpha
PKA	Protein kinase A
Pre-warmed	37 °C
PTEN	Phosphatidylinositol-3,4,5-trisphosphate 3-phosphatase
Pyruvate- Dehydrogenase	PDH
Ras	Superfamily of small GTPases
RNA	Ribonucleic acid
Room-temperature	21 °C-23 °C
ROS	Reactive oxygen species
Rpm	Rotation per minute
SCR-R	Stem cell factor receptor
SD	Standard Deviation
SDS	Sodium dodecyl Sulphate
SSC	Side scatter
TCA cycle	Tricarboxylic acid cycle
TCPS	Tissue culture plastic surface
TGF-β	Transforming growth factor-beta
TGs	Triglycerides
TNF-α	Tumour necrosis factor alpha
Trypsin P	Trypsin Polymun
Trypsin S	Trypsin Sigma
TubeSpin® bioreactor	CELLSTAR® CELLreactor™ tubes
VEGF	Vascular endothelial growth factor
α-MEM	Minimal essential medium alpha
β1-β3-AR	β-adrenoceptors

2 Introduction

Mesenchymal stem cells (MSC) are characterized as multipotent cells and have become one of the most promising cell-candidates for tissue engineering and regenerative medicine applications in recent years [1].

Their multipotency gives these cells the ability to differentiate into a variety of cell types from the mesodermal origin such as bone, muscle tendon, cartilage, ligament and fat [2].

Because of these features, MSC have been established as a powerful tool for therapeutic applications such as cell-based-therapy and tissue engineering. MSC have many applications in the treatment of burns, spinal cord injuries, graft versus host disease, liver cirrhosis or failure, progressive multiple sclerosis, diabetes mellitus, cancer research and cardiac ischemia [3, 4].

In addition to these regenerative properties MSC feature an immune regulatory capacity, releasing immune suppressive effects in a variety of physiological situations. These cells are not only immune-privileged (anergy), which means that they are able to tolerate the introduction of antigens without eliciting an inflammatory immune response, but also interfere with several cellular pathways of the immune system by means of soluble factor secretion and direct cell to cell interactions. Furthermore, *ex vivo* expanded MSC inhibit proliferation of B-cells, T-cells, DC and NKC, resulting intolerance mechanisms, known as anergy. MSCs did not preferentially target any T-cell subset and the inhibition was also extended to B-cells [5].

MSC mediated inhibition induces an unresponsive T-cell profile that is fully consistent with that observed in cell anergy [6].

Anergy is a term in immunobiology that describes a lack of reaction by the body's defence mechanisms to foreign substances and consists of a direct induction of peripheral lymphocyte tolerance. An individual in a state of anergy often indicates that the immune system is unable to mount a normal immune response against a specific antigen, usually a self-antigen. Lymphocytes are said to be anergic when they fail to respond to their specific antigen. Anergy is one of three processes that induce tolerance, modifying the immune system to prevent self-destruction and especially to avoid auto-reactive B-cells, which is a fundamental tool in autoimmune diseases [7].

Mesenchymal stem cells are able to stop several aspects of immune cell function which include B-cell maturation, cytokine secretion and cytotoxicity, antibody secretion, antigen presentation, and DC activation and maturation [8].

It must be recognized that *in vivo* studies of mesenchymal stem cells have yielded discrepancies due to immune modulatory potency. Such studies are designed to test the ability to suppress abnormal immune response in autoimmune diseases like diabetes mellitus and the prevention of allograft rejection episodes. Preclinical studies have been carried out on rabbits, baboon monkeys and rodents to demonstrate that MSC are a powerful cell type in autoimmune diseases, because the immune system may not reject them [8].

Therefore, by understanding *in vitro* cell growth and metabolism of MSC, successful therapeutic application will be achieved. Numerous metabolic pathways have been investigated since the 1980s and it is conceivable that more pathways have yet to be defined [9].

Besides, an enormous advantages is not just the usage of MSC in clinical applications and the numerous interesting pathways of such cells, which indicates the extreme variety of MSC`s potential in humans, it is also the aspect that MSC are easily isolated from tissues in the human body such as adipose tissue, muscle, umbilical cord and bone marrow [10-12].

MSC from adipose tissue represents an adequate source, because AD-MSC are easily isolated and expanded. Furthermore, AD-MSC are not subject to any ethical conflicts and there are no “medicinal-legal” limitations in their application due to cell harvest. This means that research has not been largely limited due to the ethical issues that surround their controversial procurement from fertilized embryos. In general MSC provides a lot of advantages like those mentioned above but there are still unfavorable aspects to mention.

MSC are presence in small quantities in human bodies [13] and in clinical applications, MSC must be expanded to tens of million MSC to adequate usage of them. These small quantities led to the concept of bioreactors which offers a controlled cost effective, reproducible way of cultivation, which end in large quantities of cells [14].

Expansion in bioreactors is able to take place without sub-cultivation, reducing the risk of microorganism`s contamination as well as cross-contamination with other cell lines. A control of important cultivation parameters (such as O₂, CO₂, pH, temperature, pressure, metabolic concentrations and continuous online monitoring) help to deliver optimal growth inhibitors and metabolic conditions for the cell in the bioreactor to survive [15].

Besides, a variety of cell expansion strategies are popular, including conventional static cultivation in cell culture flasks (TCPS), alternative static cultivation on a thermoresponsible surfaces, hanging-drop cultivations, and dynamic cultivations in bioreactors under precisely regulated control processes, which involves a huge field of cell culture techniques: cultivation on a 3D matrix, on polycarbonate cell carrier slides, on thermo responsible surfaces or on microcarriers [16].

In addition to these cell cultivation techniques, an important approach is cultivation under hypoxic conditions (low oxygen tension), which positively influences cell growth and causative their proliferation capacity of MSC [17-20].

In vivo tissue concentrations are never exposed to the atmospheric oxygen concentrations in which most cell culture studies are carried out [17].

2.1 Researched goals

The present study considered a variety of variables in order to tweak the processing of AD-MSC. Specifically, the roles of hypoxia and dynamic cell expansion have been investigated.

Three aims have been identified:

1. The advantages and disadvantages of static cultivation of AD-MSC under hypoxic and normoxic conditions (referring to proliferation capacity and differentiation potential) were inspected to demonstrate the identity of AD-MSC.
2. The effects of different cell detachment processes (enzyme dependent detachment in contrast to temperature reduction detachment processes with thermo-responsive surfaces) on proliferation capacity were studied.
3. The expansion of AD-MSC under dynamic cultivation conditions was examined in a Z[®]RP 2000 H bioreactor (Zellwerk GmbH, Berlin) and in a suspension disposable TubeSpin[®] bioreactor (Greiner Bio-One GmbH, Frickenhausen).

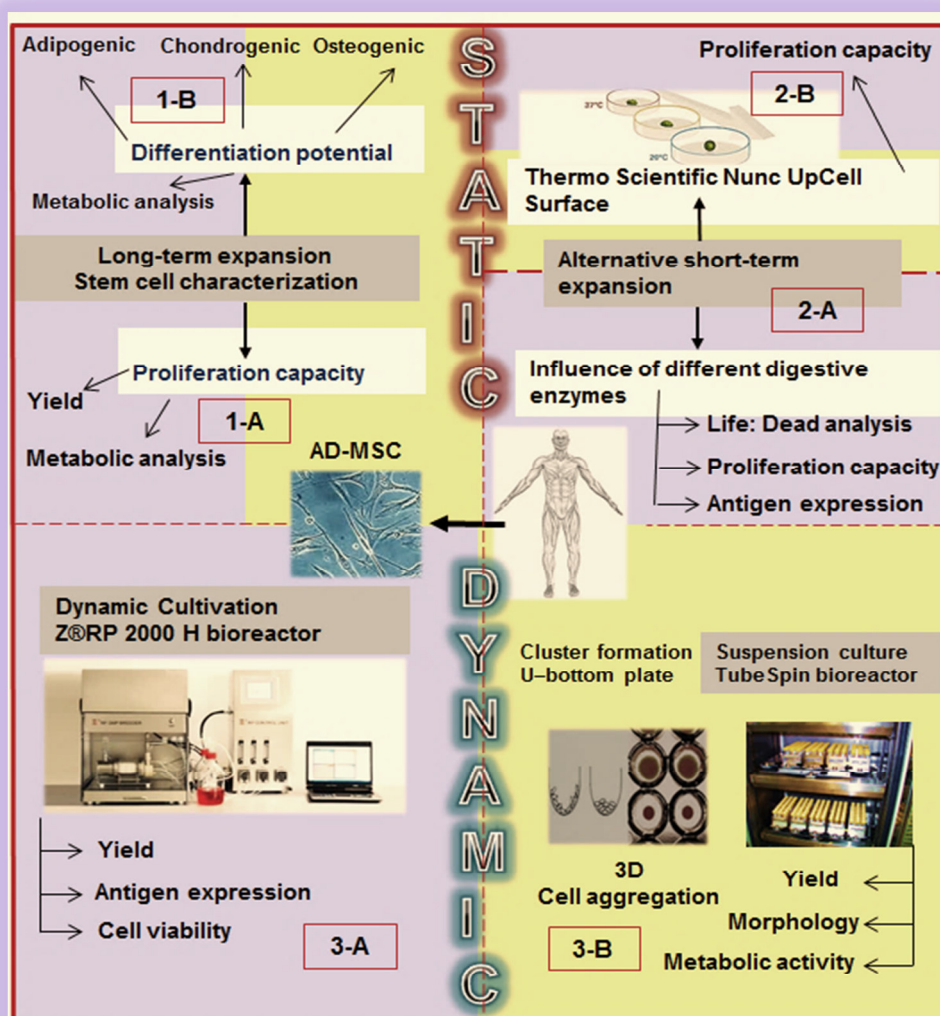


Figure 1: Graphical abstract of the three aims of the master thesis: Strategies of adipose-derived stem cell expansion. Yellow-represents the cultivation under normoxia. Blue-represents the cultivation under hypoxia.

1-A: Stem cell characterization referring to the proliferation capacity in a long-term culture.

1-B: Stem cell characterization referring to the differentiation potential in a long-term culture.

2-A: Alternative expansion strategy based on the influence of different digestive enzymes.

2-B: Alternative expansion strategy based on the principle of Thermo Scientific Nunc UpCell[™] surfaces.

3-A: Dynamic cultivation in the Z[®]RP 2000 H bioreactor. 3-B: Dynamic cultivation in the TubeSpin[®] bioreactor.

3 Theoretical background

3.1 Cellular metabolism

Metabolic control systems have developed to distinguish an adequate supply of nutrients and manage the requisite of carbon, nitrogen and free energy into generating polymers which are needed to produce a new cell. When there is a shortage of nutrients cells cease biomass production and adapt their metabolism to extract the majority of free energy from available resources to survive. Cell survival is based on strict control systems that prevent aberrant individual cell proliferation when nutrient availability exceeds the levels to support cell division [21].

Every single metabolic pathway is a multicomponent network and is interconnected with all cellular pathways. A typical mammalian cell is able to synthesise approximately 30 000 proteins, which catalyse thousands of different reactions and hundreds of metabolites, not only in one metabolic pathway, but in a combination of many. This complex system is visually available in the online-databank KEGG (Kyoto Encyclopedia of Gens and Genomes) ((taken from (1)).The metabolism is a strictly coordinated cellular activity in which many multi-enzyme systems (the so called metabolic pathways) cooperate to achieve four main functions.

First, to obtain chemical energy by capturing solar energy or degrading energy-rich nutrients from the environment, second to convert nutrient molecules into the cell's own characteristic molecules, third to polymerize monomeric precursors into macromolecules and lastly to synthesize and degrade biomolecules required in specialized cellular functions [22].

3.2 Glycolysis and the catabolism of hexoses

In mammalian cells, glucose has three main tasks, to serve as energy source, to oxidise a three-carbon compound (pyruvate) via glycolysis and to oxidise to pentoses via the pentose phosphate pathway. Glycolysis is seen as the central, universal pathway of the glucose molecule and the largest flux of carbon in most cells, especially in MSC. The breakdown of the six-carbon glucose into two molecules of the three-carbon pyruvate takes place in ten steps, seen in figure 2. The starting point of the glycolysis is known to be a preparatory phase in which the phosphorylation of glucose and its conversion to two molecules of glyceraldehyde-3-phosphate takes place.

In the second phase, oxidative conversion of glyceraldehyde-3-phosphate to pyruvate and the coupled formation of ATP and NADH take place. As a result, much of the energy is preserved by the coupled phosphorylation of four molecules of ATP and ADP.

The absolute net yield is two molecules of ATP per inserted molecule glucose. Moreover, energy is also preserved in the second phase of glycolysis via the formation of two molecules of NADH per molecule glucose. To sum up, in the ten sequential reactions in the preparatory phase and the payoff phase, three major types of chemical transformations occur. First, the degradation of the carbon skeleton of glucose yields pyruvate. Then a high energy

phosphorylation of ADP to ATP and the transfer of hydride ion with its electron to NAD^+ , followed by formation of NADH occurs [22].

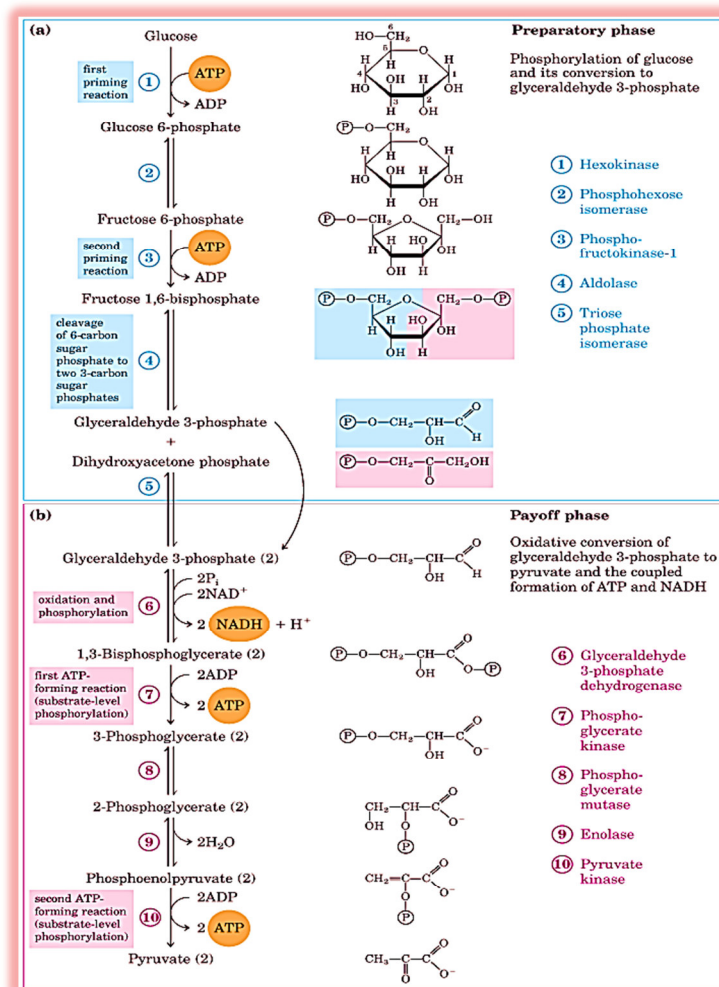


Figure 2: Glycolysis and the catabolism of hexoses (taken from (2)).

3.3 Fates of pyruvate

Interestingly, in cells as well as in MSC the pyruvate which is formed as an end product by glycolysis is further metabolized via one of three catabolic routes. This happens on the one hand under aerobic conditions and glycolysis is just the first metabolic stage in the complete degradation of glucose molecule. Pyruvate is initially oxidized and the carboxyl group is lost in the form of CO_2 and is added as an acetyl group to form acetyl-coenzyme A.

Afterwards, the acetyl group is oxidized completely to CO_2 via the citric acid cycle. From these oxidations, the electrons are passed to O_2 through a chain of carriers in the mitochondrion and H_2O is formed. This resulting energy that was created from the electron transfer reactions facilitates the synthesis of ATP (36 ATP/glucose) in the mitochondrion. The metabolic pathway is known as oxidative phosphorylation.

On the other hand the degradation of glucose takes place under low-oxygen conditions, called hypoxia, in the so called second pathway, in which NADH cannot be re-oxidized to NAD^+ and this NAD^+ will be needed as an electron acceptor for further oxidation of pyruvate. Because of this, pyruvate is reduced to lactate; accepting electrons from NADH and as a result regenerate the NAD^+ that is needed for the glycolysis to proceed. The described pathway is called anaerobic glycolysis [5].

Based on the previous mentioned metabolic activities of cells and also of MSC, few studies have investigated changes in MSC energy metabolism during differentiation to osteogenic and chondrogenic lineages [23, 24].

This was demonstrated by an increase in oxygen consumption during osteogenic and adipogenic differentiation for AD-MSC and BM-MSC. While a higher rate of ATP production resulted during glycolysis through chondrogenic differentiation compared to its proliferation. Chondrocytes have been shown to have a high level of glycolysis activity with minimal oxygen consumption compared to osteoblasts and adipocytes [25, 26].

In contrast, osteoblasts have higher oxygen consumption than chondrocytes and are known to exhibit a mixed metabolism and to utilise both glycolysis at first and oxidative phosphorylation follows for the ATP production upon culture under normoxia [27-30].

It should be mentioned that glycolysis occurs in both cases: in aerobic as well as in anaerobic fermentation, because it happens before to create pyruvate.

However it is right, that an unexpectedly high rate of glycolysis occurs during proliferation of MSC, the cells generally exhibit a mixed metabolism with a significant glycolytic component consistent with the Warburg effect. The just described 3rd metabolic route is known as aerobic glycolysis (Warburg effect). The Warburg effect is defined by an increased utilization of glucose via glycolysis as a cellular resource under aerobic conditions and is a common phenotype of tumorigenic cells and in cells with exhibit a high rate of proliferation like MSC [21].

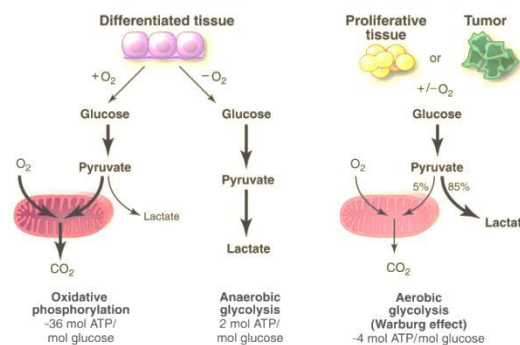


Figure 3: Fates of pyruvate: Differentiated tissue converts on the one hand in the presence of O_2 , glucose to pyruvate and end up in the formation of CO_2 , which is called oxidative phosphorylation. On the other hand differentiated tissue converts glucose directly to lactate under low oxygen tension (hypoxia), which is known as anaerobic glycolysis. In comparison to differentiated tissue proliferative tissue exhibit a mixed metabolism, which is known as the Warburg effect or aerobic glycolysis. The Warburg effect occurs during both: in the presence of O_2 or in the absence of O_2 (taken from (3)).

According to figure 3 the differences between oxidative phosphorylation, anaerobic glycolysis and aerobic glycolysis (Warburg effect) is described. In the presence of oxygen, non-proliferating (differentiated) tissues first metabolize glucose to pyruvate via glycolysis and then completely oxidize most of that pyruvate in the mitochondria to CO₂ during the process of oxidative phosphorylation. Because oxygen is required as the final electron acceptor to completely oxidize the glucose, oxygen is essential for this process. 36 ATP per mole glucose is generated during oxidative phosphorylation, which is the most efficient metabolic step. When oxygen is limiting which occurs during hypoxia, cells can redirect the pyruvate generated by glycolysis away from mitochondrial oxidative phosphorylation by generating lactate (anaerobic glycolysis). This generation of lactate during anaerobic glycolysis allows glycolysis to continue (by cycling NADH back to NAD⁺), but results in minimal ATP production (2 ATP/glucose) when compared with oxidative phosphorylation. To mentioned casually, Warburg observed that cancer cells tend to convert most glucose to lactate regardless of whether oxygen is present (aerobic glycolysis). This property is shared by normal proliferative tissues. Mitochondria remain functional and some oxidative phosphorylation continues in both cancer cells and normal proliferating cells. Interestingly, it has also been shown that even under aerobic conditions, certain tissues (erythrocytes) convert glucose to lactate during aerobic glycolysis [22].

Nevertheless, aerobic glycolysis is less efficient than oxidative phosphorylation for generating ATP. In proliferating cells, ~10% of the glucose is diverted into biosynthetic pathways upstream of pyruvate production [31].

In connection with the three fates of pyruvate it is a fact that the contributions of glycolysis and oxidative phosphorylation vary depending on oxygen as well as glucose concentration, which is consistent with the Pasteur and Crabtree effects, respectively. The Crabtree effect describes the observation that respiration is inhibited when high concentrations of glucose are added to the culture medium. This phenomenon takes place in numerous cell types, particularly in proliferating cells. The Pasteur Effect (suppression of glycolysis by oxygen) is the converse of the Crabtree effect (aerobic glycolysis to lactate). Also cancer cells differ from normal cells by reversibly down-regulating the oxygen consumption in response to increases in glucose availability. This phenomenon as also occurs during the Crabtree effect [32].

This metabolic route is to protect and contribute to tumour cell survival in a dynamic environment that is periodically undergoing hypoxia [33].

3.4 Glycolysis is under tight regulation

Louis Pasteur proved that the rate and total amount of glucose consumption in cells are greater under anaerobic than under aerobic conditions. This is termed as the Pasteur effect, which can be explained by the fact that the ATP yield from glycolysis under anaerobic conditions (2 ATP per investigated molecule glucose) is smaller than the ATP yield from the

complete oxidation of glucose to CO₂ under aerobic conditions (36 ATP/molecule glucose). As a consequence, about 15 times more glucose must be processed under anaerobic conditions than under aerobic conditions to yield the same amount of ATP.

As a result also MSC increase their rate of glycolysis upon culture under hypoxic condition, consistent with the Pasteur Effect [34-36].

3.5 The role of aerobic glycolysis on proliferating cells

Most differentiated cells metabolize glucose to carbon dioxide by oxidation of glycolytic pyruvate in the citric acid cycle in which NADH is reduced to NAD⁺. Afterwards, it fuels oxidative phosphorylation to produce free energy (36 ATP/glucose) with minimal production of lactate. Differentiated cells produce large amounts of lactate only under anaerobic conditions. The aerobic glycolytic metabolism provides sufficient energy for cell proliferation. Anaerobic glycolysis generates only 2 ATP per molecule of glucose, whereas oxidative phosphorylation produces up to 36 ATP during the oxidation of just one glucose molecule [22].

This fact raises the question of why a less efficient metabolism would be used for proliferating cells, especially in MSC, because during aerobic glycolysis (Warburg effect) only 4 ATP are produced compared to 36 ATP during oxidative phosphorylation. One explanation could be that inefficient ATP generation is only a problem when cellular fuel is scarce. This is not the case with proliferating mammalian cells, because these cells get a continuous supply of different nutrients via medium exchange or the circulating bloodstream. ATP is never limited in proliferating cells, no matter how much they are stimulated to divide. As a consequence, the aerobic glycolysis is no problem for proliferating cells [37, 38]. Moreover, even minor perturbations in the ratio of ATP/ADP can influence cell growth and if this flux does not occur, cells undergo apoptosis [39, 40].

The ability to produce ATP from glucose can be compromised by using reactive catabolism metabolism like aerobic glycolysis [41, 42].

The primary way a cell maintains a viable ATP/ADP ratio is by using the enzyme adenylate kinase, which buffers declining ATP production by converting two molecules of ADP to only one molecule of ATP and one molecule of AMP. However, the accumulation of AMP stimulates AMP-activated protein kinase (AMPK). The activation of AMPK is dependent on the tumour suppressor protein LKB1 (liver kinase B1) and as a result, this leads to phosphorylation of a variety of targets to improve energy amount in cells, which positively accompanied with the aerobic glycolysis [43].

Another explanation for using aerobic glycolysis is the fact that proliferating cells also have metabolic requirements other than ATP. A proliferating cell has to replicate all of its contents to create two viable daughter cells during mitosis and this step requires available nucleotides, amino acids, and lipids. When a cell is growing, ATP production and hexose are necessary for the new generation of biomass. It is true that ATP hydrolysis dispenses free energy for a

variety of biochemical reactions but regardless, additional requirements are essential for a complete biomass replication. For example, the synthesis of palmitate requires 7 molecules of ATP, 28 electrons from 14 molecules of NADPH and 16 carbons from 8 molecules of acetyl-CoA. The synthesis of amino acids as well as nucleotides also requires several equivalents of carbon and NADPH, even more than ATP. One mole of glucose produces up to 36 ATP or 30 ATP and 2 NADPH if glucose is diverted into the pentose phosphate pathway or allocates 6 carbons for macromolecular synthesis.

That means that to create a 16-carbon fatty acyl chain, one single glucose molecule gives five times the ATP required, whereas 7 glucose molecules are the postulate to generate the NADPH requirement. It seems clear that this 35-fold ratio is just partially compensated by the consumption of 3 glucose molecules in acetyl-CoA synthesis to correlate to the carbon requirement of the 16-carbon fatty acyl chain. Therefore, it is evident that the amount of the glucose cannot be committed to carbon catabolism for ATP by proliferating cells. If this is the case, the ratio of ATP/ADP would impair the flux through glycolytic intermediates, followed by the limitation of the acetyl-CoA and NADPH requirement for the synthesis of macromolecules [22].

Besides, glucose and glutamine are the main sources of nitrogen, carbon, ATP and reducing equivalents to enable cell growth and division. This leads inevitably to the awareness that converting all of glucose to carbon dioxide via the oxidative phosphorylation to achieve a maximum of ATP is counterintuitive to the requirements for cell proliferation. Therefore, glucose has to be branched to macromolecular precursors such as ribose for nucleotides, acetyl-CoA for fatty acids, and glycolytic intermediates for amino acids. This fact may be a third explanation for the advantage why proliferating cells undergo aerobic glycolysis [44].

3.6 *In vivo* oxygen concentration

As a fact, just a few cells in human beings are exposed to atmospheric O₂ tension (21% O₂). These cell types are cells of the corneal epithelium, macrophages and pneumocytes in lung alveoli and keratinocytes in the epidermis. The rest of the cell pool proliferate and function under lower oxygen tensions, seen in figure 4.

For better understanding all explained oxygen values are calculated as volumetric O₂ concentrations (figure 4).

Every tissue has a different intensity of vascularization and this leads to different oxygen tensions in human body. Depending on this, oxygen tensions less than 6% were measured in bone marrow and approximately 15% in adipose tissue [45-47].

Moreover, the oxygen tension in the deep zone of cartilage is less than 1% and 7% on the surface [48, 49].

In the retina the oxygen tension is at its maximum 5% and in the circulation a value of 16% is measured [50, 51].

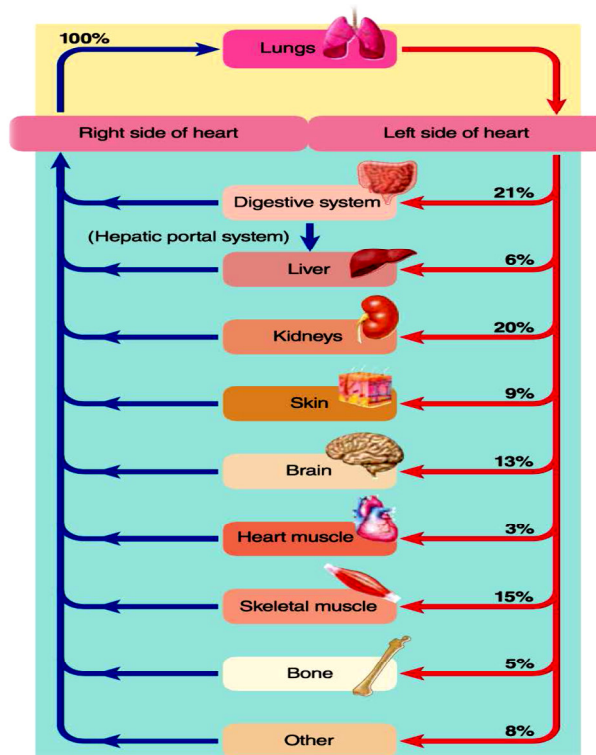


Figure 4: *In vivo* oxygen concentration. Red arrows present O₂ uptake. Blue arrows present CO₂ release (taken from (4)).

All tissue types except the digestive system and parts of the kidney develop a hypoxic atmosphere, which is associated with low oxygen (hypoxia) concentration, especially bone marrow and the skin. As a result it can be said that adipose-derived mesenchymal stem cells function under low oxygen tension. These data show that low oxygen concentrations (less than 15% O₂ tension) present a physiological hypoxia.

The term describes a so-called steady state of oxygenation *in situ*. The definition of hypoxia is a reduction of oxygen supply to a tissue below physiological levels (21% O₂) despite an adequate perfusion of the tissue by blood [52].

Based on this fundamental cognition, MSC function, independent of their origin, the best under much lower oxygen concentrations as those used in classically cell culture systems [53].

3.7 Oxygen concentration and its impact on MSC

Recent studies describe the influence of oxygen concentration on the proliferation capacity and differentiation potential on MSC, seen in table 1. The effect of hypoxia is dependent on diverse parameters like the type of MSC, the presence or absence of cell culture media supplements and the degree of achieved hypoxia levels [17].

Table 1: Influence of different oxygen concentration on MSC's proliferation and differentiation potential.

Oxygen concentration	Type of MSC	Observed effect	Reference
$\leq 1\%$	hBM-MSC	Decreased osteogenesis	[54]
1%	hBM-MSC	Decreased proliferation and differentiation	[55]
2%	hBM-MSC	Increased proliferation	[35]
2%	hBM-MSC	Increased proliferation	[17]
5%	hAD-MSC	Increased proliferation and chondrogenesis	[56]
5%	hAD-MSC	Decreased osteogenesis and increased chondrogenesis	[57]

To sum up all these data, it is clear that cultivation of MSC, especially hAD-MSC under hypoxic condition may be beneficial for stem cell proliferation and differentiation. This leads inevitable to the fact that under hypoxia higher cell yields and different types of cells (chondrocytes, osteoblasts and adipocytes) may be achieved [58].

3.8 Glucose catabolism is similar in cancerous tissue and MSC under hypoxia

Cancer is nowadays one of the main causes of mortality in developed countries and is also increasing in low income countries because the global population increases as well as ages and improvements in detection are implemented [59].

Most of cancer is associated with the elderly, but some occur in the young and both phenomena represent the accumulation of genetic, epigenetic cell damage and changes in metabolism [60].

Investigating and understanding all metabolic links between growth control and cellular metabolism may ultimately lead to better treatments for human cancer.

A main feature of tumours under hypoxia is that the availability of oxygen decreases, which increases resistance to treatment and favours tumour progression. How cells respond to hypoxia and how hypoxic conditions are generated are fundamental questions in understanding the cycle of metastasis and tumour progression [61].

Some factors related to the tumour microenvironment are now recognized as essential in tumour progression, such as increasing resistance and metastasis. Hypoxia is one of these factors which is common in all cancer types [62].

Glycolysis proceeds and glucose is metabolized about 10 times faster in most tumours than in non-cancerous tissues. This abnormal regulation of glycolysis is particularly interesting in cancer research. In 1928, Otto Warburg proposed that glycolysis in most cancer cells proceeds at a higher level than in non-cancer cells, albeit oxygen is available. Tumour cells mostly experience hypoxia (limited oxygen supply) because these cells initially lack a considerable capillary network to supply the tumour with oxygen. As a consequence, tumour cells, not

farther than 100 to 200 μm from the nearest capillaries, depend on aerobic glycolysis for most of the ATP production.

The increase of tumour growth requires the presence of a local vascular network, which supplies oxygen and nutrients to cancer cells. As a result, a higher proliferating rate of tumour cells accrues faster than the vasculature and cancer cells quickly meet up with an avascular environment which results in hypoxia. This is one of the consequences of the diffusion limit of oxygen within tissues, which is approximately 150 μm [63, 64].

Cancer cells need more glucose than normal cells, transferring it to pyruvate and finally to lactate as they recycle NADH. The output of ATP (2 ATP/molecule glucose) is less than the complete oxidation of pyruvate to CO_2 (approximately 36 ATP/molecule glucose). This fact serves as the basis for the idea that cancer cells need more glucose than normal cells [22].

By regarding the cellular metabolism of BM-MSC, there was a strong adaption to low oxygen atmosphere. When BM-MSC are cultured at 2% O_2 , these cells presented a higher specific consumption rate of glucose during the first week of culture, corresponding to the beginning of the exponential growth phase similar to the behaviour of cancerous cells. The reason for the higher consumption rate of glucose can be explained by the higher requirement of carbon for the higher rate of cell proliferation, which is induced by low oxygen tension (hypoxia), which is also likely to cancerous cells. A fact is that BM-MSC metabolism is not first-hand based on mitochondrial oxidative phosphorylation, as it had also been reported [21, 35, 65, 66].

It is also reported that proliferating cells, such as stem cells or cancer cells depend on aerobic glycolysis to produce energy (Warburg effect). Although aerobic glycolysis is not that efficient in terms of ATP (4 ATP/glucose) production, it is counterbalanced by non-limited availability of glucose provided by the cell culture medium and as a result, the production of ATP is not impaired or extenuated for these cells throughout culture time. It has been investigated that the metabolism of all proliferating cells (including MSC and cancer cells) is assimilated to enable the uptake and incorporation of nutrients into biomass [17].

Another important condition is that adipose tissue is well supplied and surrounded with many blood vessels, which suggests that in such cells, aerobic conditions dominate and therefore most of the cell metabolism is based on the complete oxidation of glucose to CO_2 or aerobic glycolysis [22].

The up-regulation of glycolysis is achieved through an increased synthesis of glycolytic enzymes and plasma membrane transporters (GLUT1 and GLUT3), which supply cells with glucose. The hypoxia-inducible transcription factor (HIF-1) is a protein that acts on RNA level and increases the production of 8 glycolytic enzymes. These enzymes increase the glucose transport if the oxygen level is limited (hypoxia). Hypoxia activates HIF-1 and results in the inhibition of the hydroxylation of the alpha subunit. The alpha subunit permits hetero dimerization, stabilization, and binding to hypoxia response elements (HRE) in target genes [67-69] and [70-73].

Because of this, the rate of glucose increases and cancer cells as well as MSC are able to survive under hypoxic conditions until the new building of blood vessels obtains the growth

of cells. Another protein which expresses because of the induction of HIF-1 is known as VEGF (vascular endothelial growth factor). VEGF improves angiogenesis in the direction of the tumour.

HIF-mediated expression of gene products also include the angiopoietin-2 (Ang-2) factor, which allows cancer cells to reverse the hypoxic situation by inducing re-growth of the vascular network [74].

Glucose transporter GLUT-1 and pyruvate kinase isoform M2 are responsible for elevated glycolysis and VEGF/erythropoietin production, [75] which are up-regulated because of the influence of HIF-1 α and HIF-2 α [76].

A few tumour cells (proliferating tissue) over-produce some glycolytic enzymes. One of them is an isozyme of hexokinase that interacts with the cytosolic face of mitochondrial inner membrane and is responsible for feedback inhibition by glucose 6-phosphate, which may monopolize the ATP production in mitochondria. After using ATP, glucose is converted to glucose 6-phosphate, and commits the cell to proceed with glycolysis. The protein products of tumour suppressor genes like p53 and Ras are also involve in the increased production of glycolytic enzymes in tumour cells. Cells with a mutated p53 have a defect in mitochondrial electron-transport chain and are forced to produce ATP via glycolysis.

In addition, metabolic regulation via HIF-1 also brings products of tumour suppressors and oncogenes into play such as the previous mentioned p53, Ras, c-Myc and Act [68, 77, 78].

Another pathway related to the availability of nutrients, which is also modified by HIF-1, is that of the mammalian target of rapamycin (mTOR). In one respect, energy depletion and hypoxia suppress mTOR, saving energy on protein synthesis, allowing cellular survival. Conversely, nutrients and growth factors potentiate the mTOR pathway in hauling signals of survival and growth through increased protein synthesis [69].

The strong dependency of tumours on glycolysis provides an avenue for therapeutic possibilities in cancer research. Inhibitors of the glycolysis are able to target cancer cells as they disconnect the ATP accommodation. 2-desoxyglucose, lonidamin, and 3-bromopyruvate are inhibitors of hexokinase. By using these chemotherapeutics, the formation of glucose-6-phosphate is not possible and a surplus of ATP is available. 2-desoxyglucose, lonidamin and 3-bromopyruvate prevent the formation of pentose phosphate via the pentose phosphate pathway, which also starts with glucose-6-phosphate. Without the subsistence of pentose phosphate, cells are not able to synthesize nucleotides, which are essential for DNA and RNA assembly. As a result the cell is not able to proliferate. The understanding of hypoxia, which drives cancer research, is an important investigation, especially the relevance of HIF-1 as a marker of prognosis [61].

In summery it is possible to say that cancerous cells and mesenchymal stem cells exhibit similar metabolic activities under low oxygen tension (hypoxia).

3.9 A lack of oxygen leads to the formation of ROS

Under hypoxic condition (low oxygen level) there is disequilibrium between the supply of electrons from the oxidation of fuels in the mitochondrial matrix and the transfer of electrons to molecular oxygen. This leads to a decreasing formation of reactive oxygen species (ROS). Every cell has different defensive strategies against ROS and beside the glutathione-peroxidase-system; the regulation of the pyruvate-dehydrogenase (PDH) is available.

This enzyme transfers pyruvate to acetyl-CoA for use in the citric acid cycle. Under hypoxia, the PDH-kinase phosphorylates the mitochondrial PDH.

As a consequence, PDH is inactivated and the preparation of FADH₂ and NADH is retarded from the citric acid cycle for the respiratory chain. Another possibility to inhibit the formation of ROS is an exchange of a subunit of complex IV, which is known as COX4-1 with the COX4-2 subunit. This subunit is more suitable under hypoxic conditions than COX4-1 and the metabolism is assimilated to a lower oxygen level. The change of PDH activity as well as the total amount of COX4-2 of complex IV is arranged by HIF-1. HIF-1 accumulates under hypoxic conditions and acts as a transcription factor. HIF directs glucose towards glycolysis by repressing mitochondrial respiration and optimizes low levels of respiration by regulating the ratio of isoforms of cytochrome c oxidase, which is located in the respiratory chain [79].

This strategy protects cells from oxidative damage under hypoxic condition. Studies have demonstrated that the predominant use of oxidative phosphorylation metabolism in MSC generates higher ROS levels. It is proven that reactive oxygen species are produced by mitochondria. Besides, the mitochondrial genome is specifically susceptible to ROS-mediate damage [80].

3.10 Damaged glucose assimilation by Insulin-dependent diabetes mellitus

The glucose metabolism is limited because of the rate and the phosphorylation of glucose via hexokinase. The glucose assimilation in the bloodstream is possible because of the GLUT-family, which act as glucose transporters. These transporters are located in the liver (GLUT1, GLUT2), or in neural networks (GLUT3). Transporters in adipose tissues (GLUT4) function based on the principle of insulin signal cascade, which regulates the steps of glycolysis.

As a result, the assimilation of glucose and its metabolism in adipose tissue depends on insulin release via β -cells of the pancreas as a response to high glucose concentration in the blood. β -cells do not exist in insulin-dependent diabetes (diabetes mellitus type 1) and therefore an accumulation of glucose results, known as hyperglycaemia. Because of this damaged assimilation, adipocytes use triacylglycerol as a fuel. In the liver, acetyl-CoA is converted into acetoacetate, ketones, and β -hydroxybutyrate, which exports to a variety of tissues (brain). Generally, insulin activates the integration of GLUT4-transporter in the plasma membrane, whereas GLUT4-vesicles merge with the membrane and cause the

assimilation of glucose out of the bloodstream. When the insulin-level is not maintained in the bloodstream, GLUT4 is packed in vesicles via endocytosis. This step is inhibited by Insulin-dependent diabetes and as a result, the absence of insulin marks the assimilation via GLUT4. As a consequence, a lack of glucose in cells results and therefore the glucose concentration in the bloodstream increases. Because of this response, the energy metabolism is not able to proceed and adipocytes start to remove triacylglycerol, converting it to fatty-acids which are used for mitochondrial ATP production. Two chemical by-products (acetoacetate and β -hydroxybutyrate) accumulate in the liver and distribute throughout the bloodstream. These products are fuel for the brain but acetoacetate and β -hydroxybutyrate also decrease the physiological pH in the bloodstream and this phenomenon leads to ketoacidosis, which is a life-threatening condition for MSC. The solution is the injection of insulin because the hormone reverses all steps that lead to ketoacidosis.

To sum up all these issues, it is clear that diabetes mellitus (type 1 and 2) has a fundamental influence in the glucose as well as lipid metabolism in MSC [22].

MSC also show an extracellular pH that is much lower than the corresponding tissue [81].

The acidotic nature is the result of a modification in the metabolism of mesenchymal stem cells and Insulin-depend diabetes, in particular that of glucose. Interestingly it should be mentioned that the same phenomena also occurs on cancerous cells [82].

3.11 Glycolysis at limiting concentration of oxygen (hypoxia)

First of all there are 6 major metabolic pathways which occur during hypoxia in MSC. These pathways are known as Cori cycle, oxidative phosphorylation, glycogenolysis, pentose phosphate pathway and the alanine cycle. The mentioned metabolic routes are unavoidable during MSC metabolism. As a start, the cycle of reactions that involves glucose conversion to lactate in muscle by anaerobic glycolysis (hypoxia) and lactate conversion to glucose in liver is called the Cori cycle. This pathway is generally active when nutrients may be scarce, especially in non-proliferating cells. The pathway functions to recycle the overage of lactate and alanine dumped during proliferating cells. The Cori cycle (located in the liver) is able to recycle lactate generated from proliferating tissues to glucose. Moreover, similar pathways are also known to recycle the alanine generated from glutamine metabolism [22].

The ability to recycle cellular waste results in a minimal impact on energy reserves within the organism. This leads inevitably to emerging evidence that metabolism within tumours can be heterogeneous, with cells utilizing the overproduction of lactate and generated as a fuel for oxidative phosphorylation [83].

Another prominent pathway which occurs during hypoxia is known as glycogenolysis. The breakdown of glycogen releases glucose in form of glucose-1-phosphate.

The G-1-P is converted to G-6-P by the enzyme phosphoglucomutase. G-6-P not only is used in glycolysis, it can also be a part of another metabolic route which is named the pentose phosphate pathway if the concentration of G-6-P is high enough. These processes provide

ATP to the muscle cells as the main energy resource. When the supply of oxygen is effectual, ATP comes from feeding pyruvate, the end product of glycolysis, into the citric acid cycle. When the oxygen supply is not sufficient, energy has to be released through anaerobic metabolism, in which pyruvate is converted to lactate and regenerates NAD^+ , maintaining the NAD^+ concentration which allows the glycolysis reaction to occur. The production of lactate is considerably lower for MSC, which are expanded under hypoxia referring it to the glucose consumption under hypoxia [17].

Last but not least, the alanine cycle is very similar to the first described metabolic pathway, the so called Cori cycle. During times of decreased oxygen, the cells also produce alanine, which is shuttled to the liver where it is used to create glucose. The ATP generation is lower than in the Cori cycle however, NADH is conserved because lactate is not formed. This allows for it to be oxidized via the electron transport chain. This pathway requires the presence of alanine aminotransferase [22].

3.12 Regulatory enzymes act as metabolic valves

In multistep processes like the 10 step catabolic glycolysis, many of the reactions are inevitable at equilibrium in the steady state, in which the rates of these substrate limited reactions fall and rise with the amount of substrate concentration.

Other reactions are too slow to produce instant equilibration of substrate as well as product and are therefore out of equilibrium. This phenomenon is termed as enzyme limited reaction and they are often highly exergonic reactions in which the Gibbs energy is less than zero and as a result irreversible [5].

The enzymes which catalyse these reactions are primarily at the steps by which the flux through the pathway is regulated. Glycogen phosphorylase, hexokinase, phosphofructokinase-1 and pyruvate kinase are the exergonic regulating enzymes in the glycolytic pathway from glycogen to pyruvate (conversion of the glycolysis). To prevent futile cycling of glucose, the enzyme-limited reactions of the glycolysis and gluconeogenesis, which is the opposite of the glycolysis, are under allosteric control.

This means when the reactions of gluconeogenesis are stimulated, the glycolysis reaction is blocked and vice versa. For example fructose 2, 6-biphosphate is an allosteric activator of PFK-1 in glycolysis and an allosteric inhibitor of fructose 1, 6-bisphosphatase in the gluconeogenesis [5].

A lot of regulatory enzymes are located at critical branch points and their activities dictate the allocation of metabolite to several pathways through which each might pass. For instance, glucose-6 phosphate is able to be metabolized either by glycolysis or by the pentose phosphate pathway. PFK-1 and 6-phosphate dehydrogenase are the first enzymes unique to each of these pathways. The main route of glucose is the glycolytic breakdown to pyruvate, and then being oxidized via the citric acid cycle and finally the ATP synthesis in the oxidative phosphorylation to CO_2 . Glucose has other catabolic fates which lead to specialized products

needed by the cell and this route of glucose is manifested in the synthesis of pentose phosphate pathway. This result in the oxidation and decarboxylation at the C1 position of glucose produce NADPH and finally the product, pentose phosphate. The reducing power for biosynthetic reaction provides NADPH and pentose phosphate, which is essential for every cell to synthesize nucleotides and nucleic acids. In mammalian cells and especially in MSC, the role of NADPH is very prominent in adipose tissue, in which fatty acids and steroids are synthesised. The function of NADPH is the reduction of double bonds and carbonyl groups of intermediates [22].

3.13 Adipose tissue

Adipose tissue, which is composed of adipocytes, is amorphous and distributed through the body. It is concentrated around deep blood vessels, under the skin, and in the abdominal cavity. Collagen fibres and many capillaries are around adipocytes in fatty tissue. Almost the entire volume of these metabolically active cells is taken up by fat droplets.

Adipose tissue makes up about approximately 15% of the body mass of a young adult human and about 65% of the adipose tissue is comprised of triacylglycerol. The metabolic activity of adipocytes is very active, responding to hormonal stimuli in a metabolic interplay with the liver, the skeletal muscles, and the heart. Additionally, it has been shown that adipocyte's main metabolic pathway is mainly the active glycolytic metabolism, in which these cells use the citric acid cycle to oxidize pyruvate and fatty acids and they also execute mitochondrial oxidative phosphorylation. Over a period of high carbohydrate input, adipocytes are able to metabolize glucose via pyruvate and acetyl-CoA into fatty acids, from which triacylglycerol are composed of and stored as huge and large fat globules. In humans most fatty acid syntheses are carried out in hepatocytes instead of adipocytes, which have the function to store triacylglycerol arriving from the liver (carried in the blood stream as VLDL) and from the intestinal tract. When the organism needs fuel, triacylglycerol is hydrolysed by lipase within the adipocytes to extricate free fatty acids, which may enter the bloodstream to skeletal muscles and the heart. This release is greatly accelerated by the hormone epinephrine. Insulin suppresses this effect of epinephrine and as a result decreases the activity of triacylglycerol lipase [22].

The metabolism of fatty acids is derived from glucose in which glucose is converted to acetyl-CoA in the mitochondrial matrix then utilized to synthesize citrate in the citric acid cycle. At a high ratio of ATP/ADP and NADH/NAD⁺ this citrate is transferred back into the cytosol where lipids are created by proliferating cells. Acetyl-CoA is trapped from citrate and utilized as the carbon source for building up acyl chains in the cytosol. It is interesting that by the synthesis of acetyl-CoA from citrate the enzyme ATP citrate lyase (ACL) engages a fundamental role because by cleaving ACL tumour growth impairs [84].

Another critical parameter for lipid biosynthesis is the uptake of glutamine in that it supplies carbon in form of oxaloacetate to offer citrate production in the first step of the TCA cycle [44].

Hence, the metabolism of glucose as well as the metabolism of glutamine is fiddle to support the production of acetyl-CoA and NADPH which are required for fatty acid synthesis [21].

3.14 Glutamine or glucose, which nutrient is more efficient in terms of growth, metabolism and growth inhibitors?

Glucose and glutamine are typically used as nutrients in cell culture for the generation of cellular energy (ATP), which is essential for cell growth and maintenance. This raises the question of whether glutamine or glucose is more efficient due to growth, metabolism and growth inhibitors of MSC. In mammalian cells, glucose is seen as the main source for ATP production. This fuel is utilized either by oxidative phosphorylation (yielding about 36 mol ATP/molecule glucose) or by anaerobic glycolysis (yielding 2 mol of ATP and 2 mol lactate per molecule glucose). The lactate production and glucose consumption can be monitored to act as indicators for which metabolic route the cells take to produce ATP from glucose [85-88].

Apart from the use of glucose as a primary energy source, glutamine is also an important energy source for mammalian cell culture and an essential constituent of proteins. This pathway is common in protein biosynthesis, in which glutamine is metabolically de-aminated to glutamate, then converted to α -ketoglutarate by either the transamination pathway (yielding alanine) or the de-amination pathway utilizing glutamate dehydrogenase (GDH) yielding ammonium. Afterwards, α -ketoglutarate is transferred to pyruvate and this route from glutamine as precursor to pyruvate as end product is popular as glutaminolysis. Subsequent pyruvate has three fates. It can be converted to lactate or alanine or it can be broken down completely in the citric cycle. Glutaminolysis can be energy efficient or totally energy inefficient. The energy efficient route, utilizing GDH and the whole oxidation to CO_2 , results in 27 mol of ATP and 2 mol ammonium. The yield of the inefficient catabolism is about 1 mol lactate, 1 mol ammonium and 9 mol ATP by using GDH and 1 mol alanine, 1 mol ammonium and 9 mol ATP by using the transamination pathway [85-88].

If cells use glutamine as a nutrient, monitoring glutamine consumption and ammonium production can indicate whether glutamine is utilized by the cells for either efficient or inefficient ATP production or just for protein biosynthesis [88, 89].

One side effect when cells consume glucose and glutamine is the production of the toxic metabolites like lactate and ammonium. These metabolites are suspected to inhibit cell growth [90].

One toxic side effect of lactate and NH_3 may be the result of pH changes which affect electrochemical gradients necessary for proper function of all membrane transporters [89-91].

A consequence of low pH is the inhibition of cell growth and the proliferating capacity of MSC. The non-ionized NH_3 diffuses through the plasma membrane and inner membrane causing the increase of the pH of acidic intracellular compartments. The key is an optimal nutrient and metabolite concentration of the cell culture medium, which will increase proliferation rate [66].

It should also be mentioned that under hypoxic conditions, the rate of glutamine is higher than compared to cultures, which are expanded under normoxic conditions. Glutamine is known to have the main role in initiation of cell proliferation, acting as a supplier of carbon in the form of mitochondrial oxaloacetate, which is vital to maintain citrate production in the citric acid cycle and nitrogen for amino acid synthesis [21].

Other studies suggested that glutamine is not an important energy source for human MSC [66].

Furthermore, an interesting observation is that the specific production rate of ammonium is significantly lower under hypoxic condition throughout the entire culture. It may pertain to a more efficient internal cell metabolism to equilibrate ammonia accumulation owing to the rapid glutamine consumption. The ammonium molecule releases in the conversion of glutamate to α -ketoglutarate, then transfers to oxaloacetate or pyruvate to form aspartate or alanine, respectively [92].

As a consequence, under hypoxic condition the ammonium concentration never reached inhibitory values, while the higher accumulation of ammonium in MSC under normoxic condition might have contributed to low cell expansion [21].

In contrast to the low cell expansion, because of ammonium, an interesting point is that the conversion of glucose and glutamine to lactate as an end-product includes the popular enzyme lactate dehydrogenase (LDH), which impairs cell proliferation, if the enzyme is inhibited. Not only by interfering with the ability of the cells to excrete immoderate carbon but also by eliminating the excess of carbon might be important to produce sufficient bulks of NADPH with the goal of supporting cell proliferation [93].

To sum up, glutamine and glucose are efficient due to growth, metabolism and growth inhibitors of MSC. An optimal compound ratio of both is a major prerequisite for efficient cell growth.

3.15 Lipolysis

MSC derived adipocytes are focused due to their molecular and cellular mechanisms underlying obesity and its consequences. However, there is a lack of understanding about the adipocyte-specific function of fat cells derived from hMSC. Do they have the same regulatory mechanism for lipolysis as mature fat cells? Do they display endocrine functions like secretion of adipocyte-specific hormones, leptine and adiponectin? Triglycerides (TGs) are hydrolysed during lipolysis by hormone-sensitive lipase (HSL) which releases free fatty acids

and glycerol. Natural catecholamines, adrenaline, and noradrenaline stimulate the hormone sensitive lipase, which binds to any of the three β -adrenoceptors (β 1- β 3-AR).

In general, β 3-AR is the most prominent lipolytic AR, whereas β 2-AR has the superior role in stimulating lipolysis in human adipose tissue [94].

Human fat cells also express the antilipolytic α 2A-AR [95].

β - and α 2A-AR play together and are coupled to intramembranous G-proteins. G-proteins activate or inhibit adenylyl cyclase. The result of this is an increment or decrement of the concentration of cyclic AMP (cAMP) [75].

Cyclic AMP activates protein kinase A (PKA) which phosphorylates several proteins in the lipolytic cascade, which are also activated by PKA, especially HSL. Elevated cAMP concentrations inhibit sustained lipolytic stimulation.

Since A/NA bind to both β -and α 2A-AR, the result on lipolysis is depending on the relative expression of the cell surface receptors of a specific cell.

The functional importance of α 2A-AR effects in human cells is not clear but it has been hypothesized that an increased antilipolytic response to catecholamines may improve fat accumulation in adipocytes [96].

Another human-specific lipolytic pathway is induced by tumour necrosis factor alpha (TNF- α), which stimulates the lipolysis as a cytokine in human fat cells through several mitogen activated protein kinase (MAPK) pathways [97].

The intracellular pathways for TNF- α signalling appear to be identical to those in human pre-adipocytes and the lipolysis is also stimulated by β -AR and cAMP and inhibited by α 2A-AR. Given this understanding, hMSC are a necessary source for cell biology research in the obesity field because these cells are able to differentiate into adipocytes [98].

3.16 Immunosuppressive properties of MSC

MSC are known to be one of the most promising cell types for therapeutic applications and have been isolated from a variety of tissues such as adipose tissue [99].

Furthermore, MSC become an important tool in regenerative medicine for two issues. First and foremost, they are able to expand in culture while maintaining their multipotency [100]. They are also able to differentiate into osteoblasts, chondrocytes and adipocytes [101].

Additionally, MSC are able to secrete a huge number of bioactive molecules that will promote tissue regeneration from damaged tissue progenitors [102].

The expression of these factors opens up a variety of possibilities; the survival and proliferation [103], an induced angiogenesis [104], immune responses and inhibited inflammatory responses, and lastly apoptosis [105].

MSC hold an immune-regulatory capacity and also induce immunosuppressive effects. They are immune privileged cells, referring to the low expression of class II Major Histocompatibility complex (MHC II). MSC also interfere with different pathways of the immune response regarding direct cell-to-cell interactions and soluble factor secretion. Cell

proliferation of T cells, B cells, NKC and DC are all inhibited by MSC. In addition, MSC have the potential to stop a variety of immune cell functions, some of which are DC maturation and activation, B cell maturation, antibody secretion, cytokine secretion and cytotoxicity of T and NK cells, and antigen presentation. It is necessary to activate MSC's immunomodulation skills and therefore some inflammation-related molecules like tumour necrosis factor- α and interferon- γ might be implicated [8].

3.17 The linking pathway between growth control and glucose metabolism

The link between cell growth control and glucose metabolism is based on the principle of the phosphoinositide 3-kinase (P13K) signalling pathway. First of all by the activation of P13K most cells are pended on high levels of a glucose flux [106].

Phosphatidylinositide 3-kinases are involved in cellular functions such as growth, proliferation, and motility, which in turn are involved in cancer. PI3Ks are a family of intracellular signal transducer enzymes and are suitable for phosphorylating the 3 position hydroxyl group of the inositol ring of phosphatidylinositol. The pathway with tumour suppressor PTEN (gene) and oncogene PIK3CA is involved in resistance of cancer tumours to insulin and IGF1[107].

PI3Ks interact with the IRS (Insulin receptor substrate) which poses the idea to regulate glucose uptake through a series of phosphorylation events [108].

P13K regulates cell growth and proliferation and many of these functions relate to the ability of class I of P13K to activate protein kinase B (Akt) as in the PI3K/AKT/mTOR pathway. P13K is also a key component of the insulin signalling pathway, making it of great interest with regard to signalling in Diabetes mellitus [44].

Because of P13K, most cells are dependent on a high level of glucose intermediates, whereas small molecules are able to disrupt P13K, leading to a decrease of glucose uptake by tumours. As a result, the glucose uptake causes cell death [109].

There is also growing evidence that some enzymes are able to collaborate to engage in carcinogenesis. Mutations in the germline of the enzymes in the TCA cycle which are fumarate hydratase and succinate dehydrogenase have been identified in several cancers [110]. Because of such mutations in the P13K pathway, a new activation of the famous HIF-1 α -mediated glucose utilization is induced. In addition, it is proved that modifications in NADPH production affects cellular proliferation and therefore is also an important indicator for cellular growth capacity in the P13K pathway [111].

Moreover the growing evidence that activation of P13K causes increased dependency on glycolysis suggests that these agents may exert some of their effect by disrupting glucose metabolism. As a consequence, a huge number of clinical studies have proven that this signalling metabolism principle in the P13K pathway may offer a possible benefit in cancer prevention and therapies [112].

Better understanding in the P13K pathway will guarantee optimal control in cell proliferation and survival.

3.18 Future prospects

Cell metabolism and its regulation are associated directly or indirectly in essentially every cellular function.

The evidence for cross talk between metabolic control and signalling pathways in every single mammalian cell, especially in hMSC has been elucidated.

In this complex network of several pathways, there is still much to learn about how proliferating cell metabolism and the metabolism of differentiated cells are regulated. The past is filled with a long and rich history of research on this subject and the complex connection between metabolism and proliferation raises many questions and opportunities for exciting investigations in the future.

However, a variety of new metabolic pathways have been discovered as recently as the 1980s [9].

4 Results

Static cultivation

4.1 Stem cell characterization

4.1.1 Long-term AD-MSK cultivation under varying oxygen tensions

To emphasize the importance of high cell numbers for clinical applications, it is necessary to expand the cells over several passages. In this experiment AD-MSKs were isolated and then cultivated over 20 passages under normoxic (21% O₂) and hypoxic (5% O₂) conditions. Expanded AD-MSK under hypoxic and under normoxic conditions were split at identical time points to get a rational comparison of the cell numbers, population doubling levels and metabolic concentrations during these long-term cell cultivations.

Before every cell division (passage 5 to passage 20) AD-MSK, under both conditions, proliferated 3 days in culture. A total cultivation-time of exactly 35 days was achieved in these long-term cell expansions.

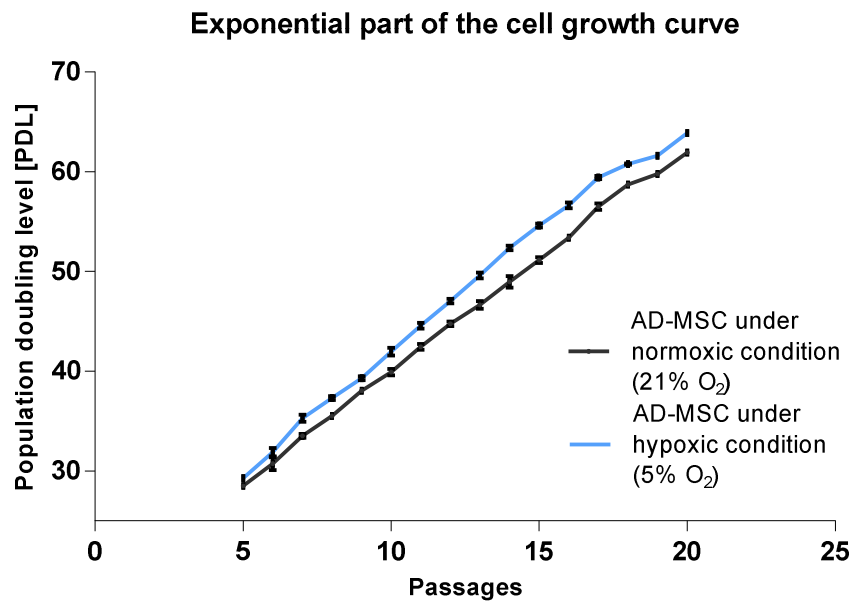


Figure 5: The effect of hypoxia (5% O₂) on AD-MSK long-term culture. One donor's cells were cultivated over 20 passages under 21% O₂ despite of 5% O₂. Exposition of the population doubling level (PDL). Data represent MN ± SD from one donor. The number of replicates was 4 (n=4).

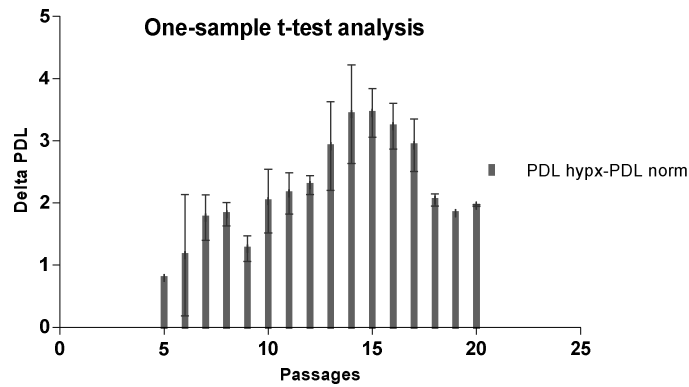


Figure 6: Delta (Δ) PDL (PDL hypoxic-PDL normoxic) for one-sample t-test analysis. P-value (<0.0001) shows that the expansion under hypoxia in comparison to the expansion under normoxia was significantly effective, calculated by one-sample t-test with $\alpha=0.05$ (data are given in table 2).

Figure 5 demonstrates the expansion of long-term cultivation of AD-MSC in up to 20 passages under normoxic and hypoxic conditions.

The curves already start at Passage 5 and ends at Passage 20 (35 days of cultivation). In general the curves look quite parallel but overall, it seems that under hypoxic condition, AD-MSC divided about approximately 37x within 35 days in culture, while under normoxic condition the cells divided 35x in the same time range.

That is just a small difference, thus one-sample t-test analysis followed to verify statistically the difference between these two long-term cell expansions, seen in figure 6 and table 2.

The one-sample t-test assumes that you have sampled your data from a population that follows a Gaussian distribution. While this assumption is not too important with large samples, it is important with small sample sizes, especially when N is less than 20. N=16 in this analysis.

A one-sample t test compares the MN of a single column of numbers against a hypothetical MN that you provide. The P value answers the following question: If the data were sampled from a Gaussian population with a MN equal to the hypothetical value you entered, what is the chance of randomly selecting N=16 data points and finding a MN as far (or further) from the hypothetical value as observed here, seen in table 2.

For this one-sample t-test column statistics were used to identify the differences between cell cultivation under 21% O_2 and 5% O_2 tension. PDL MN values from each passage (normoxia) were subtracted from each passage (hypoxia) for this one-sample t-test analysis.

Table 2: One-sample-t test. Analysis of significantly differences between columns MN (Δ PDL).

One-sample t-test							
Number of values	Actual mean	Discrepancy	95% CI of discrepancy	t, df	P value (two tailed)	Significant alpha=0.05	
16	2.191	-2.191	1.763 to 2.620	t=10.91 df=15	< 0.0001	Yes P<0.05	

If the P value is small, as well as in this analysis, seen in table 2 (usually defined to mean less than 0.05), then it is unlikely that the discrepancy which was observed between sample MN and hypothetical MN is due to a coincidence arising from random sampling. You can reject the idea that the difference is a coincidence and conclude instead that the population has a MN different than the hypothetical value you entered. The difference is statistically significant (p-value <0.0001) and as a result it can be said that hypoxic cultures resulted in a slightly increased population doubling levels in 5% O₂ than in cultures with 21% O₂ concentrations, seen in table 2 and figure 6.

Table 3: PDL during AD-MSC cell expansion under normoxic (21% O₂) and hypoxic (5% O₂) conditions. Data represents MN values (n=4) from passage 5 to passage 20.

Passages	PDL (MN) 21% O ₂	PDL (MN) 5% O ₂
5	28.50	29.30
6	30.72	31.88
7	33.52	35.28
8	35.51	37.32
9	38.05	39.31
10	39.91	41.94
11	42.43	44.59
12	44.76	47.05
13	46.67	49.58
14	48.95	52.38
15	51.17	54.62
16	53.39	56.63
17	56.51	59.43
18	58.73	60.77
19	59.77	61.61
20	61.91	63.87

To sum up, cultivating under 5% oxygen concentrations quantitatively shows a higher population doubling level and, as a consequence, an effective expansion behavior of AD-MSC, seen in table 3 and figure 5. In attention to these results also deliverables were discussed by Nekanti and colleagues [18].

These results showed that AD-MSC can cultivate over longer time periods without loss in proliferation capacity. This is important for the potential use of AD-MSC in clinical applications, where large amounts of cells are required. Furthermore, these data indicated that proliferation was enhanced under hypoxic condition. In future this finding might be useful to be able to generate the required cell numbers in shorter times.

However, it must be mentioned that AD-MSC's *in vitro* proliferation is not unlimited. Prolonged cultivation can either result in generation of tumorigenic cells by spontaneous immortalization [113] or lead to growth arrest due to senescence. In both cases cells are rendered inadequate for clinical application. Senescence is usually accompanied by a clear alteration of the cellular morphology. Stem cells for example obtain elongated, thin spindle-shape morphology. Some senescence tests, for example β -galactosidase staining test would need to be done to confirm such an assumption, but this test was not performed in this approach [114, 115].

The results show that both normoxic (21% O₂) and hypoxic (5% O₂) conditions decelerate the speed of confluence, seen in figure 7. The morphology of cells in passage 20 is different to cells in passage 5. AD-MSC become longer and thinner at higher passage numbers, as seen in Figure 7-C, D.

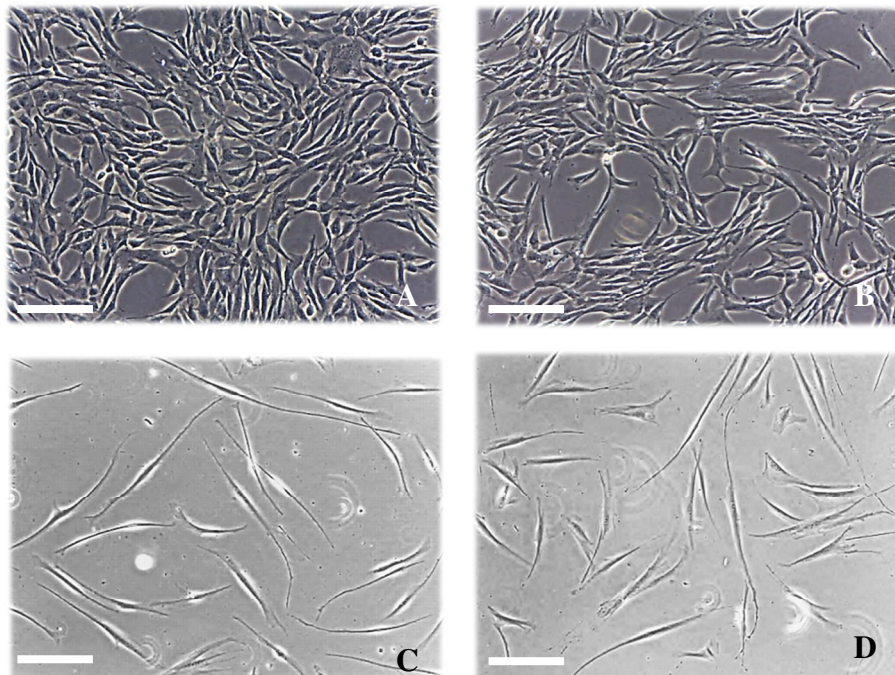


Figure 7: Morphological examination of AD-MSC after long-term cultivation. A–Passage 5 under hypoxic condition (5% O₂); B–Passage 5 under normoxic condition (21% O₂); C–Passage 20 under 5% oxygen concentration; D–Passage 20 under 21% oxygen concentration. Original magnification: 10x.

Figure 7 shows the morphological examination of AD-MSC's long-term cell cultivation. In all 4 cases (figure 7–A, B, C, D) the seeding cell number was exactly 4000 cells/cm². The pictures were taken after 3 days of seeding, to be exact before each splitting.

Last but not least, it should be mentioned that the idea of cultivation under 5% oxygen tension, which imitates physiological conditions, is therefore the solution to achieving higher cell numbers in a shorter time when compared to standard conditions (21% O₂).

4.1.2 Metabolic activity of AD-MSC under varying oxygen tensions

According to previously mentioned results (see section 4.1.1) the metabolic activity of AD-MSC under different oxygen tensions was investigated.

The analysis of glucose and lactate over 20 passages in the static cell culture system demonstrated that the limiting factor in cell growth was glucose. The initial concentration of glucose in α -MEM cell culture medium (+10% HS and 0.5% gentamicin) had a value of 1 g/l glucose. After each passaging step fresh cell culture media was added and always the same seeding cell number was used.

First, a fact is that theoretically, much higher glucose consumption under hypoxic conditions would be expected in comparison to the glucose consumption under normoxia, seen in figure 8-C. The reason for this assumption is well-founded. On the one hand lower oxygen supply (in this case 5% O₂) is more efficient for cell proliferation compared to higher oxygen (21% O₂) supply for the cells and on the other hand, hypoxia provides less energy in terms of ATP to the cells. As described in section 3.3 this metabolic route is also known as anaerobic glycolysis, where just 2 ATP per glucose molecule is generated.

36 ATP per mole glucose is generated under normoxia (oxidative phosphorylation).

As a result 18 times more in comparison to the anaerobic glycolysis and this lack of energy supply was compensated in this case as more glucose consumption. Proliferated AD-MSC under hypoxia are stronger depended of glucose supply (via media) to generate enough energy for cell expansion.

To sum up, cells which were cultivated under low oxygen levels consumed more glucose under hypoxia in comparison to normoxia to produce enough energy for cell proliferation.

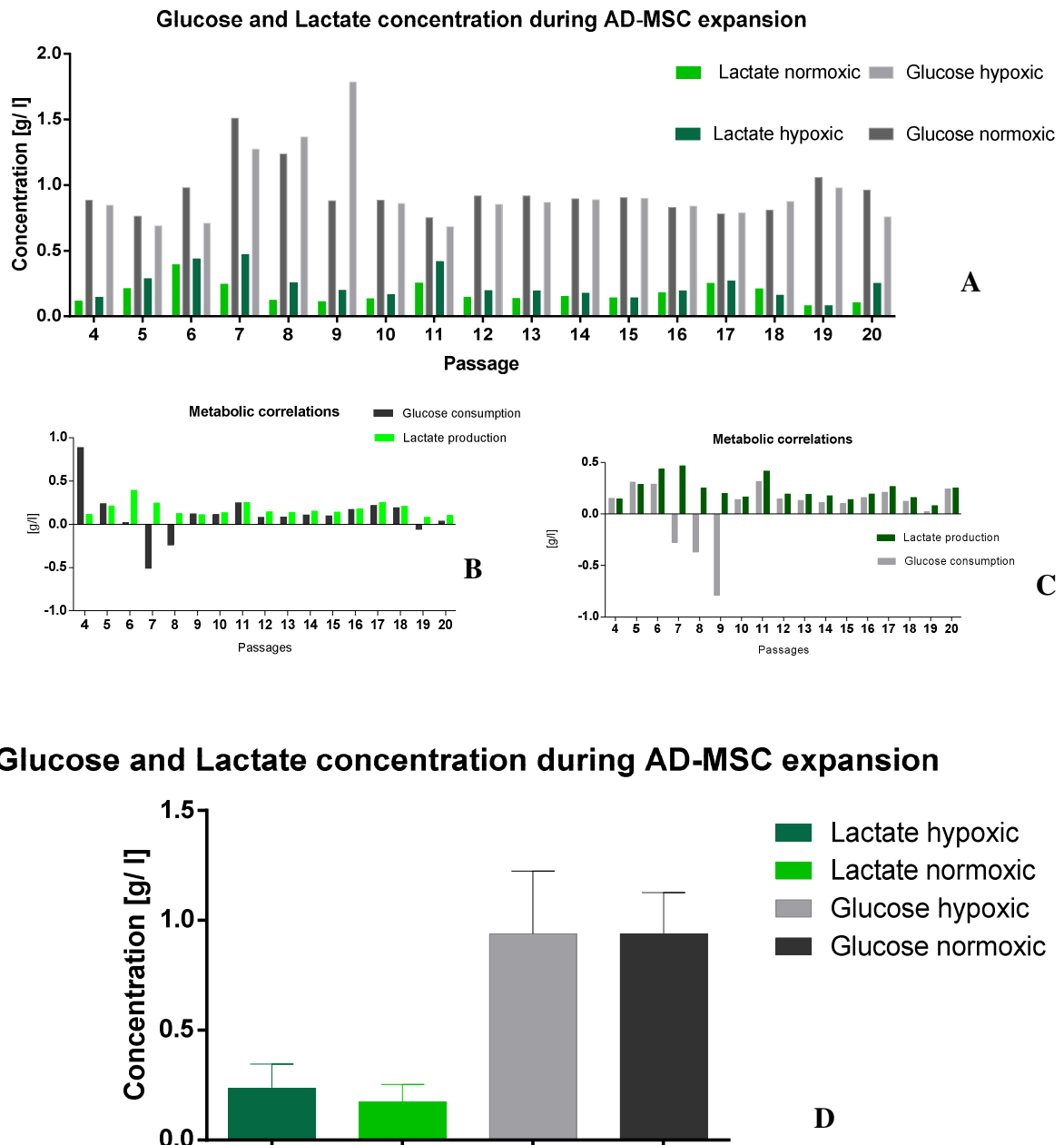


Figure 8: Glucose and lactate profile in conventional cell culture flask over an expansion-time of 35 days (passage 5 to passage 20). A-Overview of metabolic activity under 21% and 5% O₂ tension; both lactate concentration and glucose concentration were measured. P-value >0.0001. B-Data represent the glucose consumption and the lactate production under normoxic condition. C-Data represent the glucose consumption and the lactate production under hypoxic condition. D-Data represent MN \pm SD of the metabolites (concentration in g/l).

Glucose and lactate concentration of AD-MSC were measured before every passaging step. To illustrate the issue being presented, at the end of e.g. passage 5 before split into passage 6. The relation of both metabolites (glucose and lactate) under two oxygen concentrations was determined. The results are shown in Figure 8-B, C. Under normoxic conditions, the glucose concentration does not modify considerable (from 0.886 g/l at passage 5 to 0.962 g/l at

passage 20). These values seem very similar. A random fluctuation of both metabolites is observed under normoxic condition. All in all, this observation implies that enough glucose in the cell culture medium was existed. AD-MSC cultivated under normoxia had enough glucose to consume during cell growth. An optimal glucose concentration was therefore available in the α -MEM cell culture medium (+10% HS and 0.5% gentamicin) for cell expansion. On the other hand a lactate production under normoxia was not observed (the values rise from 0.15 g/l to 0.103 g/l), seen in figure 8. It is true that also the lactate concentration in the cell culture medium does not change significantly during these 35 days in culture under normoxic condition. This phenomenon is based on the principle of the oxidative phosphorylation, as described in section 3.3. Under 21% O₂ tension cells tend to use the oxidative phosphorylation for ATP generation and during this metabolic way the cells do not produce lactate in comparison to the anaerobic glycolysis, where the end-products consist of lactate and 4 ATP/glucose.

Similar results demonstrated the metabolic activity under hypoxic conditions, where the glucose concentration decreases from 0.848 g/l at passage 5 to 0.758 g/l at passage 20 and the lactate concentration increased from 0.145 g/l at passage 5 to 0.252 g/l at passage 20, seen in figure 8-A. Based on the these data the glucose consumption [initial glucose concentration (g/l) – measured glucose concentration (g/l)] and lactate production can be calculated, seen in table 4.

Table 4: Glucose consumption (g/l) and lactate production (g/l) under normoxic (grey) and hypoxic (blue) conditions during the long-term cell expansion. Data were measured from passage 4 to passage 20 in ascending order.

Glucose consumption	Lactate production	Glucose consumption	Lactate production
0,886	0,115	0,152	0,145
<u>0,238</u>	<u>0,210</u>	<u>0,309</u>	<u>0,286</u>
0,021	0,393	0,289	0,436
-0,508	0,244	-0,275	0,469
-0,237	0,122	-0,369	0,255
0,120	0,111	-0,786	0,199
0,114	0,133	0,140	0,164
0,249	0,253	0,317	0,418
0,081	0,144	0,147	0,195
<u>0,082</u>	<u>0,136</u>	<u>0,131</u>	<u>0,192</u>
0,105	0,151	0,112	0,176
0,095	0,140	0,101	0,140
0,171	0,179	0,159	0,194
0,218	0,252	0,211	0,268
0,190	0,209	0,124	0,161
-0,057	0,080	0,021	0,080
<u>0,038</u>	<u>0,103</u>	<u>0,242</u>	<u>0,252</u>

According to table 4, the glucose consumption as well as the lactate production under different (21% and 5%) oxygen tensions is represented. At passage 5 AD-MSC which were cultivated under hypoxia consumed 1.3x more glucose and produced 1.4x more lactate in comparison to the cultivation under normoxia. At passage 13 AD-MSC (hypoxia) consumed 1.8x more glucose and produced also 1.4x more lactate compared to the expansion under 21% O₂ tension and at passage 20 6.3x more glucose and 2.4x more lactate was consumed or produced under hypoxic condition than under normoxic condition. At both conditions (passage 7-9) very low levels of the glucose consumption; considerably less than all other measured values are represented. These values show negative glucose consumption (< zero). There is a high probability that the reason for these negative values is preferable to instrumental errors. All in all, 17 of 20 measurements show values below 1 g/l (initial glucose concentration) which leads to the maintenance that the glucose consumption was similar at each passage with insignificant random fluctuations in both environmental conditions, seen in figure 8-B, C.

According to these results it seems clear that cells, which were cultivated under hypoxia, tend to use other metabolic routes to generate enough ATP for cell expansion (see section 3.3). One would imagine that AD-MSC, which were expanded under low oxygen tension (5% O₂) consumed much more glucose and produced in comparison much more lactate for an optimal cell growth. It is true that AD-MSCs consumed more glucose under hypoxia in comparison to normoxia, but these values are not significantly different (p-value > 0.0001) to the values which were observed under normoxia. If the P value is large, the data do not give you any reason to conclude that the population mean differs from the hypothetical value you entered. This is not the same as saying that the true mean equals the hypothetical value. You just don't have evidence of a difference. All in all, the glucose consumption and the lactate production are a little bit more under hypoxia than under normoxia but not statistically, significant different. These observation leads to the result that both cell culture media had enough metabolites (no cell starving) for cell expansion under both oxygen conditions. Additional, these results are realistic and go well together because after each passage step fresh media was added to each culture to guarantee optimal nutrient supply. This optimal supply was assured that no strong changes in the metabolite concentrations were observed during 35 days in culture.

In summary it should be mentioned that the average relation of consumed glucose to produced lactate from passage 5 to passage 20 shows that under hypoxic conditions (a glucose concentration of 0.94 g/l ± 0.28 g/l and a lactate concentration of 0.24 g/l ± 0.11 g/l) glucose consumption, as well as lactate production, are slightly higher than under normoxic conditions (glucose concentration of 0.93 g/l ± 0.19 g/l and lactate concentration of 0.17 g/l ± 0.08 g/l) as seen in Figure 8-D.

To conclude, it seems that under hypoxic condition (5% O₂) metabolic activity is slightly more efficient than under normoxic condition (21% O₂) and an optimal glucose consumption

as well as lactate production was available during these long-term cell proliferation under both conditions, seen in figure 8-B,C.

4.1.3 Differentiation potential of AD-MSK under varying oxygen tensions

The ability of AD-MSK to be responsive to external differentiation factors is a fundamental capacity of these cells. The reason why MSK lose their differentiation property is that the cells expanded *in vitro* over quite a few passages. This effect is named *in vitro* cell aging. Due to this issue, the solution would be cultivation in a physiological cellular environment. The differentiation capacity of AD-MSK used in this work was tested to prove the cells were indeed MSK. The cells were cultivated under 5% and 21% O₂ concentrations, and differentiation toward osteocytes, adipocytes and chondrocytes with special cell type dependent media was inspected. The cultivation ended after 21 days in culture. During these 21 days of cultivation, a methodical and strictly regulated cycle of media exchange was performed.

For osteogenic differentiation the cells were stained with Von Kossa staining, Calcein staining and Alizarin Red staining. To prove adipogenic differentiation cells were stained with Oil Red O. Cells were stained with Alcian Blue to prove chondrogenic differentiation. All cells were differentiated on fibronectin coated plates (see section 8.8.1)

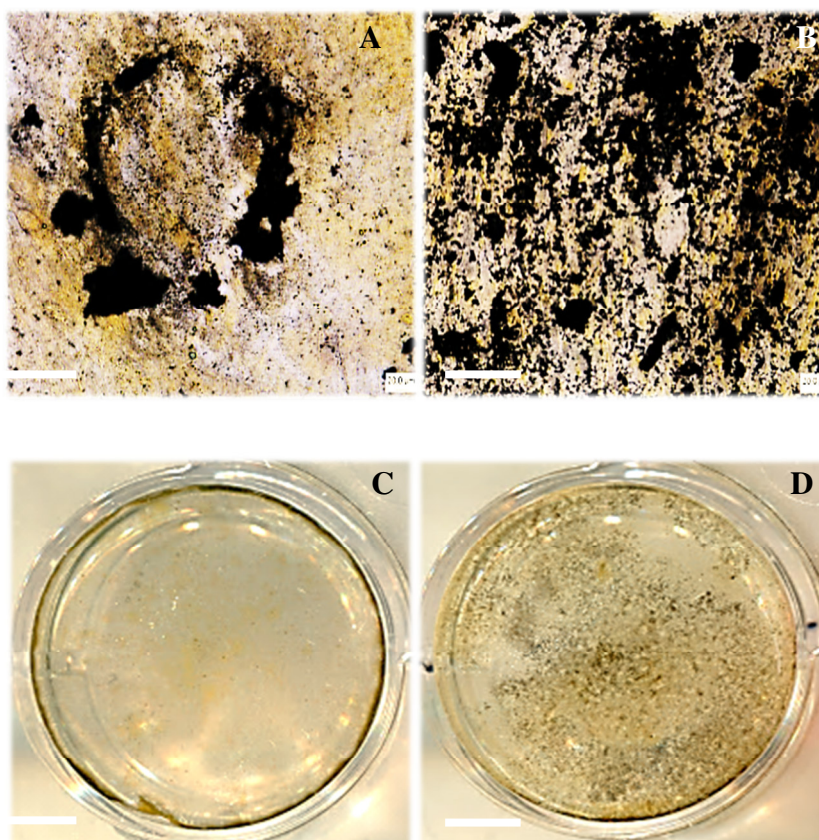


Figure 9: Osteogenic differentiation potential of AD-MSK after cultivation under 5% O₂ (A, C) in comparison to 21% O₂ (B, D). A, B-Von Kossa staining; C, D-wells overview (Von Kossa staining). A-B: Original magnification: 20x.

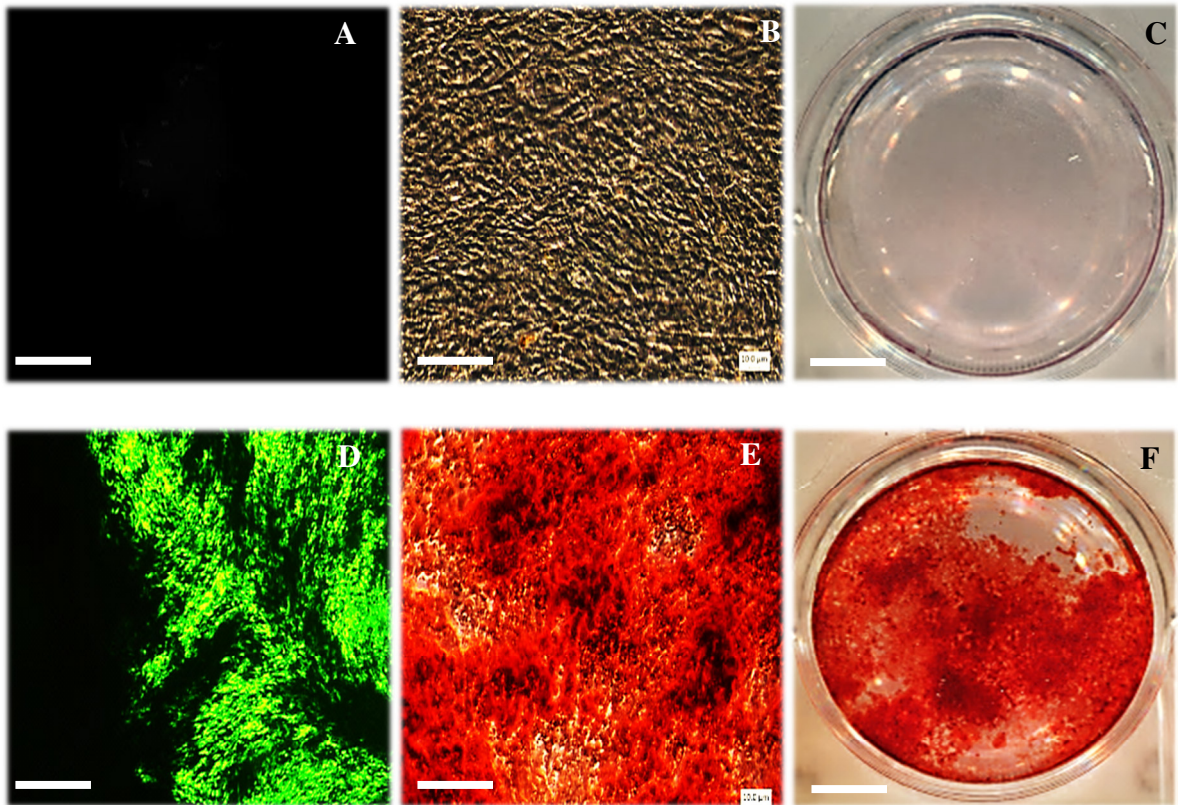


Figure 10: Osteogenic differentiation potential of AD-MSC after cultivation under 5% O₂ (A, B, C) in comparison to 21% O₂ concentration (D, E, and F). A, D-Calcein staining; B, E-Alizarin Red staining; C, F-wells overview (Alizarin Red staining). Original magnification: 10x

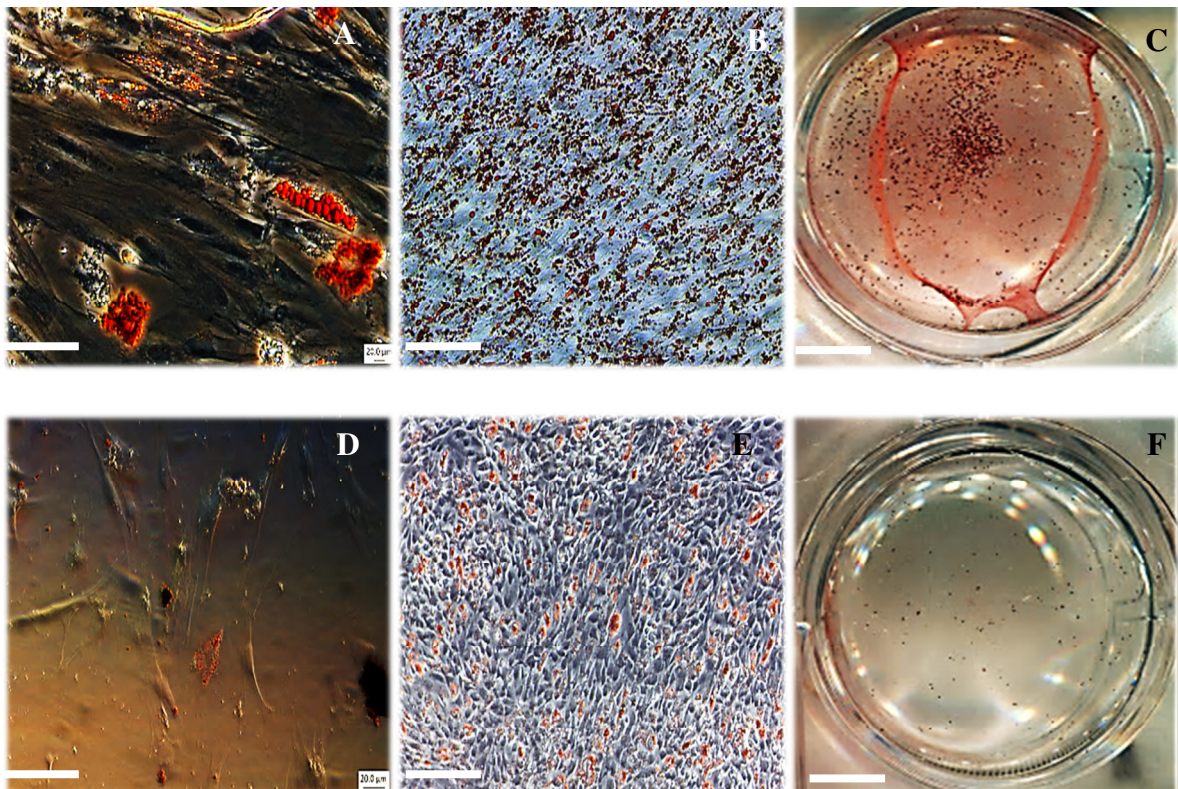


Figure 11: Adipogenic differentiation potential of AD-MSC after cultivation under 5% O₂ (A, B, C) in comparison to 21% O₂ (D, E, and F). A, B, D, F-Oil Red O staining; C, F-wells overview (Oil Red O staining). A-D original magnification: 20x; B-E original magnification: 10x.

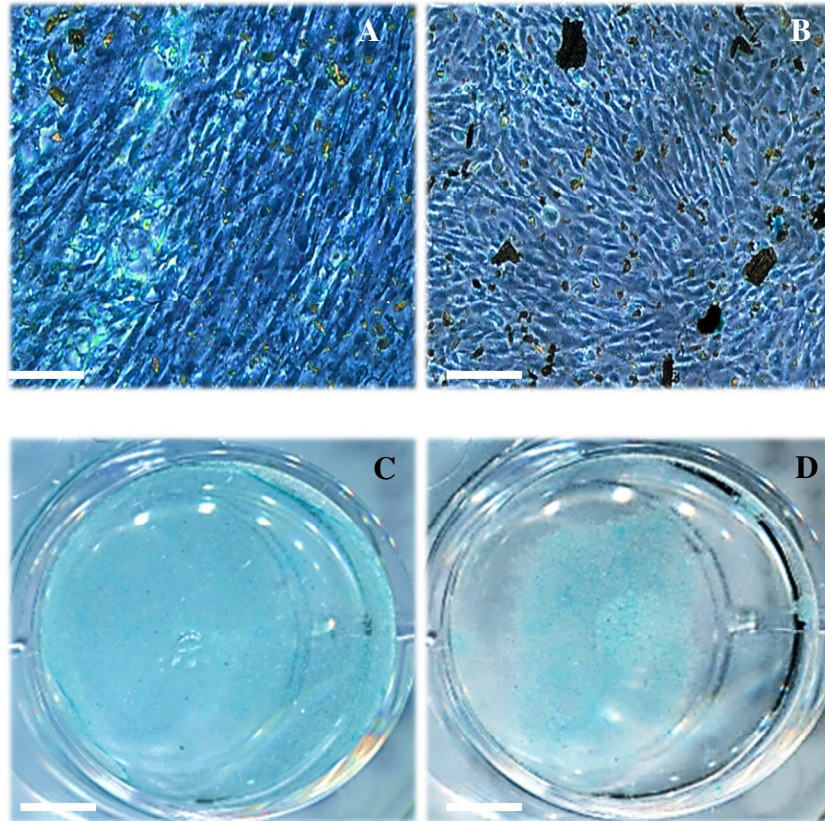


Figure 12: Chondrogenic differentiation potential of AD-MSC after cultivation under 5% O₂ (A, C) in comparison to 21% O₂ (B, D). A, B-Alcian Blue staining; C, D-wells overview (Alcian Blue staining). A-B: Original magnification: 10x.

The result of osteogenic differentiation is shown in figure 9 and figure 10. It can be determined that cultivating AD-MSC under normoxic conditions (21% O₂) had a higher degree of differentiation towards osteoblasts and, strictly speaking, of a higher calcium and phosphate deposition. These mineralisation processes are detectable with The Von Kossa staining, the Calcein staining and the Alizarin Red staining in which different minerals (calcium or phosphate) are visible. The Von Kossa stain based on a precipitation reaction in which silver ions react with phosphate (in this staining not to calcium) in the presence of acidic material. Additional, photochemical degradation of silver phosphate to silver then occurs under light illumination which is seen as grey to black mineralisation, seen in figure 9. Further methods to provide the existence of osteoblasts can be done with Alizarin Red staining. This staining confirms the presence of calcific deposition by cells of an osteogenic lineage, seen in figure 10. Over and above, osteoblasts produce a calcium and phosphate-based mineral that is deposited, in a highly regulated manner, into the organic matrix forming a very strong and dense mineralized tissue which is known as the mineralized matrix. This mineralized tissue can be detected with Calcein staining, in which the green fluorescence spots are the so called mineralized matrix, seen in figure 10.

In comparison to the osteogenic lineage, adipogenic differentiation exhibited more lipid droplets (seen as red vacuoles) under 5% O₂ compared to 21% O₂ which are visible with the Oil Red O staining. The differentiation potential towards adipocytes is higher under hypoxic conditions (5% O₂), seen in Figure 11. Staining for chondrogenic differentiation using Alcian blue yielded only faint blue staining. Therefore the success of chondrogenic differentiation could not be proven with certainty. However, Alcian blue staining was similar under normoxic conditions to results under hypoxic conditions, demonstrated in Figure 12.

4.1.4 Metabolic activity of AD-MSK during differentiation under varying oxygen tensions.

In addition to previously mentioned staining procedures (see section 4.1.3), biochemical functions were analyzed based on glucose and lactate measurement during differentiation. Fibronectin coated plates (see section 8.8.1) were also used for the metabolic analysis.

In addition, the differentiation under 5% O₂ and 21% O₂ tensions on fibronectin coated cell culture ware was also tested to investigate the metabolism during differentiation. During this long-term cell differentiation, on day 3, 7, 14, and 21, glucose and lactate measurements were performed, (see figures 13-18). All analyses were tested with the specific differentiation media (Miltenyi) to a reference media (α -MEM +10% HS +0.5% GM). Especially for glucose plotting the values [g/l] in the supernatant (explicit from the CuBIAN[®]XC photometric measurement analyzer) does not make a lot of sense, since the media already have different glucose concentrations to begin with. As a consequence, the glucose consumption vs. time was plotted, seen in figure 13-18. As mentioned in section 8.7.2 the glucose consumption is calculated according to the following formula [initial glucose (g/l) – measured glucose (g/l)], see formula 7. All indications of the initial glucose and lactate concentrations in the fresh media are seen in table 5.

Table 5: Glucose and Lactate concentrations (g/l) in the initial fresh media. Different media (see section 7.4) were used for stem cell differentiation.

α -MEM (+10% HS, +0.5% gentamicin)		StemMACS ChondroMedia, Miltenyi		StemMACS AdipoMedia, Miltenyi		StemMACS OsteoMedia, Miltenyi	
Glucose [g/l]	Lactate [g/l]	Glucose [g/l]	Lactate [g/l]	Glucose [g/l]	Lactate [g/l]	Glucose [g/l]	Lactate [g/l]
1	-	3.52	-	4.4	-	4.83	-

Glucose consumption during adipogenic differentiation

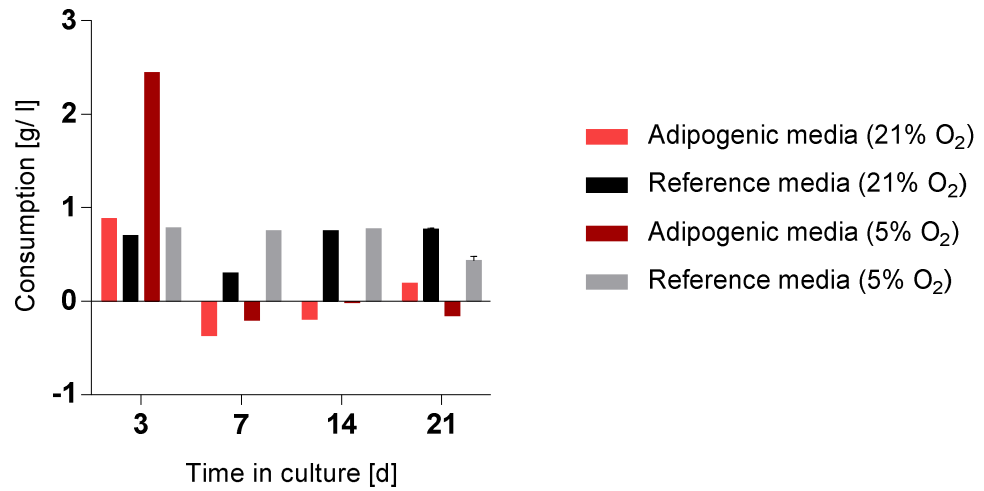


Figure 13: Metabolic profile during differentiation under 21% oxygen and 5% oxygen concentrations. Glucose consumption during adipogenic differentiation. Data represent MN \pm SD.

Glucose consumption during chondrogenic differentiation

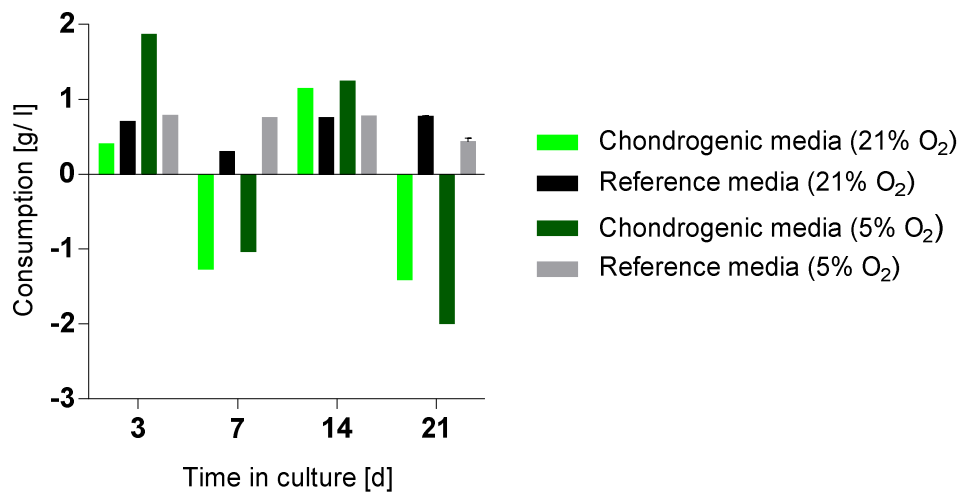


Figure 14: Metabolic profile during differentiation under 21% oxygen and 5% oxygen concentrations. Glucose consumption during chondrogenic differentiation. Data represent MN \pm SD.

Glucose consumption during osteogenic differentiation

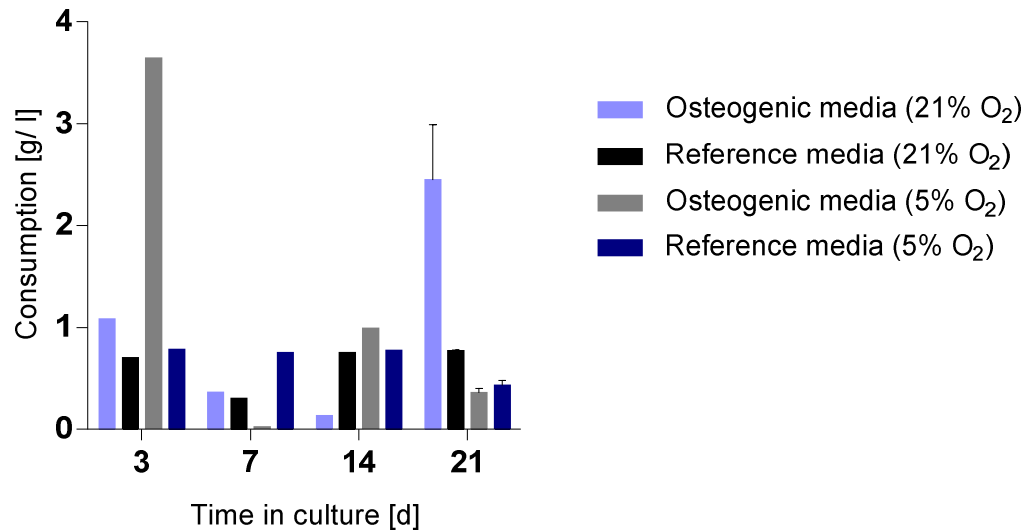


Figure 15: Metabolic profile during differentiation under 21% oxygen and 5% oxygen concentrations. Glucose consumption during osteogenic differentiation. Data represent MN \pm SD.

Lactate production during adipogenic differentiation

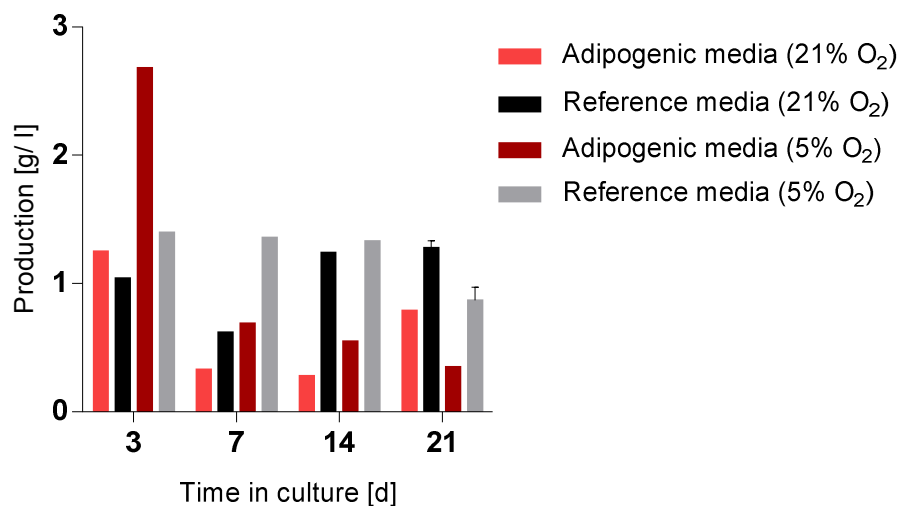


Figure 16: Metabolic profile during differentiation under 21% oxygen and 5% oxygen concentrations. Lactate production during adipogenic differentiation. Data represent MN \pm SD.

Lactate production during chondrogenic differentiation

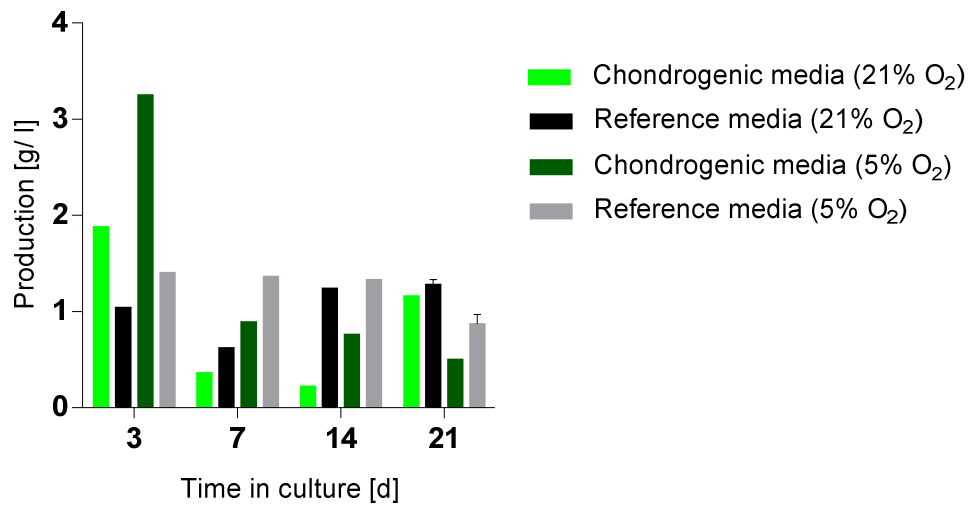


Figure 17: Metabolic profile during differentiation under 21% oxygen and 5% oxygen concentrations. Lactate production during chondrogenic differentiation. Data represent MN \pm SD.

Lactate production during osteogenic differentiation

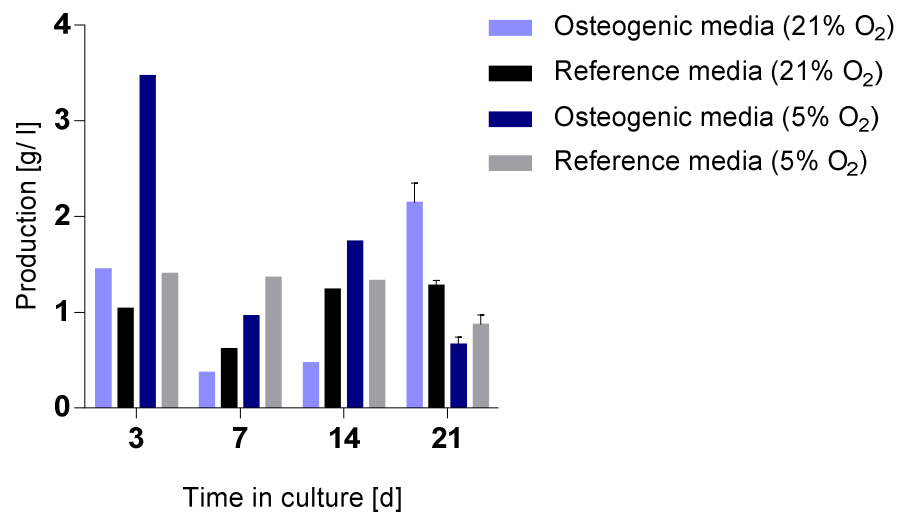


Figure 18: Metabolic profile during differentiation under 21% oxygen and 5% oxygen concentrations. Lactate production during osteogenic differentiation. Data represent MN \pm SD.

In figure 13-18 metabolic profiles of glucose consumption as well as lactate production during adipogenic, chondrogenic and osteogenic differentiation are described.

Considering the overall fluctuations of the measured values a conclusive identification of the metabolic trend of differentiated AD-MSC is not clear. However, to discuss the matter in detail, the glucose consumption during adipogenic differentiation under hypoxia was in general higher than under normoxia. After 3 days in culture AD-MSC consumed 2.8 times more glucose, after 7 and 14 days both (hypoxia and normoxia) measured values were negative (-0.01 g/l and -0.19 g/l), which indicates that AD-MSC consumed more glucose as existing in the initial fresh media. After 21 days AD-MSC which were differentiated under hypoxia consumed also more glucose as available (-0.19 g/l of consumed glucose concentration) whereas a glucose consumption of 0.19 g/l was measured under normoxia. All in all, AD-MSC which were differentiated under normoxic condition over 21 days consumed less glucose as compared to the differentiation under hypoxic condition, seen in figure 13. The lactate production during adipogenic differentiation showed that after 3 (2.1x lactate production), after 7 days (2.1x for lactate production) and after 14 days (1.9x lactate production) differentiation under hypoxia produced more lactate in comparison to the differentiation under normoxia. All measured values except the lactate production after 21 days of differentiation showed the same trend. After 21 days 0.4 times more lactate was produced under normoxia compared to hypoxia. Similar values resulted for the glucose consumption and lactate production during chondrogenic differentiation. Hence, the glucose consumption during hypoxic differentiation after 3 days was higher compared to the differentiation under normoxic condition (4.7 times more). After 7 days of differentiation both measured glucose concentrations (hypoxia and normoxia) were negative (-1.03 g/l and -1.26 g/l) and after 14 days the glucose consumption was 1.1 times more during differentiation under 5% O₂ compared to 21% O₂. The last measurement point (after 21 days) resulted also in both negative values (-1.9 g/l and -1.4 g/l). The glucose consumption during chondrogenic differentiation resulted during adipogenic differentiation also in more glucose consumption under hypoxic condition. The lactate production during chondrogenic differentiation showed the following values: After 3 days (hypoxic culture produce 1.7 times more lactate than normoxic culture), after 7 days (hypoxic culture produce 2.5 times more lactate than normoxic culture), after 14 days (hypoxic culture produce 3.5 times more lactate than normoxic culture) and last but not least after 21 days (normoxic culture produce 2.3 times more lactate than hypoxic culture). To sum up, chondrogenic differentiation resulted in increased glucose consumption under hypoxic condition and in an increased lactate production (except after 21 days of differentiation, seen in figure 14 and 17). The glucose consumption and lactate production during osteogenic differentiation showed strong

fluctuations in the metabolic profile. This means that on the one hand the glucose consumption after 3 days (hypoxic culture consumed 3.4 times more glucose) and after 14 days (hypoxic culture consumed 7.6 times more glucose) and on the other hand after 7 days (normoxic culture consumed 18 times more glucose) and after 21 days (normoxic culture consumed 6.9 times more glucose). All in all, a clear statement to the glucose consumption during osteogenic differentiation is not possible. The lactate production during osteogenic differentiation showed that after 3 days (hypoxic culture produce 2.4 times more lactate), after 7 days (hypoxic culture produce 2.6 times more lactate), after 14 days (hypoxic culture produce 3.7 times more lactate) and after 21 days in culture (normoxic culture produce 6.9 times more lactate). To sum up, it can be said that the metabolic behaviour of both cultures during osteogenic differentiation did not result in a clear trend. It might be possible that the differentiation of AD-MSCs under hypoxic conditions may result in inhibited osteogenesis, while adipogenesis was improved and chondrogenesis was unaffected [116], as seen in figure 13 to 18.

Respectively to the previously mentioned results, several studies have investigated changes in MSC energy metabolism during differentiation toward the chondrogenic as well as the osteogenic lineages [23, 24], see also section 3.3.

However, in this metabolic analysis at selected time points (3, 7, 14, 21 days) the medium was aspirated from each well for glucose and lactate analysis. According to these figures, the results might indicate that AD-MSCs have a mixed metabolism, utilizing both, oxidative phosphorylation for ATP generation and glycolysis for energy production, see section 3.3. During adipogenic and chondrogenic differentiation after 21 days in culture, AD-MSCs tend to consume more glucose under hypoxic conditions compared to the glucose consumption under normoxic conditions. At each step of the glucose consumption measurement the lactate production might indicate exactly the opposite of what was measured of the glucose consumption. This means that high glucose consumption values resulted in less lactate production values and the way around. This might indicate that AD-MSCs under hypoxic condition during differentiation toward chondrogenic and adipogenic lineages have a tendency to consume more glucose and produce less lactate. Last but not least it should be mentioned that the production of lactate under normoxia is termed as the Warburg effect [33] and that MSCs increase their rate of glycolysis upon differentiation under hypoxia, which is termed the Pasteur effect [34-36], see also section 3.3.

Above all, this metabolic capacity provides further support for a theoretical link between MSC's differentiated progeny and their differentiation state, which could provide novel avenues to control differentiation.

4.2 Alternative expansion strategies

4.2.1 Short-term cell expansion with alternative surfaces

Thermo Scientific Nunc™ UpCell surfaces are composed of a temperature-responsive polymer, which is covalently immobilized to the polystyrene surface of the cell culture area and becomes hydrophobic above 32 °C. At 32 °C AD-MSCs are allowed to adhere to these surfaces. Incubating the cells above 32 °C (preferably at 37 °C) is recommended and more effective. Reducing the temperature below 32 °C causes cell detachment, seen in figure 19.

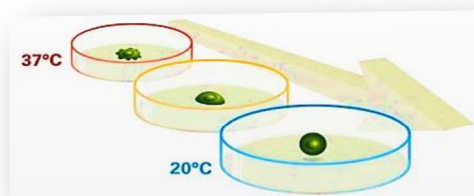


Figure 19: Detachment of AD-MSCs. The covalently immobilized polymer poly (N-isopropyl acrylamide), or PIPAAm layer is hydrophobic at 37 °C, allowing cells to attach and grow. When the temperature is reduced to below 32 °C, the PIPAAm layer becomes hydrophilic, binds water and swells, resulting in the release of adherent cells (taken from (5)).

This technique is based on physical and chemical principles and offers a major advantage in comparison to conventional cell detachment techniques. Cells are gently detached by reducing the temperature rather than using digestive enzymes (in this case Accutase) which can be harmful to the cells. MSCs need extensive *ex vivo* proliferation within prolonged durations of *in vitro* culture [117, 118].

To avoid pathogenic transmission, it is imperative to minimize animal and human-derived products, like digestive enzymes and serum within MSC culture. When using digestive enzymes, it is necessary to add serum to the cell culture because cells become heavily damaged after too long incubation of digestive enzymes. The digestive reaction stops by adding cell culture media with serum, which includes protease inhibitors that inactivate the digestive enzyme. It has been shown that serum-free medium allows better expansion than classical α -MEM media [119].

Enzyme-free cell dissociation is instead sometimes preferred to preserve the structural integrity of membrane surface proteins [120].

The objective of this project was to study the different effects of enzyme dependent detachment processes (used enzyme was Accutase) in contrast to temperature dependent detachment processes with UpCell™ surfaces (Nunc™) on the short-term cultivation of AD-MSC to prove the proliferation capacity. AD-MSC, which generally detach from conventional culture ware (tissue culture plastic surface, TCPS) by enzymatic methods, may benefit from alternative culture ware, known as culture ware with UpCell™ surface. As previously mentioned, this technology is based on temperature reducing processes and, as a consequence, cell detachment is improved and guaranteed. This investigation compared the absolute yield of AD-MSC harvested from different UpCell™ surface formats using temperature reduction with those harvested from traditional culture ware (T-25 flask and 6 well plate) using Accutase as digestive enzyme under normoxic (21% O₂) and hypoxic (5% O₂) conditions. The cell proliferation capacity and the cell morphology were inspected in both types of cell culture ware. In the first attempt, all cultivations were performed under normoxic condition (21% O₂) and in the second one under normoxic (21% O₂) and hypoxic (5% O₂) conditions.

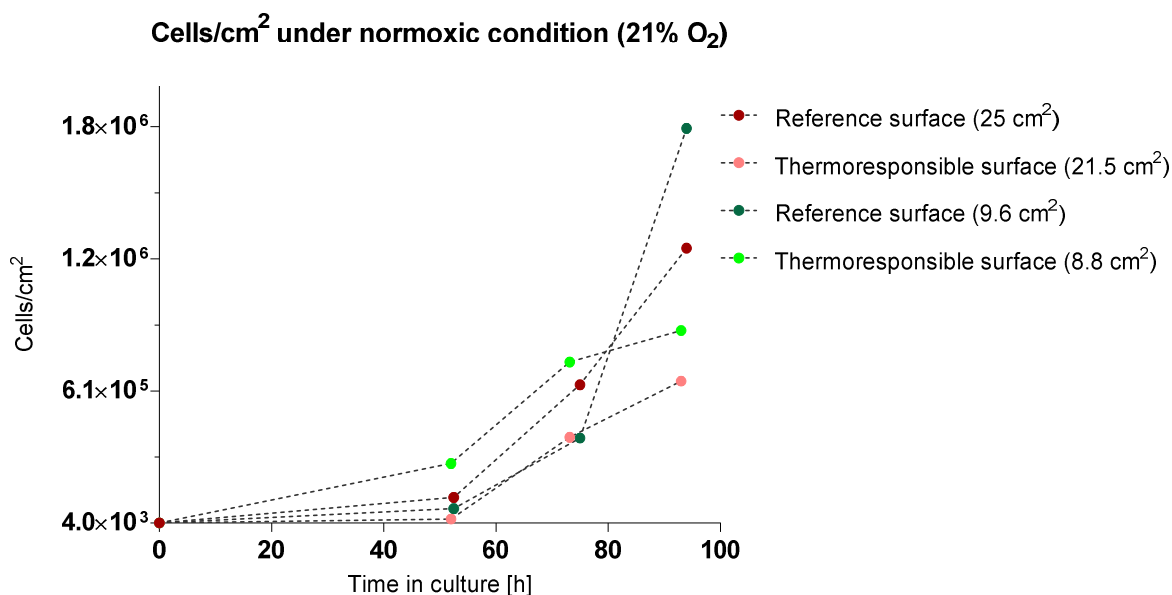


Figure 20: Cell proliferation capacity (cells/cm²) of AD-MSC under normoxic condition (21% O₂), by using different cell culture wares. (n=1.)

The first reference with a surface area of 9.6 cm² was chosen to enable a comparison to the thermoresponsible surface with 8.8 cm² (3.5 cm dish). The second reference with a surface area of 25 cm² was chosen to provide a comparison to the thermoresponsible surface with 21.5 cm² (6.0 cm dish). Still the TCPS surface areas are about 10% or more different it is better to compare the cell proliferation capacity in cells/cm² instead of the absolute cell number. The reason behind the comparison of these references to the tested surfaces is just to get a comparative value of the proliferation capacity on nearly similar surfaces. There exists a

difference if the seeded cells (4000 cells/cm²) are cultivated on surfaces with inferior surface than taller ones because cultivated cells had less more (depend on the size of the TCPS) cell-to-cell contact.

As seen in Figure 20, the thermoresponsible surface (8.8 cm² dish) shows obviously higher cell numbers after 52.5 (3.9 times more cells) and 73.15 (1.9 times more cells) hours of incubation time, but not after 93 hours (reference surface resulted in 2.0 times more cultivated cells) compared to the reference TCPS (9.6 cm²).

The highest proliferation capacity at the end of the cultivation is demonstrated by expanding AD-MSC on a 9.6 cm² cell culture surface (TCPS) with 1.8×10^6 cells/cm², seen in figure 20 and table 6.

The comparison of the thermoresponsible surface (21.5 cm²) to the reference surface (25 cm²) demonstrated that the total cell number of the reference at each time point was higher than that of the thermoresponsible surface, as seen in Figure 20 and Table 6.

Table 6: Cells/cm² after AD-MSC expansion on TCPS and thermoresponsible surfaces: The reference surface (9.6 cm²) in comparison to the thermoresponsible surface (8.8 cm²), the reference surface (25 cm²) in comparison to the thermoresponsible surface (21.5 cm²).

	Cells/cm ²			
	Time point			
	T ₀	T ₁	T ₂	T ₃
Reference surface (9.6 cm ²)	4.0×10^3	7.0×10^4	3.92×10^5	1.81×10^6
Nunc UpCell™ surface (8.8 cm ²)	4.0×10^3	2.76×10^5	7.4×10^5	8.84×10^5
Reference surface (25 cm ²)	4.0×10^3	1.21×10^5	6.36×10^5	1.26×10^6
Nunc UpCell™ surface (21.5 cm ²)	4.0×10^3	2.2×10^4	3.96×10^5	6.52×10^6

4.2.2 Morphological examination

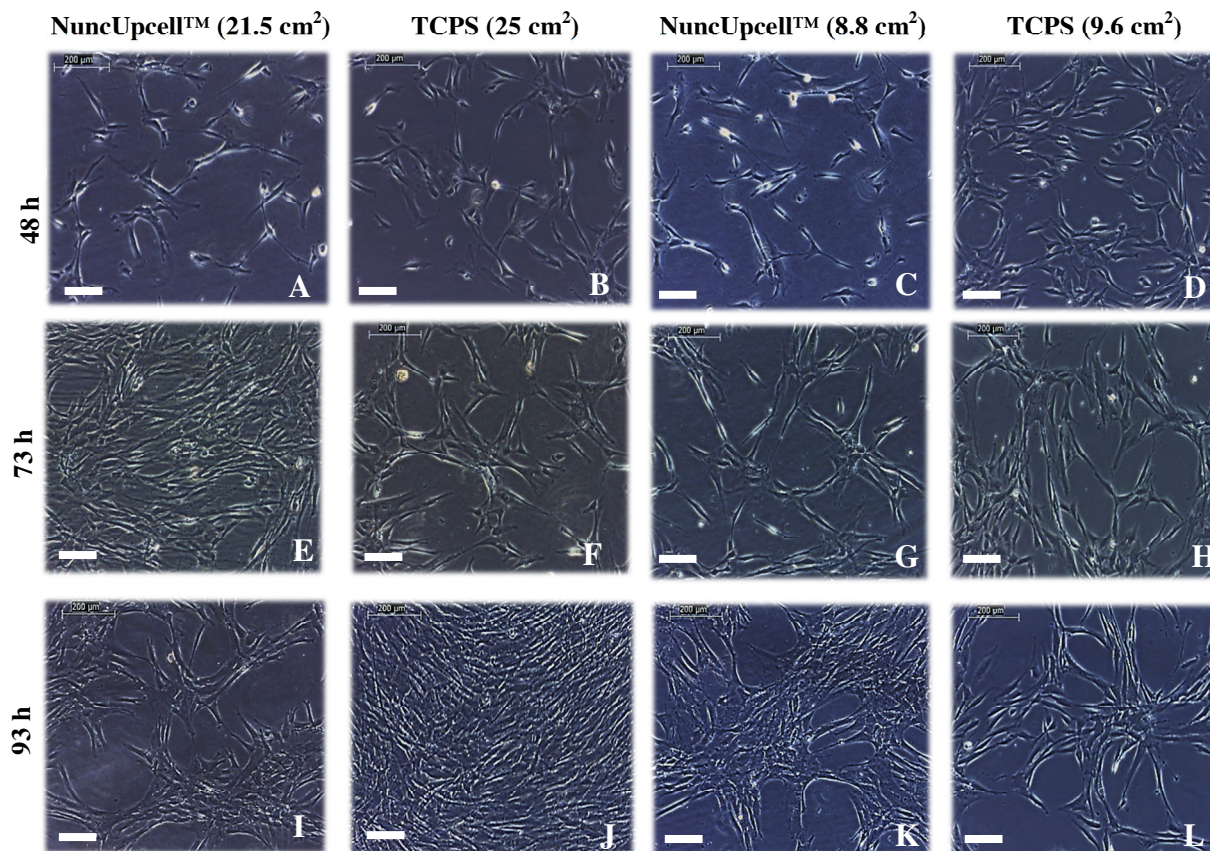


Figure 21: Morphological examination of AD-MSCs after expansion on different surfaces. First row (after 48 hours in culture). Second row (after 73 hours in culture). Third row (after 93 hours in culture). Original magnification: 10x.

A – Thermoresponsible surface (21.5 cm²) after 48 hours cultivation.

B – TCPS (25 cm²) after 48 hours cultivation.

C – Thermoresponsible surface (8.8 cm²) after 48 hours cultivation.

D – TCPS (9.6 cm²) after 48 hours cultivation.

E – Thermoresponsible surface (21.5 cm²) after 73 hours cultivation.

F – TCPS (25 cm²) after 73 hours cultivation.

G – Thermoresponsible surface (8.8 cm²) after 73 hours cultivation.

H – TCPS (9.6 cm²) after 73 hours cultivation.

I – Thermoresponsible surface (21.5 cm²) after 93 hours cultivation.

J – TCPS (25 cm²) after 93 hours cultivation.

K – Thermoresponsible surface (8.8 cm²) after 93 hours.

L – TCPS (9.6 cm²) after 93 hours cultivation.

AD-MSC after 48 hours in culture showed approximately the same behavior on the different surfaces, seen in figure 21. This means that the degree of confluence was roughly the same in all four cell culture wares. Nearly the same trend was cognizable after 73 hours of cultivation, with one exception. The degree of confluence was obviously higher on the thermoresponsible surface (21.5 cm²) compared to the other three surfaces. All in all, it is a contented result that AD-MSC were able to expand on thermoresponsible cell culture as good as on standard TCPS. In all cases the morphology of AD-MSC as well as the grow behavior was similar. Even at the last time point, AD-MSC survived for at least 93 hours on thermoresponsible cell culture ware, which positively accompany with the proliferation capacity of AD-MSC on alternative cell culture ware.

This qualitative analysis (figure 21) shows that AD-MSC`s morphology was, on traditional surfaces, as good as thermoresponsible surfaces. MSC are characterized morphologically by a small cell body with a few cell processes that are long and thin which is visible in all cases (figure 21). AD-MSCs, which are long and thin, are widely dispersed. To amplify, these cell bodies contain a large, round nucleus, which is surrounded by finely dispersed chromatin particles, giving the nucleus a clear appearance [121].

Furthermore, it should be recognized that the observed confluence of AD-MSC correlates with the counted cell number, seen in section 4.2.1. According to these results it may come to the realization that these tested thermoresponsible surfaces will be as good as classically TCPS in action, especially in the field of regenerative medicine or clinical applications which are involved with MSC.

4.2.3 The expansion of AD-MSC on Thermo Scientific Nunc™ UpCell surface under varying oxygen tensions

The previously mentioned experiment (section 4.2.1 and 4.2.2) demonstrated that thermoresponsive surfaces were appropriate for the expansion of AD-MSC and therefore an additional expansion for approximately 63 hours was performed to investigate the proliferation capacity under varying oxygen tensions (hypoxic condition (5% O₂) compared to normoxic (21% O₂) condition). The idea was to examine the expansion behavior of AD-MSC on a thermoresponsive surface in addition to low oxygen concentrations, seen in figure 22.

Expansion behaviour under varying oxygen tensions

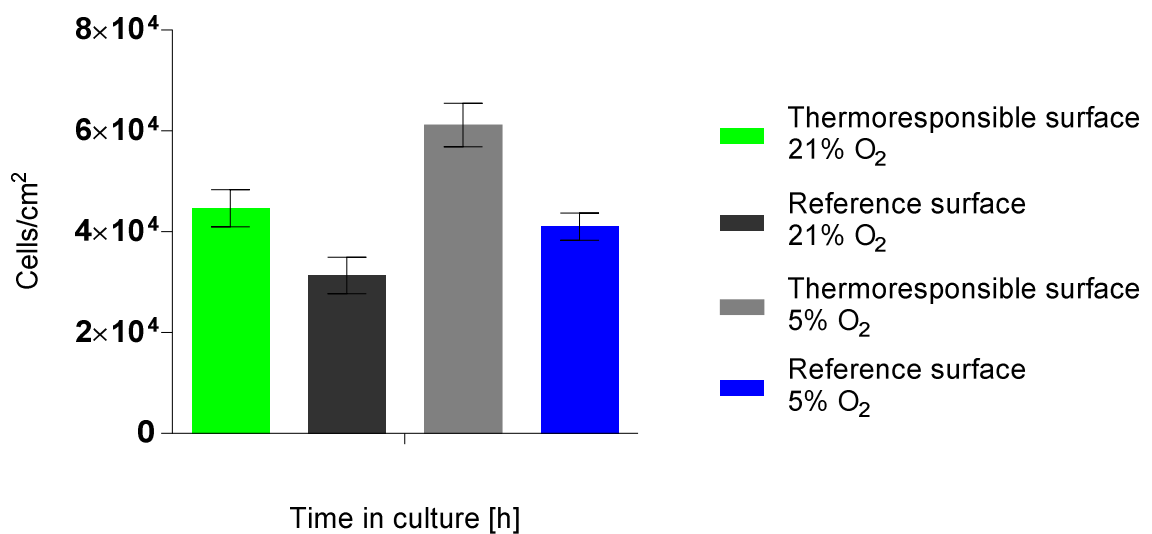


Figure 22: The effect of hypoxia (5% O₂) on AD-MSC short-term cultivation on different cell culture ware surfaces. The cells were harvested from two different cell culture ware under two conditions (5% O₂ and 21% O₂). Cells/cm² after incubating for 63 hours. Data represent MN ± SD. (n=6)

Figure 22 demonstrates the result of the cultivation of AD-MSC on conventional TCPS (6 well plate, Sarstedt) and thermoresponsive (Nunc™ Multidishes 6-well with UpCell™ surfaces) cell culture ware under normoxic (21% O₂) and hypoxic (5% O₂) conditions. Both cell culture wares demonstrated an indent surface area of exactly 9.6 cm². AD-MSC, which were cultivated on thermoresponsive cell culture ware, illustrated a slightly higher cell number (cells/cm²) of $6.12 \times 10^4 \text{ cells/cm}^2 \pm 4.37 \times 10^3 \text{ cells/cm}^2$ than on standard surface ware with $4.10 \times 10^4 \text{ cells/cm}^2 \pm 2.68 \times 10^3 \text{ cells/cm}^2$. Both were incubated under hypoxic (5% O₂) condition. According to this graph, the cell harvest on a thermoresponsive with $4.47 \times 10^4 \text{ cells/cm}^2 \pm 3.72 \times 10^3 \text{ cells/cm}^2$, in contrast to the conventional surface with $3.13 \times 10^4 \text{ cells/cm}^2 \pm 3.63 \times 10^3 \text{ cells/cm}^2$, also represented a slightly higher cell count per square centimetre. Both are incubated under normoxic conditions (21% O₂).

Table 7: Overview of the counted cell number (cells/cm²) of AD-MSC on different surfaces under normoxic (21% O₂) and hypoxic (5% O₂) conditions.

Surfaces (9.6 cm ²)	Time in culture [h]	Cells/cm ²	
		MN	SD
Thermoresponsible surface normoxic	63	4.47 x 10 ⁴ cells	3.72 x 10 ³ cells
Reference surface normoxic	63	3.13 x 10 ⁴ cells	3.63 x 10 ³ cells
Thermoresponsible surface hypoxic	63	6.12 x 10 ⁴ cells	4.37 x 10 ³ cells
Reference surface hypoxic	63	4.10 x 10 ⁴ cells	2.68 x 10 ³ cells

To sum up, the proliferation capacity showed slightly higher results by using alternative surfaces than conventional surfaces and the effect of hypoxia (5% O₂) on AD-MSC culture improved supplementary, seen in figure 22 and table 7.

4.3 Influence of different digestive enzymes for passaging on AD-MSC

Digestive enzymes are enzymes that break down polymeric macromolecules into smaller building blocks, in order to facilitate a detachment of them from TCPS. Trypsin as an example cleaves peptide chains mainly at the carboxyl side of the acids lysine or arginine [122].

It is used for numerous biotechnological processes, which are commonly referred to as trypsin proteolysis and proteins that have been treated with trypsin are said to have been trypsinized [123].

This study was done to determine the effectiveness of diverse digestive enzymes on potential differences in cell phenotype and growth because cell passaging relies on a variety of enzymatic processes to assess whether different digestive enzymes limits the rate of proliferation of AD-MSC or influence surface antigens on AD-MSC, which may change the cell's phenotype. As such, the influence of digestive enzymes on AD-MSC for cell detachment capability, optimal incubation time of the digestive enzymes, and the influence on cell growth and surface markers need to be determined.

4.3.1 Comparison of different enzymatic means of dissociation adherent monolayers of AD-MSC

This study compared the detachment capacity of adherent AD-MSC monolayers with four of the most commonly used enzymes for dissociation: Accutase (PAA), TrypLE™ Express (Gibco Invitrogen), Trypsin S (Sigma) and Trypsin P (Polymun). Cells were incubated by these enzymes for 5 min, followed by 15 min and 45 min incubation time for each specific enzyme. The cell viability of the newly created dissociated AD-MSC was evaluated by a

trypan blue exclusion assay through the use of a haemocytometer. The influence on cell growth and cell abatement was then analysed after each incubation step.

4.3.1.1 Cell viability assessment

The proportion of viable and dead AD-MSK was compared as seen in figure 24. This analysis was performed to get the ratio of viable and dead cells after incubation with different digestive enzymes. The proportion of viable as well as dead cells was analysed after 5, 15 and 45 min of incubation with each enzyme to get information of these different enzymes would influence the cell viability.

For statistical conclusion at each time point three samples were proven (n=3).

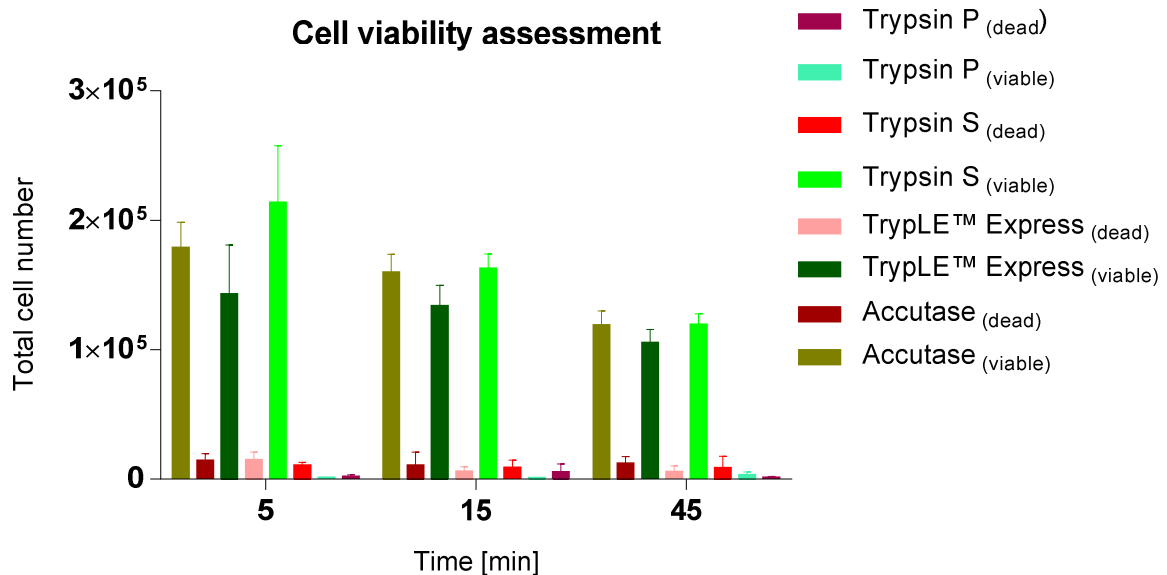


Figure 23: Overview of the proportion of viable (green coloured) vs. dead (red coloured) AD-MSK upon dissociation with Accutase, TrypLE™ Express, Trypsin S and Trypsin P after an incubation time of exactly 5, 10 and 45 min. Data represents MN \pm SD. (n=4)

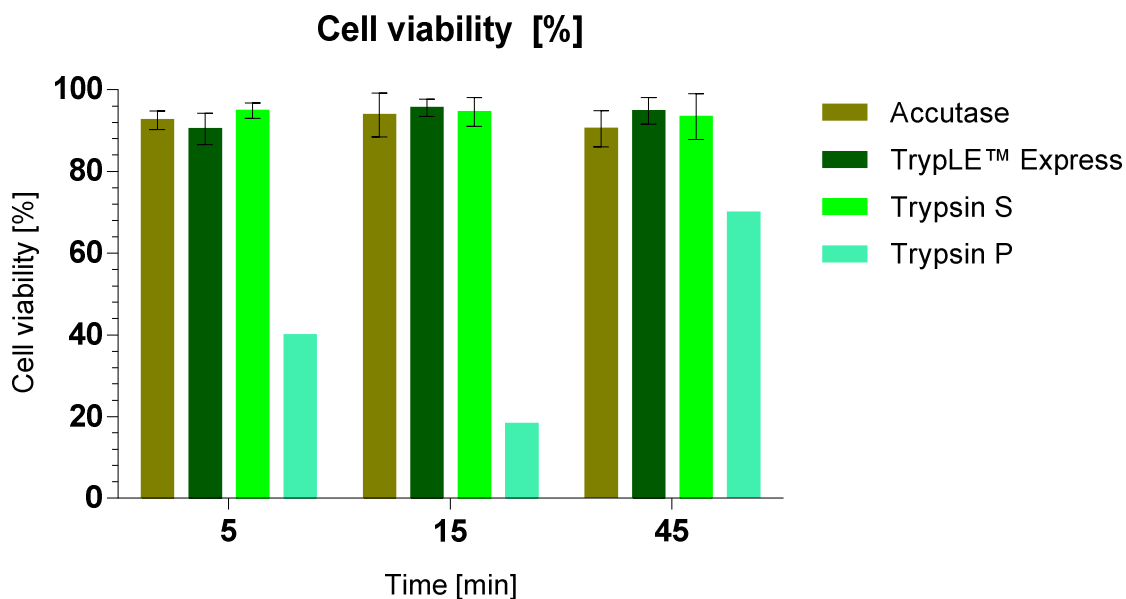


Figure 24: Cell viability (%) after the treatment of Accutase, TrypLE™ Express, Trypsin S and Trypsin P, after an incubation time of exactly 5, 10 and 45 minutes. Data represents MN \pm SD. (n=4).

According to figures 23-24, the first result after 5 min incubation with these digestive enzymes demonstrated that the cell viability of $94.91\% \pm 1.88\%$ by using Trypsin S was slightly higher than under the influence of the other three enzymes. By using Accutase $92.55\% \pm 2.33\%$, by using TrpLE™ Express $90.41\% \pm 3.81\%$ and by using Trypsin P 40.00% of the total cell viability was achieved. After 15 min incubation time of the enzymes, TrpLE™ Express with $95.61\% \pm 2.12\%$ of the cell viability was the highest in comparison to all others. Trypsin S showed $94.60\% \pm 3.41\%$, Accutase $93.85\% \pm 5.36\%$ and Trypsin P 18.18% of the cell viability. After 45 min the detachment with TrpLE™ Express demonstrated a cell viability of $94.83\% \pm 3.27\%$. Trypsin S represented $93.44\% \pm 5.59\%$, Accutase $90.51\% \pm 4.34\%$ and Trypsin P 70.00% cell viability.

Furthermore, the enzyme activity in this attempt is defined as a measurement of the ability of an enzyme to catalyse a specific reaction and is indicated as the number of viable cells per unit time [given in %] after the treatment with digestive enzymes.

The “maximum” or most of the measured so called enzyme activity (expressed as cell viability) was achieved by using Trypsin S after 5 min, by using TrpLE™ Express after 15 min or by using Accutase after 15 minutes. The detachment with Trypsin P did not work, as seen in figure 23 and 24. Hypothetically, this phenomenon is due to a loss in activity resulting from varying storage times of the enzymes and as a result Trypsin P did not work like the other enzymes. Because of this malfunction of Trypsin P, this digestive enzyme was not used for further enzymatically analysis.

Another interesting point is that the number of total cells, expressed as viable + dead cells decreases with increasing incubation time, seen in table 8. In general the number of total cells has to be the same after each time point because the seeded cells of 4000 cells/cm^2 was equal

in each cultivated well. A possible explanation for this phenomenon may be that AD-MSC exhausted and lost as cell-debris. After the treatment of all enzymes on AD-MSC, except Trypsin P (did not work), a loss of the total cell number was observed, seen in table 8.

Table 8: Loss of the total cell number [%] after an incubation time of 5, 15 and 45 min with varying digestive enzymes.

Time point [Min]	Total cell number [%]	Loss of cells [%]
Accutase		
5	100.00	-
15	88.29	11.71
45	68.04	20.24
TrpLE™ Express		
5	100.00	-
15	88.87	11.13
45	70.67	18.19
Trypsin S		
5	100.00	-
15	76.48	23.52
45	57.18	19.29
Trypsin P		
5	100.00	-
15	183.33	+83.33 (increased, malfunction)
45	133.33	50 (extremely decreased, malfunction)

To sum up, this enzymatic attempt with varying digestive enzymes was successful and pleasant because after the treatment with all enzymes (except Trypsin P), a cell viability of greater than 90% was observed at each time point with Accutase, TrpLE™ Express and Trypsin S. This result demonstrated that the usage of all of them (except Trypsin P in this case) was applicable for cell detachment processes.

4.3.2 Influence on cell growth and surface markers via flow cytometric analysis of surface antigen expression

Enzymatic dissociation inevitably results in some degradation of surface proteins as well as glycoproteins. Hence, the digestive enzymes were tested in regard to the structural integrity of stem cell biomarker surface proteins for ligand binding and were analysed by using flow cytometry [124, 125].

The immune-phenotype of the adipose-derived mesenchymal stem cell based on flow cytometric analysis may be changed progressively with the influence of digestive enzymes. One of the three major criteria to define the identity of MSC is that $\geq 95\%$ of the MSC population must express CD105, CD73 and CD90. In addition these cells must lack expression ($\leq 2\%$ positive) of CD45, CD34, CD14 or CD11b, CD79 α or CD19 and HLA class II [126].

Interestingly is that accutase is well known for gentle dissociation [127] of adherent AD-MSC, whereas trypsin doesn't preserve cells at all and these enzymatic influences on surface markers of MSC were proven to confirm the cell equivalence of AD-MSC after being acted upon by digestive enzymes. In this trial AD-MSC were expanded over 5 passages to get the necessary information about the influence of different enzymes relating to cell growth and the proliferation capacity, seen in figure 25.

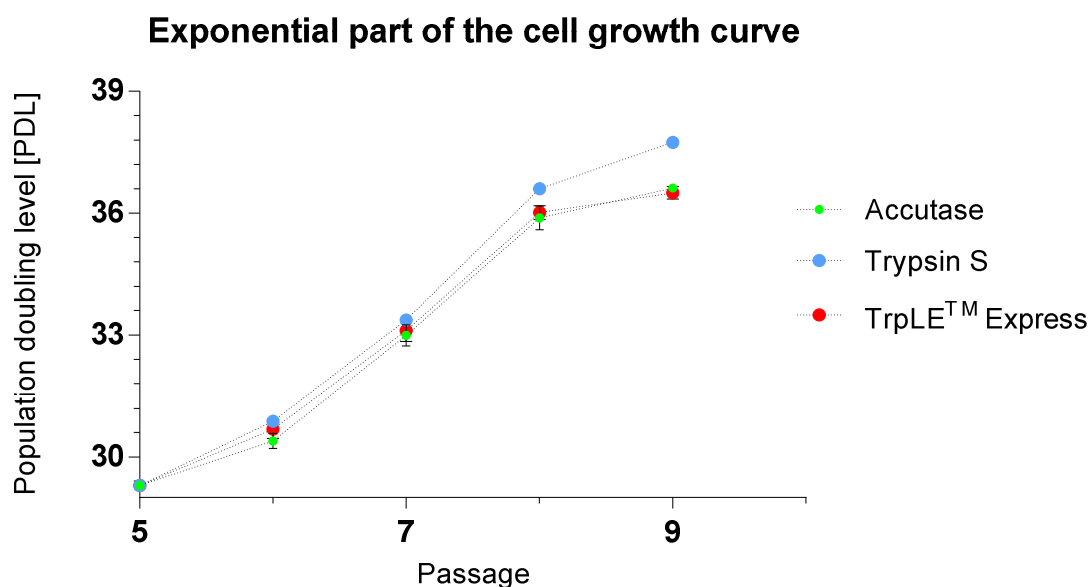


Figure 25: The effect of different digestive enzymes on AD-MSC short-term cell expansion over 5 passages (passage 5 to 9). Data represent population doubling level. (n=4).

The first part of this approach started by calculation of the influence on cell growth after incubation with Accutase, Trypsin S and TrpLE™ Express.

Cell population doublings over 5 passages by using different digestive enzymes for cell detachment are shown in figure 25. Because of the assumption that Trypsin P lost its enzyme activity, this enzyme was no investigated for this approach, see section 4.3.1.1. The population doubling level at passage 9 achieved a maximum of 37.73 ± 0.09 after the influence of Trypsin S, (36.61 ± 0.16) by Accutase and TrpLE™ Express (36.5 ± 0.16).

As a result, it is definitely clear that by using Trypsin S as digestive enzyme, most of the proliferation capacity will be reached compared to the other ones, as seen in figure 25.

The second parts of this approach followed by flow cytometric analyses of AD-MSC, previously sub-cultivated with Accutase, Trypsin S and TrpLE™ Express by standard procedure, see section 8.9.2 and 8.9.3.

Flow cytometric analysis was performed at passage 6 and passage 9 of AD-MSC to investigate the influence of surface markers via flow cytometric analysis of surface antigen expression. Cultured AD-MSC were stained with the phenotype (red) and isotype cocktail (grey) against CD14, CD20, CD34, CD45, CD73, CD90, CD105 and isotype control IgG-

conjugated fluorophores, as seen in figure 26 (treated with Accutase) and section 9 (rest of the tested enzymes, which were Trypsin S and TrpLE™ Express).

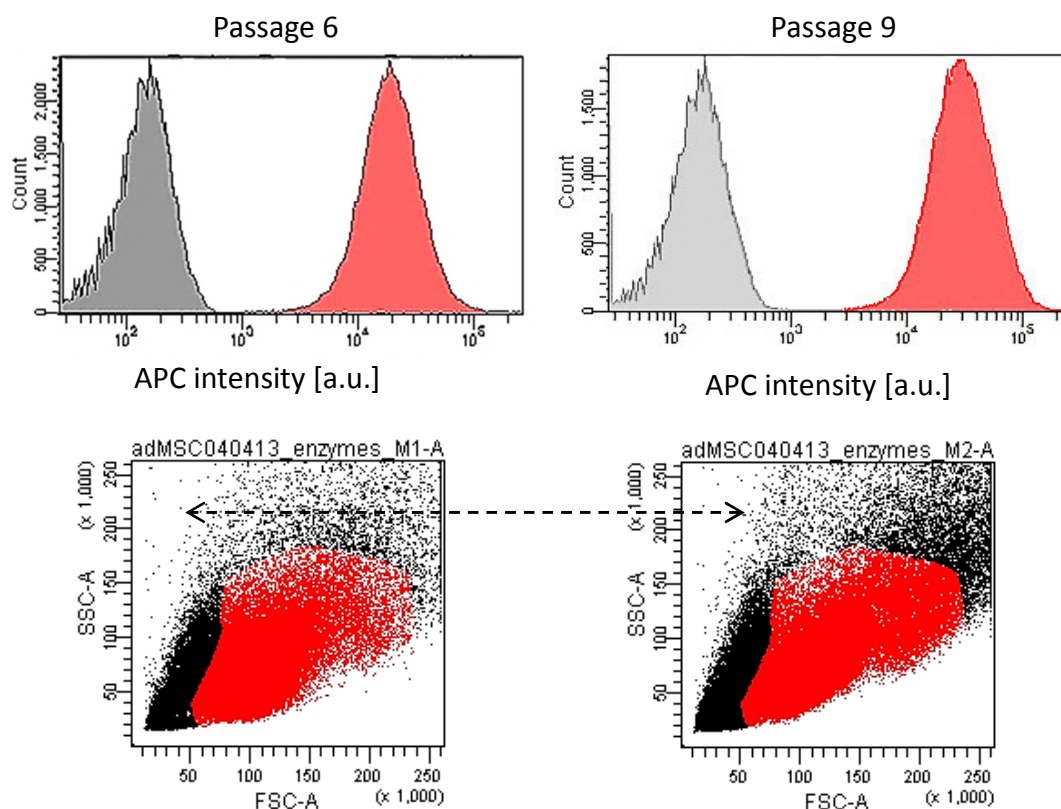


Figure 26: Flow cytometric analysis of cultured AD-MSC after passage 6 and 9, detached with Accutase.

A-APC intensity after passage 6. B-APC intensity after passage 9. C, D-gated population (red) with cell fragments (arrow).

According to figure 26 and section 9, flow cytometric analysis of AD-MSC showed that AD-MSC were negative for hematopoietic (CD34, CD45, CD20) and endothelial (CD14) markers and that they were positive for specific immune-phenotypic MSC markers (CD73, CD90, CD105) after passage 6 and 9 by using Accutase, as seen in figure 26 and section 9.

For the data using TrpLE™ Express and Trypsin S, see section 9. These histograms showed that after using all three digestive enzymes the adipose-derived cells still have an MSC-like immuno-phenotype, as defined by ISCT (International Society of Cellular Therapy) standards [126].

Interestingly, the same result is also demonstrated by the digestive enzyme Trypsin S, as seen in section 9, whereupon trypsin is well known as less gentle for detachment of AD-MSC as Accutase [128].

These results showed that by using Accutase, TrpLE™ Express and Trypsin S, the MSC population expressed CD105, CD73 and CD90 and lacked expression of CD45, CD34 and CD14.

For evaluation of the flow cytometric data, first the cell population was identified from the forward and side scatter dot-plots.

Gates were drawn to select the cell population and only events within a gate were considered for further analysis (e.g. histograms) (see section 9 and figure 26).

Figure 27 shows similar percentages of gated events in all cases (enzymes), indicating comparable underlying populations.

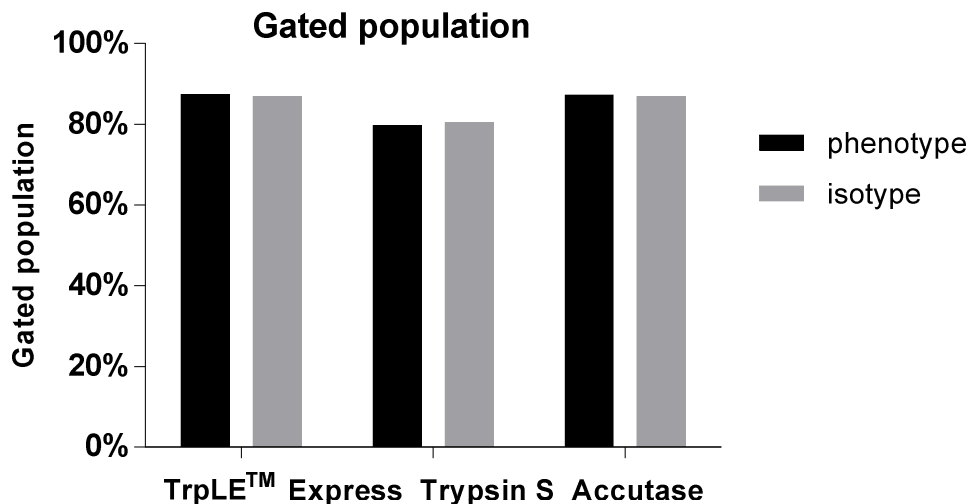


Figure 27: Gated population of AD-MSC under the influence of TrpLE™ Express, Trypsin S and Accutase.

The gated population of AD-MSC after incubation with TrpLE™ Express (phenotype with 87.40% and isotype with 86.80% of gated AD-MSC), Trypsin S (phenotype with 79.70% and isotype with 80.40% of gated AD-MSC) and Accutase (phenotype with 87.20% and isotype with 86.80% of gated AD-MSC) is demonstrated in figure 27.

In addition to the gated population, the calculation of the mean fluorescence intensity was estimated (phenotype:isotype) to demonstrate the expression of CD73 (APC), CD90 (FITC) and CD14, CD20, CD34, CD45 (PerCP-Cy5.5).

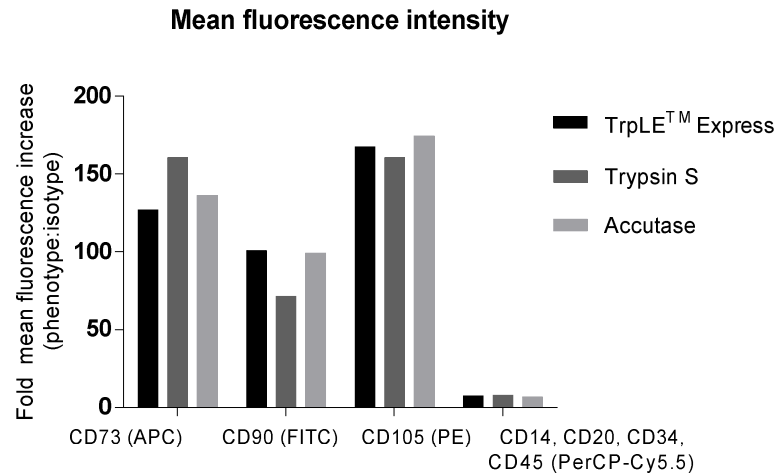


Figure 28: Mean fluorescence intensity.

According to figure 28, there is an expression of stem cell markers CD73, CD90 and CD105. By comparison, it is negative for CD45, CD34, CD20 and CD14.

The expanded AD-MSC by detaching with TrpLE™ Express, Trypsin S, and Accutase based on ISCT standard has defined minimal criteria for a common definition of human MSC)[126]. In summary, there exist no significant difference between using Trypsin S, TrpLE™ Express or Accutase as digestive enzymes in stem cell based experiments, because flow cytometric analysis show the existence of all necessary specific surface antigens, which are one indicator for the existence of mesenchymal stem cells, regardless of what enzyme was used.

Dynamic cultivation

4.4 Expansion of AD-MSK in the Z[®]RP 2000 H bioreactor

The idea of expanding AD-MSK in one-way (single-use) disposable bioreactors is in great demand because it offers two main advantages; the achievement of high cell numbers without frequent sub-cultivations of cells and less safety requirements. Dynamic cultivation conditions have more advantages in matters of cell expansion compared to static cultivation conditions. In dynamic cultivation systems, the Z[®]RP 2000 H bioreactor had optimal mass transfer. The maintenance of different composition of nutrients is guaranteed as well as the removal of toxic primary and secondary metabolite. In addition to mass transfer, gas and liquid transfer (diffusion) is present and offers the best condition in a closed system, because diffusion based on the principle of concentration differences. This supports an optimal flow of gas, which is known as Fick's law of diffusion [129].

This advantage also gives rise to the principle that cultivation in a closed system without the need to change the cell culture medium in a clean bench reduces the risk of contamination. Furthermore, the quality of cells and the avoidance of human errors are assured because the Z[®]RP 2000 H bioreactor is based on a programmed system that controls all parameters of cultivation combined with continuous documentation. With automatically systems in bioreactors, production costs can be minimized, which is an advantage of MSK in clinical applications. In this work, AD-MSK was expanded over 5 days in the Z[®]RP 2000 H bioreactor at 5% oxygen tension.

4.4.1 Cell growth in the Z[®]RP 2000 H bioreactor under hypoxia

This approach examined the expansion behaviour in dynamic cell culture system under low oxygen tensions (5% O₂). In several fields of biotechnological and medical research, the use of static cell culture cultivation ware has its limits. To mimic a more natural *in vivo* cell environment, it is useful to establish dynamic conditions which are regarded as physiologically more relevant cell culture models. In this approach, a dynamic bioreactor, composed of polycarbonate cell carrier slides (seen in figure 29), on which AD-MSK were expanded and used as a scaffold for this dynamic cell cultivation.

The aim of this experiment was to compare the growth properties of a dynamic cultivation system to standard plastic TCPS under static conditions. The absolute yield, cell viability with metabolic activity assay (MTT assay) and flow cytometric analysis were performed.

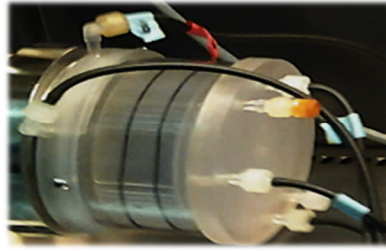


Figure 29: Z®RP 2000 H (Zellwerk GmbH, Oberkrämer) with rotating bed consisted of polycarbonate cell carrier slides, total surface area 2000 cm² (reactor size 4.6 x 8.8 cm).

AD-MSCs were seeded at a cell density of exactly 1500 cells/cm² in the Z®RP 2000 H bioreactor and in a standard TCPC (T-75 flask) as a static control under hypoxic condition (5% O₂). The total surface area of the Z®RP 2000 H bioreactor was 2000 cm² and 75 cm² in the TCPS, seen in figure 30. As a result, the entire cell number was 3 x 10⁶ cells in the Z®RP 2000 H bioreactor and 1.13 x 10⁵ cells in the reference TCPS (seen in formula 1).

$$\text{Entire cell number} = \text{Total surface area} \times 1500 \text{ cells/cm}^2$$

Formula 1: Calculation of the entire cell number for dynamic and static cell expansion.

After 5 days in culture, AD-MSCs were harvested and compared to the proliferation capacity to a reference (TCPC 75 cm²), seen in table 9 and figure 30.

Table 9: Cells per cm² and the total cell number of AD-MSCs expansion in a dynamic bioreactor (Z®RP 2000 H bioreactor) and in a static reference TCPS (75 cm²) at the beginning (T₀) and after 5 days (T₁) in culture. (n=4, Z®RP 2000 H), (n=1, reference).

	Time in culture [d]		Surface [cm ²]	Fold increase
	T ₀	T ₁		
Cells/cm ²				
Dynamic expansion	1.5 x 10 ³	1.11 x 10 ⁴ ± 1.12 x 10 ³	2000	
Static expansion	1.5 x 10 ³	3.85 x 10 ⁴ ± 3.60 x 10 ³	75	
Total cell number				
Dynamic expansion	3 x 10 ⁶	2.22 x 10 ⁷ ± 2.23 x 10 ⁶	2000	7.4
Static expansion	1.125 x 10 ⁵	2.88 x 10 ⁶ ± 2.70 x 10 ⁵	75	

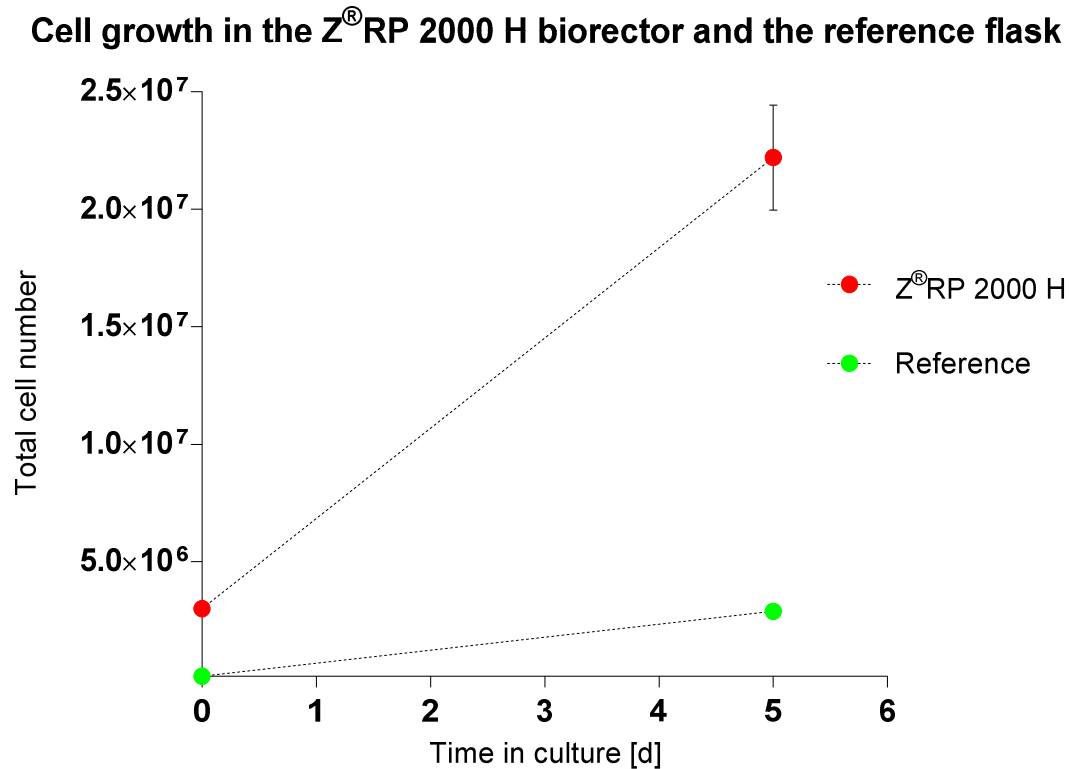


Figure 30: Total cell number of AD-MSK expansion in a dynamic bioreactor (Z[®]RP 2000 H bioreactor) and in a static reference flask (75 cm²) after 5 days in culture. Data represents MN ± SD (Z[®]RP 2000 H bioreactor).

According to figure 30, the result of this 5 day long dynamic cell cultivation in a Z[®]RP 2000 H bioreactor under hypoxic (5% O₂) tension, demonstrated a total cell number of $2.22 \times 10^7 \pm 2.23 \times 10^6$ cells at the end of this 5 days long expansion. In addition, the total population doublings were 2.88 ± 0.14 and the population doubling time was 33.35 ± 1.60 hours. In comparison to the dynamic expansion, the static control flask resulted in $2.88 \times 10^6 \pm 2.70 \times 10^5$ cells and the population doubling time was 20.54 ± 0.58 hours. The total calculated population doublings in this static cultivation were 4.68 ± 0.13 .

It can be seen that in figure 31 that the total cell number was increasing during 5 day cultivation in the Z[®]RP 2000 H bioreactor (22.2×10^6 cells $\pm 2.23 \times 10^6$ cells and 7.4-fold expansion) as well as in the static control ($2.88 \times 10^6 \pm 2.70 \times 10^5$ cells).

To sum up, the expansion of AD-MSK in the Z[®]RP 2000 H bioreactor resulted in a 7.4-fold increase of the expansion-rate (expressed as total cell number) compared to the inoculum (3×10^6 cells) after a cultivation time of 5 days. An essential advantage by using just one Z[®]RP 2000 H bioreactor as a cultivation system is that more than approximately 50 TCPS would be necessary to ensure the same cell yield.

All in all, the expansion of AD-MSK in the dynamic bioreactor system was successful which may offer a new approach in AD-MSK expansion strategies.

4.4.2 Morphological examination

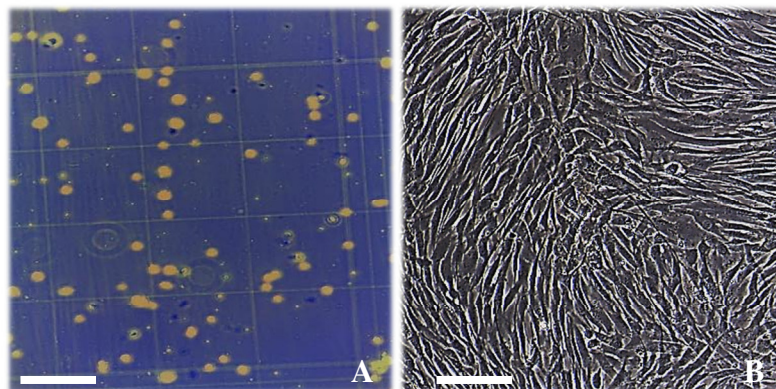


Figure 31: Cell growth of AD-MSC after 5 days of cultivation in the dynamic Z[®]RP 2000 H bioreactor system and in a static control flask (75 cm²). A-Detached cells after incubation with accutase in the Z[®]RP 2000 H bioreactor after 5 days in culture. B-Attached AD-MSC in a static control flask (75 cm²) after 5 days in culture. B-Original magnification: 10x. A- image: light microscope with an original magnification of 10x.

According to figure 31-A, microscope images of the dynamic bioreactor system's detached cells after 5 days of cultivation demonstrated that under dynamic cultivation, the morphological appearance of the expanded cells was similar to cultured cells in a conventional cell culture flask. The dimension, density, and the number of viable cells, which are cognizable as white round cells (figure 31-A) were satisfying for this dynamic cultivation because not a single cell cluster was observed and there were less dead cells visible, which is an indicator for the right amount as well as incubation time of accutase.

4.4.3 Glucose consumption

The glucose concentration during the expansion in the Z[®]RP 2000 H bioreactor was analysed daily for over 5 days. AD-MSC samples were taken and measured via the Bioprofile 100 Plus Analyser (Nova Biomedical Corporation, USA), see section 8.11.1, and table 10.

Table 10: Overview of the glucose concentration of the α -MEM cell culture media (+10% HS +0.5% GM) during the expansion of AD-MSC in the Z[®]RP 2000 H bioreactor over 5 days in culture.

Time in culture [d]	Glucose concentration [g/l]
Day 1	1.33
Day 2	0.95
Day 3	0.98
Day 4	1.00
Day 5	0.88

In the dynamic cell culture system, a total glucose concentration of 0.88 g/l was measured on day 5 in comparison to the initial glucose concentration of 1.33 g/l (table 10). During the

5-days dynamic expansion, approximately 78 ml cell culture medium was added per day, which was in sum exactly 390 ml. The effect of this is that the total glucose consumption reached 175.5 mg per day.

4.4.4 Metabolic activity assessment (MTT assay)

In order to test if the Z[®]RP 2000 H bioreactor cultivation changes the metabolic activity a MTT test was performed. AD-MSCs were harvested from the Z[®]RP 2000 H bioreactor and from the static control TCPS (to get a reference value) after 5 days in culture and both were compared, as seen in figure 32.

Metabolic activity (assessment) MTT assay

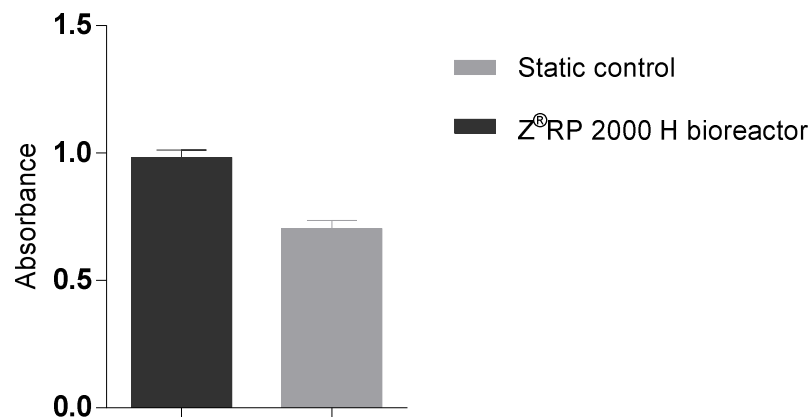


Figure 32: After 5 days in culture the final results from the metabolic activity were presented. The data were calculated according to the standard SOP MTT assay; see section 8.11.2. Static reference cultivation (75 cm²) and dynamic cultivation (Z[®]RP 2000 H bioreactor) showed a positive outcome as a result of metabolic activity. SD is presented via error indication in the plot. P-value (0.021) was analyzed by one-sample student t-test, see section 4.1.1.

The proportion of the metabolic activity was significantly higher ($p=0.021$) after 5 days cultivation in the Z[®]RP 2000 H bioreactor compared to the expansion after 5 days in the reference TCPS (75 cm²), as seen in figure 32. The results from the data set were expressed as mean \pm standard deviation. Differences between these data were analysed by a one-sample t- test, with a value of $p < 0.05$ being considered significantly different (see section 4.1.1). The final results demonstrated an evident difference in growth potential between static and dynamic cultivation, represented as 7.4 fold increase of the expansion in the Z[®]RP 2000 H bioreactor, seen in figure 30. The results presented a slightly higher metabolic activity in the bioreactor samples, which was regarded as significant due to the p-value of 0.021. As expected, dynamic and static samples showed a positive outcome in metabolic activity.

4.4.5 Surface immuno-phenotype characterization of AD-MSC after expansion in the Z[®]RP 2000 H bioreactor

Subsequent to the expansion in the Z[®]RP 2000 H bioreactor, AD-MSC were inspected by flow cytometry (see section 4.3.2). The staining was performed with a phenotype-isotype cocktail (MSC Phenotyping Kit human, 130-095-198, MACS Miltenyi Biotec) against CD14, CD20, CD34, CD45, CD73, CD90, CD105 and isotype control IgG-conjugated fluorophores. Flow cytometric analysis of AD-MSC demonstrated that they were negative for hematopoietic (CD34, CD45, CD20) and endothelial (CD14) markers, and that they were positive for specific immune phenotypic MSC markers (CD73, CD90, CD105) [126], as seen in figure 33.

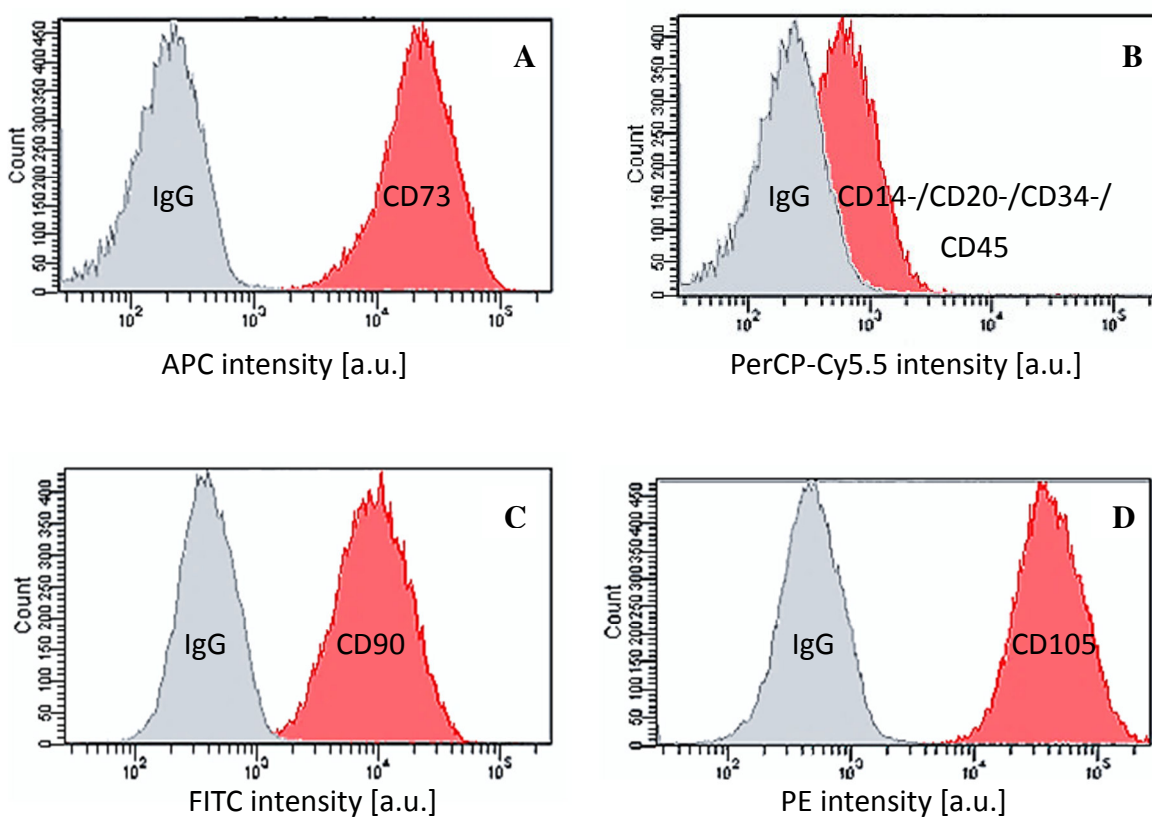


Figure 33: In the Z[®]RP 2000 H bioreactor expanded AD-MSC after 5 days under hypoxic (5% O₂) condition, analysed by Flow cytometric analysis. A-APC intensity, B-PerCP-Cy5.5 intensity, C-FITC intensity, D-PE intensity.

The gated population of the phenotype and the isotype was calculated (see section 4.3.2). A cell was stained with the specific antigen markers and the gated population, which was selective for the antigen, is pictured in figure 34.

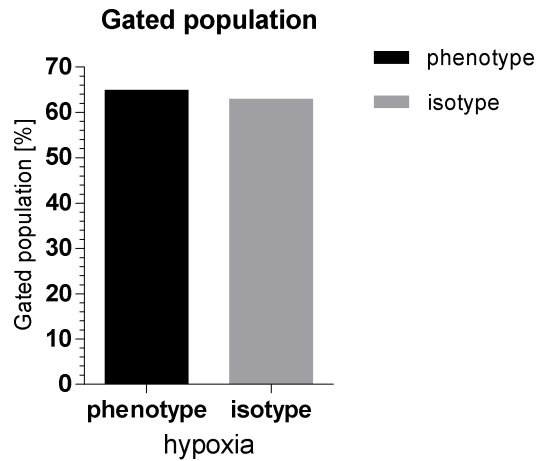


Figure 34: Gated population of AD-MSC under hypoxic (5% O₂) condition.

Table 11: Flow cytometric analysis of the gated population after expansion for 5 days in the Z[®]RP 2000 H bioreactor und 5% O₂ concentration.

Gated population [%]	
Phenotype	64.90
Isotype	62.90

This selection of a specific cell population is important because the extrinsic/fluorescent CD marker data (shown in the histogram) directly reflects the population "gated" in the histogram. In addition to the gated population, the calculation of the mean fluorescence intensity was estimated (phenotype:isotype) to demonstrate the expression of CD73 (APC), CD90 (FITC) and CD14, CD20, CD34, CD45 (PerCP-Cy5.5), seen in figure 35 (see also section 4.3.2).

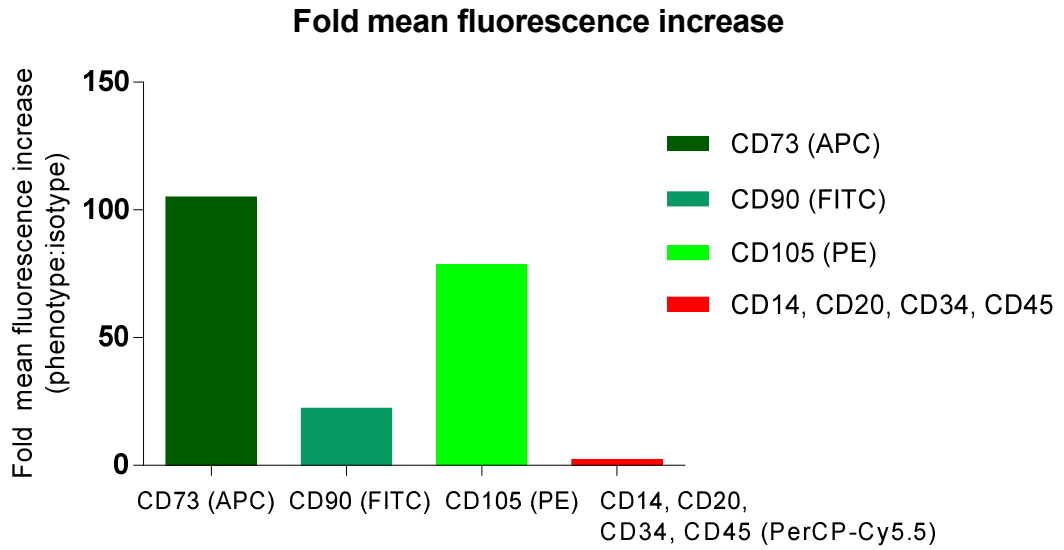


Figure 35: Fold mean fluorescence increase of CD73, CD90, CD105 and CD14, CD20, CD34, CD45.

There is a clear expression of stem cell markers CD73, CD90 and CD105 and it is negative for CD45, CD34, CD20, and CD14. Based on this data, we concluded that AD-MSC expanded in the Z[®]RP 2000 H bioreactor system under hypoxic (5% O₂) condition, based on ISCT standard (The International Society for Cellular Therapy) [126].

4.5 Expansion of AD-MSK in the TubeSpin[®] bioreactor

Three-dimensional (3D) suspension culture systems are able to provide a convenient *in vitro* model for the study of complex cell-matrix and cell-cell interactions in the absence of exogenous substrates and may benefit from the development of regenerative medicine strategies. Dynamic cultivation conditions have several advantages in comparison to static cell expansion. The contamination risk is reduced to a minimum, as there is no stirring mechanism extending into the tube. The suspension bioreactor offers an economical and fast approach for performing many parallel cell cultivations and achieves the highest yield in the shortest time. Dynamic cultivation systems like bioreactors provide active mass transfer and supply AD-MSK with nutrients and gases because the systems are operated in an orbital shaker, which provides a mechanism that facilitates excellent oxygen and carbon dioxide exchange rates [129] while minimizing mechanical stress.

This is particularly important during cell growth because of sensitivity to shearing forces. The TubeSpin[®] bioreactor is designed as a classic centrifuge tube and as a result, handling steps such as medium exchange are performed easily. The suspension bioreactor's screw cap is equipped with a hydrophobic membrane, which functions as a sterile barrier and therefore also minimizes loss of liquid by evaporation [130].

In this attempt, AD-MSK were first sub-cultivated in cell culture flask over 4 passages, followed by a second cultivation in U-bottom plates for over 24 hours to create 3D-cell-spheroids for the suspension bioreactor [131].

The cells were then expanded over 7 days in the disposable TubeSpin[®] bioreactor 50 (figure 36) [130].

The morphological examination of 3D-cell-clusters, the metabolic activity via MTT and the total cell yield of the cultivated AD-MSK were analysed in a suspension bioreactor.



Figure 36: DisposableTubeSpin[®] bioreactor 50 with orbitally rotating shaker consists of a sterile PITFE- filter, which is permeable to gas and has a working volume from 1 ml to 35 ml. 10 ml was the working volume in this experiment (taken from (6)).

4.5.1 Morphological examination

After the first sub-cultivation in standard TCPS over 4 passages (see section 8.4), AD-MSCs were transferred and seeded with a cell density of exactly 3×10^5 cells in a 1.5 ml reaction tubes according to protocols published by Hildner et.al [130].

The first barrier was the creation of cell-spheroids for the suspension bioreactor. An optimal diameter of the cell-spheroid was the prerequisite for the successful expansion of AD-MSCs in the suspension bioreactor. This supposed that the diameter of the cell-spheroids had not been too big or too small.

Based on this fact, two different pre-treatments for the cell-spheroid creation followed. One treatment was performed with centrifugation of the cells in the round-bottom plates and the other pass on centrifugation. The added centrifugation step relied on the principle of centripetal force to enforce the creation of cell-spheroids.

After the 24-hour cultivation, a morphological examination of these constructed cell-spheroids of AD-MSCs was performed to guarantee the existence of cell clusters, seen in figure 37-A, B.

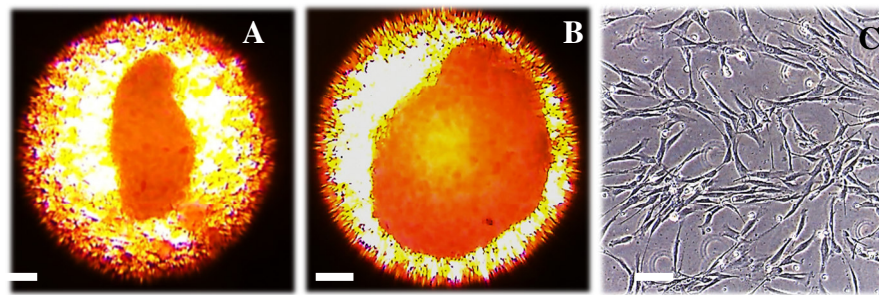


Figure 37: Morphological examination of AD-MSCs created cell spheroids after 24 hours cultivating in U-bottom plates, before transferring in the TubeSpin bioreactor. A-Created 3D-cell spheroid (without a centrifugation). B-3D-cell spheroid (with a centrifugation). C-Attached AD-MSCs in the 2D reference TCPS.

Microscopic imaging of AD-MSCs spheroid growth in U-bottom plates after 24 hours of cultivation demonstrated that cell clusters which were previously under the influence of the centripetal force were growing in a bigger and concentrically spheroid than AD-MSCs without centrifugation, seen in figure 37-B. AD-MSCs were pre-treated under centripetal force which were more suitable for the cultivation of AD-MSCs in the TubeSpin® bioreactor because the cell-cell interactions may be stronger and may benefit from the cohesion of the created spheroid. This is necessary for cultivating in the bioreactor because cells were partially growing in micro-mass formations composing 3D structures [131].

The determination of the spheroid diameter generated via centrifugation revealed between 500 μm and 1 mm (figure 37-B), which allows a comfortable handling. Unfortunately, aggregates of this size appear hard to be disrupted. As seen in section 8.12, cells of the spheroids had to be singularized through application of trypsin, lysed through addition of citric acid to disrupt

the cells and furthermore, vigorous interruption through mechanical forces (e.g. vortexing) for an effective separation of nuclei from the cellular debris. Such intense mechanical forces could also lead to damage and disruption of the nuclei themselves, which appears unfavourable with regard to cell counting, seen in figure 40. Therefore, the method of separating nuclei from spheroids with the size of 0.5-1 mm should be further optimized to guarantee a perfect balance between efficient nuclei extraction and minimal damage to cell nuclei itself.

According to figure 37-A, cell-spheroids could also successfully been established without a centrifugation step. In this case, AD-MSC were seeded as a single cell suspension directly in siliconized U-bottom plates (see section 8.12.3 for more details). AD-MSC's inability to adhere to the coated walls of the well leads to accumulation at the centre of the U-shaped bottom of the wells and moreover to a spheroid like structure. This process was only driven by the gravitational force (figure 37-A) instead of the centripetal force (figure 37-B).

To sum up, an obvious disadvantage of natural formation of spheroids through gravitational forces could be found in the loss of cells, which easily could be seen in figure 37-A.

Whereas nearly all seeded cells were existent in the spheroid generated by centrifugation (figure 37-B), the natural formed cell aggregate (figure 37-A) appears composed of approximately the half of the initial seeded cells. However, it should be noted that the focus of this work was not to find optimal procedures for spheroid generation but to analyse the proliferation of cells within spheroids in the TubeSpin[®] bioreactor. So there will be a need of further investigations, including an accurate comparison of cell counts and viability of spheroids generated either by centrifugation or the impact of gravitational forces.

In summary, according to the presented data, the centrifugation protocol to generate AD-MSC spheroids for this approach was more successful.

In addition to the morphological examination of the pleasant created 3D-cell-clusters, figure 37-C demonstrated the cell morphology of the 2D cells, as a reference, which was cultivated in standard TCPS for over 24 hours.

4.5.2 Metabolic activity assessment (MTT assay)

In order to test if the TubeSpin[®] bioreactor cultivation changes the metabolic activity a MTT test was performed. AD-MSC were harvested from the TubeSpin[®] bioreactor after 3 and 7 days in culture and were compared. Additionally the influence of either the centripetal or the gravitational force was already taken into account, as seen in figure 38.

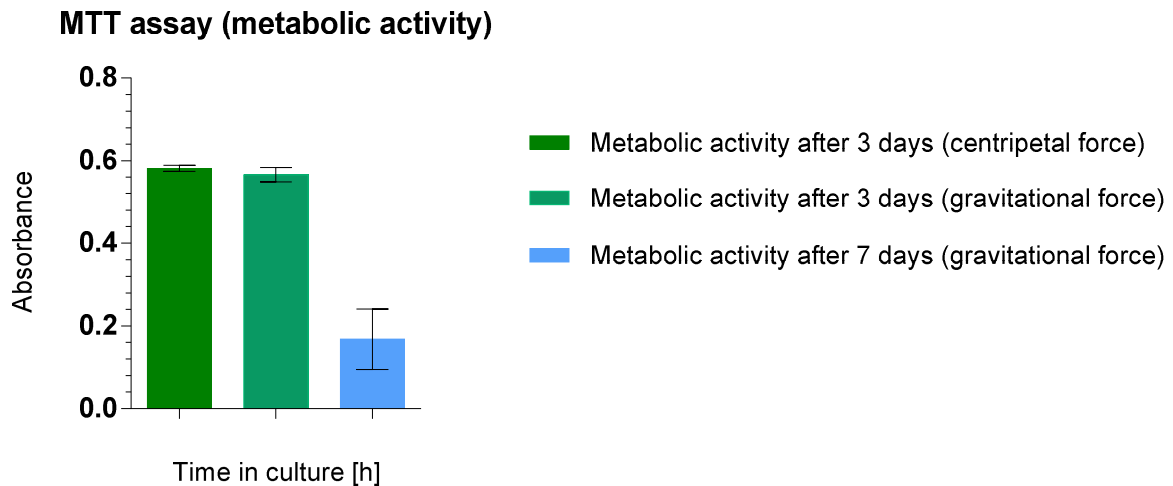


Figure 38: After 3 and 7 days in culture the final results from the metabolic activity were presented. The data were calculated according to the standard SOP MTT assay; see section 8.11.2. 3 day-cultivation as well as 7-days-cultivation of AD-MSC in the TubeSpin[®] bioreactor showed a positive outcome as a result of metabolic activity. Data were assessed by MTT assay and represent $MN \pm SD$ ($n=3$). Absorbance: 570 nm-630 nm. P-value (0.00833) was analyzed by one-sample student t-test, see section 4.1.1.

Metabolic activity (assessment) MTT assay

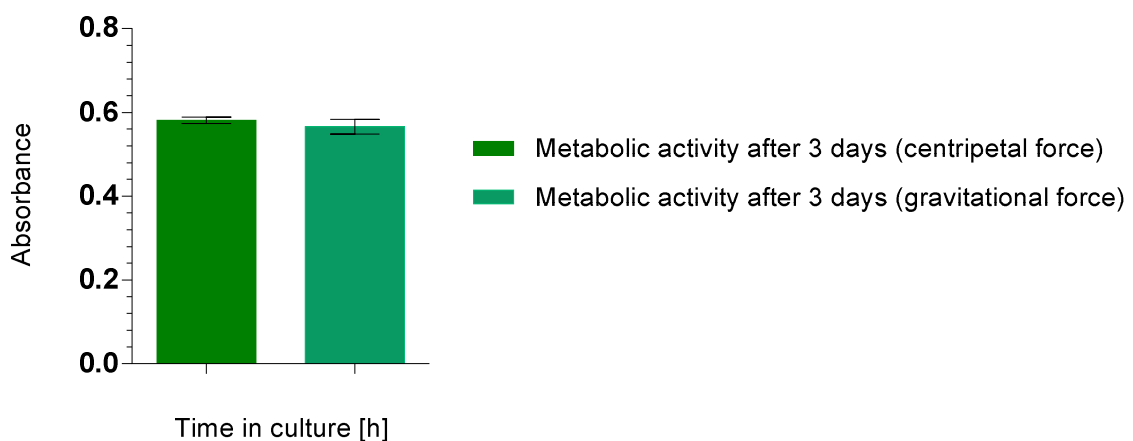


Figure 39: After 3 days in culture the final results from the metabolic activity were presented. The data were calculated according to the standard SOP MTT assay; see section 8.11.2. 3 day-cultivation of AD-MSC in the TubeSpin[®] bioreactor showed a positive outcome as a result of metabolic activity. Data were assessed by MTT assay and represent $MN \pm SD$ ($n=3$). Absorbance: 570 nm-630 nm. P-value (0.08) was analyzed by one-sample student t-test, see section 4.1.1.

According to figure 38, the proportion of viable AD-MSC was significantly higher ($p= 0.00833$) after 3 days in culture (centripetal force) compared to 7 days in culture (gravitational force). The Comparison of the metabolic activity under the influence of centripetal force and the metabolic activity under the influence of gravitational force after 3 days in culture demonstrated that there was no significant reduction in the metabolic activity of AD-MSC with or without the application of a centrifuge ($p=0.8$), seen in figure 39. The data set were expressed as $MN \pm SD$. Differences between these data were analysed by one-sample student's t test, with a value of $p < 0.05$ being considered significantly different (see section 4.1.1).

4.5.3 Cell proliferation assessment

AD-MSC were dynamically cultivated in spheroid aggregates for 7 in the TubeSpin[®] bioreactor. In addition a static reference, cultivated in standard TCPS was cultivated, with an entire cell number of 1×10^6 cells. Cell proliferation was assessed by using crystal violet cell colony staining assay and the total cell number was estimated with a haemocytometer of AD-MSC spheroids at day 1, 2, 3 and 7 to calculate the number of cells/spheroids in the suspension TubeSpin[®] bioreactor, seen in figure 40. It should be noted that the cells were in total cultivated for over 7 days, whereas data are only presented for a cultivation period of 4 days (96 hours) because cells of the spheroids are suggested to be lost during the harvesting procedure on day 7 (described below).

Table 12: Cell counts of dynamic cultivated spheroids.

DYNAMIC CULTIVATION OF SPHEROIDS					
Cell culture ware	U-bottom 96 well	U-bottom 96 well	TubeSpin [®] bioreactor	TubeSpin [®] bioreactor	TubeSpin [®] bioreactor
Time points	T ₀	T ₂₄	T ₄₈	T ₇₂	T ₉₆
Cells/4 spheroids	1.20×10^6	4.41×10^5			
MN cells/spheroid	3.00×10^5	1.10×10^5	1.11×10^5	1.23×10^5	1.59×10^5
SD cells/spheroid	0	1.46×10^4	4.76×10^4	3.54×10^2	1.02×10^4
Fluctuation (MN cells/spheroid) [%]		-63.30%	0.90%	-12,3% (*+10,8%)	+63% (*+29,3%)
Cells/T75 control (~4 spheroids)	1.20×10^6	1.60×10^6	1.90×10^6	2.90×10^6	No data
Cells/T75 control/4 (~1 spheroid)	3.00×10^5	3.93×10^5	4.63×10^5	7.40×10^5	No data
Fluctuation (MN cells/~ 1 spheroid) [%]		30.80%	17.80%	60.00%	No data

In this attempt, AD-MSC-spheroids were generated through centrifugation (t=0 h) and sub-cultured in 96 well U-bottom plates under dynamic conditions. Initial cell counts after 24 hours of sub-cultivation showed that approximately 63% of the seeded cells were lost through the centrifugation step (spheroid generation), seen in table 12. Following to transfer of the spheroids into the TubeSpin[®] bioreactor, cell counts at t=48 h, t=72 h and t=96 h showed a continuative increase of cells/spheroid. The values of T-75 controls were divided by factor 4 to obtain cell numbers which correspond (~) to one spheroid, seen in table 12.

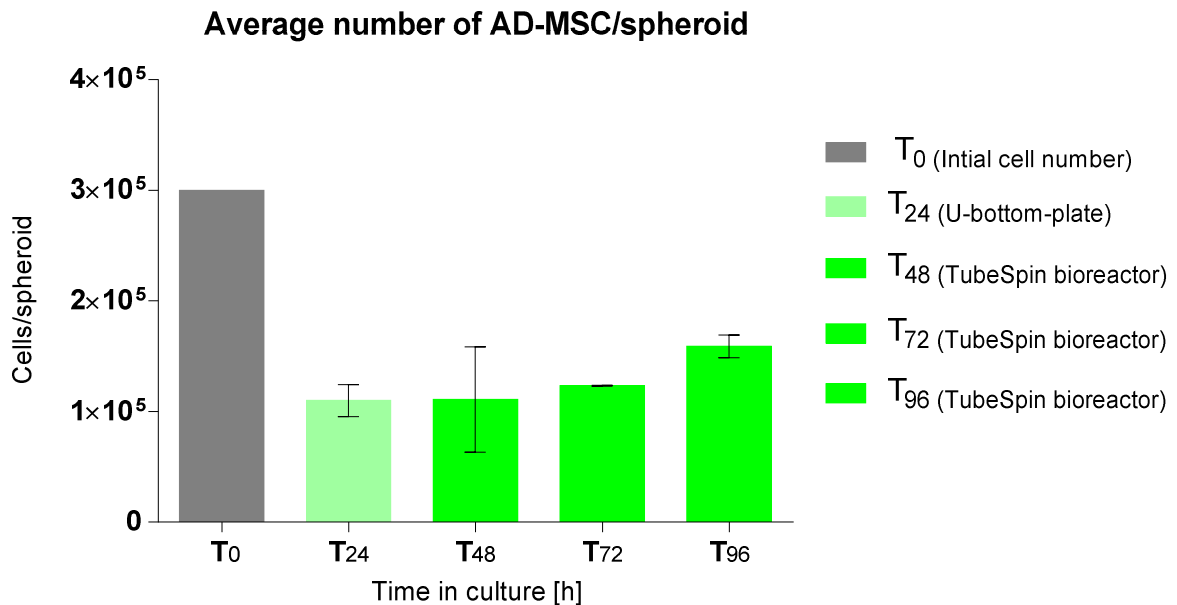


Figure 40: The calculation of the average number of AD-MSC/spheroid in a 3D suspension TubeSpin[®] bioreactor. Data represent Cells/spheroid; MN ± SD after 24, 48, 72 and 96 hours cell expansion. (n=3)

According to figure 40, the total cell numbers of spheroids which were cultivated over a period of 96 hours are represented.

The initial cell number of AD-MSC used for the generation of single cell spheroids is also seen in figure 41 (first column, T₀). Cells/spheroids were counted prior to transfer to the TubeSpin[®] bioreactor after 24 hours of dynamic sub-cultivation in U-bottom plates. Subsequently cells/spheroids were counted after 48, 72 and 96 hours of cultivation.

Figure 40 shows that the total cell number after 72 hours ($1.23 \times 10^5 \pm 3.54 \times 10^2$) in culture was slightly higher than after 24 ($1.1 \times 10^5 \pm 1.46 \times 10^4$) and 48 hours ($1.11 \times 10^5 \pm 4.76 \times 10^4$) in the 3D culture. The continued increase of the total cell number as well as the population doublings were evidence for cell growth in the suspension bioreactor, which demonstrated that AD-MSC were able to expand in a suspension bioreactor.

Even after 96 hours of cultivation an increase of the total cell number was observed ($1.59 \times 10^5 \pm 1.02 \times 10^4$).

In summary the dynamic cultivation in the suspension TubeSpin[®] bioreactor was successful and pleasant, demonstrated with an increase of the total cell number during this 3D-cell cultivation, seen in figure 40.

This experiment provides only preliminary data. Prior planning of the experiments especially with regard to controls should be revised. Summarized, the cultivation of AD-MSK in spheroid aggregates using TubeSpin[®] bioreactor offers several advantages including decreasing costs of cell culture medium, cell culture equipment (disposals), chemicals (no need of passaging), less working space requirements and an enhancement of the physiological conditions for the cultivated AD-MSK.

The latter, and most important one, arises from the fact that 3D cultures of cells mirror the natural environment within the organism. However, to include TubeSpin[®] bioreactor into standard laboratory routine, at least some steps have to be optimized:

First, as mentioned before, massive loss of cells was detected during the formation of 3D-cell-aggregates via the application of a centrifuge or without. To exclude the influence of errors emerging through the lysis/cell counting process after transfer of the generated spheroids to U-bottom plates, the supernatant should be tested to the presence of remaining cells. If cells remain in the supernatant of the 1.5 ml centrifuge tubes, the centrifugation protocol should be optimized. Optimizations could include higher g-values or prolongation of the centrifugation process. The most plausible reason for such massive cell loss, however, is thought to be a combination of both: an inefficient spheroid generation and a poorly conceived lysis/cell counting protocol which therefore should be improved for future approaches.

Second, as shown in figure 40 massive cell loss occurs between time point (T_0) and after 24 hours (T_{24}) of dynamic cultivation. It is relatively unrealistic that this amount of cells separate from spheroids or die during a distinct period of cultivation, maybe this reflects an artefact. More technical replicas can compensate the influence of such artefacts in future approaches.

Third, the complete data referring to cells analysed on day 7 was excluded from results. The reason for this exclusion is an unexplainable lack of data.

4 TubeSpin[®] bioreactors (4 spheroids/TubeSpin[®] bioreactor) were harvested by two operators. The harvesting/counting procedure was done according to current protocol described in section 8.12. AD-MSK of one TubeSpin[®] bioreactor was used for the MTT assay. Cells within the TubeSpin[®] bioreactor were clearly optical visible as spheroids with a diameter of more than 1 mm and counted twice by two different persons

(8 squares of haemocytometer/TubeSpin[®] bioreactor). No stained cell nuclei could be found within counting squares of haemocytometer. 2-3 single nuclei could be seen in the vicinity of the squares, which show evidently that the staining procedure itself was successful. No explanation can be given about the fact of this massive loss of cells, but we strongly anticipate that such cell loss could be prevented through increase of centrifugation speed.

Summarized it is clear that AD-MSK could be cultivated in suspension culture without microcarriers or scaffolds, cultivation in the TubeSpin[®] bioreactor appears possible.

This experiment demonstrated that AD-MSC spheroid aggregates could be cultivated in suspension with an increased proliferation capacity and even with a metabolic activity after 7 days in culture, seen in figure 38.

For further experiments the current used protocol maybe has to be modified to achieve higher cell numbers during AD-MSC-3D expansion in the suspension Tube Spin[®] bioreactor. This demonstrated cultivation was performed under normoxic condition. The cultivation under hypoxia could maybe improve additionally for future experiments in the suspension Tube Spin[®] bioreactor.

5 Conclusions and outlook

This study focused on two expanding strategies (dynamic and static) in order to optimize the quality and yield of *in vitro* cultured AD-MSC. In these strategies, three major approaches were investigated of adipose-derived mesenchymal stem cells expansion:

(1) To inspect the advantages and disadvantages of long-term cultivation of AD-MSC under hypoxia (5% O₂) and normoxia (21% O₂) conditions referring to the proliferation capacity and their metabolic pathways. The investigation of the stem cell differentiation capacity into different cell types such as adipocytes, chondrocytes, osteoblasts and their metabolic profiles during differentiation.

(2) To study the different effects of enzyme and temperature reduction detachment processes with UpCell™ surfaces on the short-term cell cultivation of AD-MSC to prove the proliferation capacities.

(3) Attempting the expansion of AD-MSC in a disposable Z[®]RP 2000 H bioreactor (Zellwerk GmbH, Germany) system under hypoxic (5% O₂) condition and in a disposable TubeSpin[®] bioreactor system (both based on dynamic processes).

Long-term cell expansion (over 20 passages within 5 weeks) illustrated that slightly higher cell numbers were realized at hypoxic condition (5% O₂) compared to 21% oxygen tension. Furthermore, the average relation of glucose concentration to lactate concentration from passage 5 to passage 20 demonstrated that under hypoxic condition (glucose concentration of 0.94 g/l ± 0.28 g/l and lactate concentration of 0.24 g/l ± 0.11 g/l) the glucose concentration, as well as the lactate concentration, were apparently higher than under normoxic condition (glucose concentration of 0.93 g/l ± 0.19 g/l and lactate concentration of 0.17 g/l ± 0.08 g/l). It seems that under hypoxic condition (5% O₂), the metabolic activity was more efficient than under normoxic condition (21% O₂), because AD-MSC consumed more glucose and produced more lactate. This may lead inevitably to a higher number of cells as well as a higher population doubling level under 5% O₂ tension.

All in all, cell proliferation under hypoxic condition for over 20 passages was more efficient than under normoxic conditions. This is reflected in the maximum of cell yield and exploited metabolites.

AD-MSC cultivated under hypoxia showed better retention of their adipogenic differentiation potential. Cultivating AD-MSC under normoxic condition (21% O₂) had a higher degree of differentiation towards osteocytes, suggested by a higher calcium deposition in contrast to hypoxic condition (5% O₂). Chondrogenic differentiation capacity was maintained by AD-MSC cultivated at 5% and 21% oxygen tension.

Having considered all these issues, these data suggest that 5% oxygen tension is favorable for AD-MSC expansion.

Alternative short-term cell expansion under 5% oxygen tension revealed that on Thermo Scientific Nunc™ UpCell surfaces, the yield increased, compared to conventional cell culture surfaces under hypoxic conditions.

The proliferation capacity showed an obvious increase of the total cell number higher by using a thermoresponsible surface rather than conventional surfaces. Additionally, the effect of hypoxia (5% O₂) on AD-MSC culture improved supplementary. The morphological examination of AD-MSC on Thermo Scientific Nunc™ UpCell surfaces was as viable as on traditional cell culture surfaces. Thermoresponsible culture ware is an optimal addendum to traditional culture ware, because this approach in cell culture provides many advantages such as improving cell viability and avoiding animal and human derived products in AD-MSC culture. Static cultivation on Thermo Scientific Nunc™ UpCell surfaces has several advantages in comparison to traditional static cultivation in standard TCPS. Cell detachment without any use of enzymes, cell dissociation just by temperature reduction, the influence of physical, mechanical and chemical forces instead of enzymatically forces preserves cell surface proteins, and minimal hands-on time makes this technique attractive for future MSC expansion.

Short-term cell expansion using different digestive enzymes for cell detachment demonstrated the enzymatic influences on surface markers of AD-MSC. The cell equivalence of AD-MSC after the impact of all used digestive enzymes (Trypsin P, Trypsin S, Accutase and TrpLE™ Express) was measured. Flow cytometric analysis of AD-MSC showed that they were negative for hematopoietic (CD34, CD45, CD20) and endothelial (CD14) markers and that they were positive for specific immune-phenotypic MSC markers (CD73, CD90, CD105). This major criterion to define the identity of MSC was available (according to the international society for cellular therapy position statement).

The next point to be considered is that using Trypsin S resulted in a slightly higher rate of proliferation capacity. The total cell count was increasing linearly and continuously from passage 5 to 9.

The cell viability assessment revealed that the proportion of viable AD-MSC was obviously higher upon dissociation with Trypsin S compared to the other digestive enzymes after 5 min incubation and demonstrated a cell viability of $94.91\% \pm 1.88\%$.

The peak activity of Trypsin S was observed after 5 minutes incubation time. Another trend was observed after the dissociation with Accutase, where the maximum of the cell viability ($93.85\% \pm 5.36\%$) was reached after 15 minutes incubation time. The same trend was demonstrated by using the digestive enzyme TrpLE™ Express ($95.61\% \pm 2.12\%$). After 45 min of incubation with digestive enzymes, the highest cell viability was present in the sample using TrpLE™ Express ($94.83\% \pm 3.27\%$) compared to the other enzymes.

To sum up, after 5 min of incubation the maximum of cell viability was attained by using Trypsin S, after 15 min incubation by disposing TrpLE™ Express and after 45 min incubation by utilising again TrpLE™ Express.

The detachment with Trypsin P did not work, as seen in section 4.3.1. Hypothetical, this phenomenon is due to a loss in enzyme activity due to prolonged storage.

The last part of this study comprised two dynamic cell culture bioreactors in order to investigate the expansion of AD-MSC in a rotating and in a suspension system. There are

several advantages in dynamic bioreactors in comparison to conventional static cell culture flasks. Dynamic bioreactors offer an automated control and process, lower risk of contamination, the improvement of documentation, and similar *in vivo* physiological condition. Additionally, they offer partial medium exchange, which supports the homeostatic *ex-vivo* microenvironment by producing signal molecules and cytokines, leading to increased cell growth.

AD-MSC were cultured over 5 days in the Z[®]RP 2000 H bioreactor under 5% oxygen tensions. The incubation of AD-MSC over 5 days resulted in 7.4-fold increase in terms of the proliferation capacity compared to the inoculum. AD-MSC maintained their specific surface antigen expression over this time. Additionally, the proportion of viable AD-MSC was significantly higher after 5 days in the Z[®]RP 2000 H bioreactor compared to the expansion after 5 days in the reference TCPS (75 cm²), which was reflected in the measured higher metabolic activity of AD-MSC.

This work illustrated the expansion of AD-MSC in the Z[®]RP 2000 H bioreactor under 5% oxygen tensions and provides a foundation for a new focus in cell culture research. Hypothetically, the dynamic cultivation under hypoxia could improve cell survival after transplantation because this combination can lead to the improvement of cell quality and yield during *ex vivo* AD-MSC expansion.

AD-MSC growth behavior and metabolic activity was also detected in the TubeSpin[®] disposable bioreactor. This approach supports the evidence that pellet-derived extracts may be used as an alternative in cell suspension systems. Expanded AD-MSC in a suspension bioreactor over a period of 96 hours showed an increase in the proliferation capacity (Cells/spheroids).

This study demonstrated that AD-MSC were able to cultivate as 3D-cell-aggregates in a suspension bioreactor. Metabolic active AD-MSC were even observed after 7 days in culture. The orbitally shaken TubeSpin[®] disposable bioreactor can be used for high throughput screening to determine the optimal infection parameters as well as a maximum cell yield, which is an advantage in cell culture. Traditional cell culture methods have relied on growing cells as monolayers, while three-dimensional (3D) culture systems (TubeSpin[®] bioreactor) can provide a convenient *in vitro* model for studies of cell-cell and cell-matrix interactions. The cultivation of AD-MSC in a suspension bioreactor may be a promising approach with many potential advantages in applied biotechnology but should be improved, as discussed in section 4.5.3.

To conclude, this thesis positively demonstrated that AD-MSC are a great promising cell type for future clinical applications, especially in the field of regenerative medicine. By definition, a stem cell is characterized by its ability to self-renewal and its ability to differentiate along multiple lineage pathways, which is also known as asymmetric cell division.

Based on this property, ideally, a stem cell for regenerative medicinal applications should meet the following criteria:

Firstly, AD-MSC have to exist in abundant quantities (millions to billions of cells).

Secondly, AD-MSCs have to be harvested by a minimal isolation procedure.

Third, AD-MSCs have to differentiate along multiple cell lineage pathways in a reproducible manner.

Furthermore, AD-MSCs have to be expanded in conventional and alternative expansion systems.

Moreover, AD-MSCs should be able to detach with different digestive enzymes and last but not least AD-MSCs have to be manufactured in accordance with dynamic bioreactor processes.

All these listed features of AD-MSCs demonstrate that mesenchymal stem cells of human subcutaneous adipose tissue depots are a great potential source of adult or somatic stem cells for future clinical applications which was fulfilled and evidenced in this work.

This thesis demonstrated that on the one hand the static as well as the dynamic cell expansion was successful and pleasant.

6 References

6.1 References

1. Caplan, A.I., et al., Adult mesenchymal stem cells for tissue engineering versus regenerative medicine. *Journal of cellular physiology*, 2007. 213(2): p. 341-347.
2. Tae, S.-K., et al., Mesenchymal stem cells for tissue engineering and regenerative medicine. *Biomedical Materials*, 2006. 1(2): p. 63.
3. Lee, R.H., et al., Multipotent stromal cells from human marrow home to and promote repair of pancreatic islets and renal glomeruli in diabetic NOD/scid mice. *Proceedings of the National Academy of Sciences*, 2006. 103(46): p. 17438-17443.
4. Duijvestein, M., et al., Autologous bone marrow-derived mesenchymal stromal cell treatment for refractory luminal Crohn's disease: results of a phase I study. *Gut*, 2010. 59(12): p. 1662-1669.
5. Lehninger, A.L., et al., *Lehninger Biochemie*. 2001, Springer Verlag, Berlin, Heidelberg, New York.
6. Glennie, S., et al., Bone marrow mesenchymal stem cells induce division arrest anergy of activated T cells. *Blood*, 2005. 105(7): p. 2821-2827.
7. Powell, J.D., et al., Inhibition of cell cycle progression by rapamycin induces T cell clonal anergy even in the presence of costimulation. *The Journal of Immunology*, 1999. 162(5): p. 2775-2784.
8. P De Miguel, M., et al., Immunosuppressive properties of mesenchymal stem cells: advances and applications. *Current molecular medicine*, 2012. 12(5): p. 574-591.
9. El-Maghrabi, M.R., et al., Rat liver 6-phosphofructo 2-kinase/fructose 2,6-bisphosphatase: a review of relationships between the two activities of the enzyme. *J Cell Biochem*, 1984. 26(1): p. 1-17.
10. Mizukami, A., et al., Efficient expansion of mesenchymal stromal cells in a disposable fixed bed culture system. *Biotechnology progress*, 2013.
11. Dry, H., et al., Effect of calcium on the proliferation kinetics of synovium-derived mesenchymal stromal cells. *Cytotherapy*, 2013.
12. Thirumala, S., et al., Manufacturing and banking of mesenchymal stem cells. *Expert opinion on biological therapy*, 2013. 13(5): p. 673-691.

13. Caplan, A.I., et al., Mesenchymal stem cells. *Journal of Orthopaedic Research*, 1991. 9(5): p. 641-650.
14. Pörtner, R., et al., Bioreactor design for tissue engineering. *Journal of bioscience and bioengineering*, 2005. 100(3): p. 235-245.
15. Yeatts, A.B., et al., Bioreactors to influence stem cell fate: augmentation of mesenchymal stem cell signaling pathways via dynamic culture systems. *Biochimica et Biophysica Acta (BBA)-General Subjects*, 2013. 1830(2): p. 2470-2480.
16. Diederichs, S., et al., Dynamic cultivation of human mesenchymal stem cells in a rotating bed bioreactor system based on the Z[®] RP platform. *Biotechnology progress*, 2009. 25(6): p. 1762-1771.
17. Dos Santos, F., et al., Ex vivo expansion of human mesenchymal stem cells: a more effective cell proliferation kinetics and metabolism under hypoxia. *Journal of cellular physiology*, 2010. 223(1): p. 27-35.
18. Nekanti, U., et al., Increased proliferation and analysis of differential gene expression in human Wharton's jelly-derived mesenchymal stromal cells under hypoxia. *International journal of biological sciences*, 2010. 6(5): p. 499.
19. Nekanti, U., et al., Long-term expansion and pluripotent marker array analysis of Wharton's jelly-derived mesenchymal stem cells. *Stem cells and development*, 2010. 19(1): p. 117-130.
20. Lennon, D.P., et al., Cultivation of rat marrow-derived mesenchymal stem cells in reduced oxygen tension: Effects on in vitro and in vivo osteochondrogenesis. *Journal of cellular physiology*, 2001. 187(3): p. 345-355.
21. Vander Heiden, M.G., et al., Understanding the Warburg effect: the metabolic requirements of cell proliferation. *science*, 2009. 324(5930): p. 1029-1033.
22. Nelson, D.L., et al., *Lehninger Biochemie*. 2001: Springer Berlin Heidelberg New York.
23. Chen, C.T., et al., Coordinated changes of mitochondrial biogenesis and antioxidant enzymes during osteogenic differentiation of human mesenchymal stem cells. *Stem cells*, 2008. 26(4): p. 960-968.

24. Heimbürg, D.v., et al., Oxygen consumption in undifferentiated versus differentiated adipogenic mesenchymal precursor cells. *Respiratory physiology & neurobiology*, 2005. 146(2): p. 107-116.
25. Rajpurohit, R., et al., Adaptation of chondrocytes to low oxygen tension: relationship between hypoxia and cellular metabolism. *Journal of cellular physiology*, 1996. 168(2): p. 424-432.
26. Heywood, H., et al., Monolayer expansion induces an oxidative metabolism and ROS in chondrocytes. *Biochemical and biophysical research communications*, 2008. 373(2): p. 224-229.
27. Borle, A.B., et al., Metabolic studies of bone in vitro I. Normal bone. *Journal of Biological Chemistry*, 1960. 235(4): p. 1206-1210.
28. Borle, A.B., et al., Metabolic studies of bone in vitro II. The metabolic patterns of accretion and resorption. *Journal of Biological Chemistry*, 1960. 235(4): p. 1211-1214.
29. Johnston Jr, C., et al., Studies of the metabolism of separated bone cells. *Calcified tissue research*, 1973. 11(1): p. 56-69.
30. Komarova, S.V., et al., Bioenergetics and mitochondrial transmembrane potential during differentiation of cultured osteoblasts. *American Journal of Physiology-Cell Physiology*, 2000. 279(4): p. C1220-C1229.
31. Lunt, S.Y., et al., Aerobic glycolysis: meeting the metabolic requirements of cell proliferation. *Annual review of cell and developmental biology*, 2011. 27: p. 441-464.
32. Crabtree, H.G., et al., Observations on the carbohydrate metabolism of tumours. *Biochemical journal*, 1929. 23(3): p. 536.
33. Diaz-Ruiz, R., et al., The Warburg and Crabtree effects: on the origin of cancer cell energy metabolism and of yeast glucose repression. *Biochimica et Biophysica Acta (BBA)-Bioenergetics*, 2011. 1807(6): p. 568-576.
34. Krebs, H., et al., The Pasteur effect and the relations between respiration and fermentation. *Essays in biochemistry*, 1972. 8: p. 1.
35. Grayson, W.L., et al., Effects of hypoxia on human mesenchymal stem cell expansion and plasticity in 3D constructs. *Journal of cellular physiology*, 2006. 207(2): p. 331-339.

36. Mischen, B.T., et al., Metabolic and functional characterization of human adipose-derived stem cells in tissue engineering. *Plastic and reconstructive surgery*, 2008. 122(3): p. 725-738.
37. DeBerardinis, R.J., et al., The biology of cancer: metabolic reprogramming fuels cell growth and proliferation. *Cell Metab*, 2008. 7(1): p. 11-20.
38. Christofk, H.R., et al., The M2 splice isoform of pyruvate kinase is important for cancer metabolism and tumour growth. *Nature*, 2008. 452(7184): p. 230-3.
39. Izyumov, D.S., et al., "Wages of fear": transient threefold decrease in intracellular ATP level imposes apoptosis. *Biochim Biophys Acta*, 2004. 1658(1-2): p. 141-7.
40. Vander Heiden, M.G., et al., Bcl-xL prevents cell death following growth factor withdrawal by facilitating mitochondrial ATP/ADP exchange. *Mol Cell*, 1999. 3(2): p. 159-67.
41. Shaw, R.J., et al., The tumor suppressor LKB1 kinase directly activates AMP-activated kinase and regulates apoptosis in response to energy stress. *Proc Natl Acad Sci U S A*, 2004. 101(10): p. 3329-35.
42. Lum, J.J., et al., Growth factor regulation of autophagy and cell survival in the absence of apoptosis. *Cell*, 2005. 120(2): p. 237-48.
43. Hardie, D.G., et al., AMP-activated/SNF1 protein kinases: conserved guardians of cellular energy. *Nat Rev Mol Cell Biol*, 2007. 8(10): p. 774-85.
44. DeBerardinis, R.J., et al., Beyond aerobic glycolysis: transformed cells can engage in glutamine metabolism that exceeds the requirement for protein and nucleotide synthesis. *Proc Natl Acad Sci U S A*, 2007. 104(49): p. 19345-50.
45. Chow, D.C., et al., Modeling pO_2 Distributions in the Bone Marrow Hematopoietic Compartment. II. Modified Kroghian Models. *Biophysical journal*, 2001. 81(2): p. 685-696.
46. Bizzarri, A., et al., Continuous oxygen monitoring in subcutaneous adipose tissue using microdialysis. *Analytica chimica acta*, 2006. 573: p. 48-56.
47. Harrison, J.S., et al., Oxygen saturation in the bone marrow of healthy volunteers. *Blood*, 2002. 99(1): p. 394-394.

48. Silver, I., et al., Measurement of PH and Ionic Composition of Pericellular Sites [and Discussion]. *Philosophical Transactions of the Royal Society of London. B, Biological Sciences*, 1975. 271(912): p. 261-272.
49. Fermor, B., et al., Oxygen, nitric oxide and articular cartilage. *Eur Cell Mater*, 2007. 13(11): p. 56-65.
50. Panchision, D.M., et al., The role of oxygen in regulating neural stem cells in development and disease. *Journal of cellular physiology*, 2009. 220(3): p. 562-568.
51. Dollery, C., et al., Oxygen supply to the retina from the retinal and choroidal circulations at normal and increased arterial oxygen tensions. *Investigative Ophthalmology & Visual Science*, 1969. 8(6): p. 588-594.
52. Dorland, W., et al., *Dorland's medical dictionary for health consumers*. Saunders, an imprint of Elsevier, 2007.
53. Ivanovic, Z., et al., Hypoxia or in situ normoxia: The stem cell paradigm. *Journal of cellular physiology*, 2009. 219(2): p. 271-275.
54. Yang, D.-C., et al., Hypoxia inhibits osteogenesis in human mesenchymal stem cells through direct regulation of RUNX2 by TWIST. *PLoS One*, 2011. 6(9): p. e23965.
55. Holzwarth, C., et al., Low physiologic oxygen tensions reduce proliferation and differentiation of human multipotent mesenchymal stromal cells. *BMC cell biology*, 2010. 11(1): p. 11.
56. Wang, D.W., et al., Influence of oxygen on the proliferation and metabolism of adipose derived adult stem cells. *Journal of cellular physiology*, 2005. 204(1): p. 184-191.
57. Merceron, C., et al., Differential effects of hypoxia on osteochondrogenic potential of human adipose-derived stem cells. *American Journal of Physiology-Cell Physiology*, 2010. 298(2): p. C355-C364.
58. Peterson, K.M., et al., Improved survival of mesenchymal stromal cell after hypoxia preconditioning: role of oxidative stress. *Life sciences*, 2011. 88(1): p. 65-73.
59. Bray, F., et al., Predicting the future burden of cancer. *Nature Reviews Cancer*, 2005. 6(1): p. 63-74.

60. Finkel, T., et al., The common biology of cancer and ageing. *Nature*, 2007. 448(7155): p. 767-774.
61. Brahimi-Horn, M.C., et al., Hypoxia and cancer. *Journal of Molecular Medicine*, 2007. 85(12): p. 1301-1307.
62. Moehler, T., et al., Angiogenesis in hematologic malignancies. *Critical reviews in oncology/hematology*, 2003. 45(3): p. 227-244.
63. Vaupel, P., et al., Tumor microenvironmental physiology and its implications for radiation oncology. in *Seminars in radiation oncology*. 2004. Elsevier.
64. Folkman, J., et al., Cancer: looking outside the genome. *Nature Reviews Molecular Cell Biology*, 2000. 1(1): p. 76-79.
65. Higuera, G., et al., Quantifying in vitro growth and metabolism kinetics of human mesenchymal stem cells using a mathematical model. *Tissue Engineering Part A*, 2009. 15(9): p. 2653-2663.
66. Schop, D., et al., Growth, metabolism, and growth inhibitors of mesenchymal stem cells. *Tissue Engineering Part A*, 2009. 15(8): p. 1877-1886.
67. Bilton, R., et al., ARDent about acetylation and deacetylation in hypoxia signalling. *Trends in cell biology*, 2006. 16(12): p. 616-621.
68. Brahimi-Horn, M.C., et al., Oxygen, a source of life and stress. *FEBS letters*, 2007. 581(19): p. 3582-3591.
69. Pouyssegur, J., et al., Hypoxia signalling in cancer and approaches to enforce tumour regression. *Nature*, 2006. 441(7092): p. 437-443.
70. Coleman, M., et al., Oxygen sensing and hypoxia-induced responses. *Essays Biochem*, 2007. 43: p. 1-16.
71. Schofield, C.J., et al., Signalling hypoxia by HIF hydroxylases. *Biochemical and biophysical research communications*, 2005. 338(1): p. 617-626.
72. Schofield, C.J., et al., Oxygen sensing by HIF hydroxylases. *Nature Reviews Molecular Cell Biology*, 2004. 5(5): p. 343-354.
73. Semenza, G.L., et al., Targeting HIF-1 for cancer therapy. *Nature Reviews Cancer*, 2003. 3(10): p. 721-732.

74. Ferrara, N., et al., Angiogenesis as a therapeutic target. *Nature*, 2005. 438(7070): p. 967-974.
75. Lafontan, M., et al., Fat cell adrenergic receptors and the control of white and brown fat cell function. *Journal of lipid research*, 1993. 34(7): p. 1057-1091.
76. Suchorolski, M.T., et al., Warburg and Crabtree Effects in Premalignant Barrett's Esophagus Cell Lines with Active Mitochondria. *PloS one*, 2013. 8(2): p. e56884.
77. Gordan, J.D., et al., HIF and c-Myc: sibling rivals for control of cancer cell metabolism and proliferation. *Cancer cell*, 2007. 12(2): p. 108-113.
78. Kim, J.-w., et al., Hypoxia-inducible factor 1 and dysregulated c-Myc cooperatively induce vascular endothelial growth factor and metabolic switches hexokinase 2 and pyruvate dehydrogenase kinase 1. *Molecular and cellular biology*, 2007. 27(21): p. 7381-7393.
79. Fukuda, R., et al., HIF-1 regulates cytochrome oxidase subunits to optimize efficiency of respiration in hypoxic cells. *Cell*, 2007. 129(1): p. 111-122.
80. Chen, G., et al., Different redox states in malignant and nonmalignant esophageal epithelial cells and differential cytotoxic responses to bile acid and honokiol. *Antioxidants & redox signaling*, 2009. 11(5): p. 1083-1095.
81. Cardone, R.A., et al., The role of disturbed pH dynamics and the Na⁺/H⁺ exchanger in metastasis. *Nature Reviews Cancer*, 2005. 5(10): p. 786-795.
82. Kim, J.-w., et al., Effects of hypoxia on tumor metabolism. *Cancer and Metastasis Reviews*, 2007. 26(2): p. 291-298.
83. Sonveaux, P., et al., Targeting lactate-fueled respiration selectively kills hypoxic tumor cells in mice. *J Clin Invest*, 2008. 118(12): p. 3930-42.
84. Hatzivassiliou, G., et al., ATP citrate lyase inhibition can suppress tumor cell growth. *Cancer cell*, 2005. 8(4): p. 311-21.
85. Glacken, M.W., et al., Catabolic control of mammalian cell culture. *Nature Biotechnology*, 1988. 6(9): p. 1041-1050.
86. Newsholme, P., et al., Newsholme, Rates of utilization of glucose, glutamine and oleate and formation of end-products by mouse peritoneal macrophages in culture. *Biochem. J*, 1989. 261: p. 211-218.

87. Ozturk, S.S., et al., Growth, metabolic, and antibody production kinetics of hybridoma cell culture: 2. Effects of serum concentration, dissolved oxygen concentration, and medium pH in a batch reactor. *Biotechnology progress*, 1991. 7(6): p. 481-494.
88. Ljunggren, J., et al., Catabolic control of hybridoma cells by glucose and glutamine limited fed batch cultures. *Biotechnology and bioengineering*, 1994. 44(7): p. 808-818.
89. Schneider, M., et al., The importance of ammonia in mammalian cell culture. *Journal of Biotechnology*, 1996. 46(3): p. 161-185.
90. Hassell, T., et al., Growth inhibition in animal cell culture. *Applied biochemistry and biotechnology*, 1991. 30(1): p. 29-41.
91. Dean, R.T., et al., Effects of exogenous amines on mammalian cells, with particular reference to membrane flow. *Biochem. J*, 1984. 217: p. 27-40.
92. Ozturk, S., et al., *Cell culture technology for pharmaceutical and cell-based therapies*. 2005: CRC Press.
93. Fantin, V.R., et al., Attenuation of LDH-A expression uncovers a link between glycolysis, mitochondrial physiology, and tumor maintenance. *Cancer cell*, 2006. 9(6): p. 425-34.
94. Enocksson, S., et al., Demonstration of an in vivo functional beta 3-adrenoceptor in man. *Journal of Clinical Investigation*, 1995. 95(5): p. 2239.
95. Castan, I., et al., Human adipocytes express $\alpha 2$ -adrenergic receptor of the $\alpha 2A$ -subtype only: pharmacological and genetic evidence. *Fundamental & clinical pharmacology*, 1995. 9(6): p. 569-575.
96. Valet, P., et al., Expression of human $\alpha 2$ -adrenergic receptors in adipose tissue of $\beta 3$ -adrenergic receptor-deficient mice promotes diet-induced obesity. *Journal of Biological Chemistry*, 2000. 275(44): p. 34797-34802.
97. Rydén, M., et al., Targets for TNF- α -induced lipolysis in human adipocytes. *Biochemical and biophysical research communications*, 2004. 318(1): p. 168-175.
98. Rydén, M., et al., Functional characterization of human mesenchymal stem cell-derived adipocytes. *Biochemical and biophysical research communications*, 2003. 311(2): p. 391-397.

99. Zuk, P.A., et al., Human adipose tissue is a source of multipotent stem cells. *Molecular biology of the cell*, 2002. 13(12): p. 4279-4295.
100. Pittenger, M.F., et al., Multilineage potential of adult human mesenchymal stem cells. *science*, 1999. 284(5411): p. 143-147.
101. Dominici, M., et al., Heterogeneity of multipotent mesenchymal stromal cells: from stromal cells to stem cells and vice versa. *Transplantation*, 2009. 87(9S): p. S36-S42.
102. Phinney, D.G., et al., Concise review: mesenchymal stem/multipotent stromal cells: the state of transdifferentiation and modes of tissue repair—current views. *Stem cells*, 2007. 25(11): p. 2896-2902.
103. Prockop, D., et al., “Stemness” does not explain the repair of many tissues by mesenchymal stem/multipotent stromal cells (MSCs). *Clinical Pharmacology & Therapeutics*, 2007. 82(3): p. 241-243.
104. Shyu, K.-G., et al., Mesenchymal stem cells are superior to angiogenic growth factor genes for improving myocardial performance in the mouse model of acute myocardial infarction. *Journal of biomedical science*, 2006. 13(1): p. 47-58.
105. Hung, S.C., et al., Angiogenic Effects of Human Multipotent Stromal Cell Conditioned Medium Activate the PI3K-Akt Pathway in Hypoxic Endothelial Cells to Inhibit Apoptosis, Increase Survival, and Stimulate Angiogenesis. *Stem cells*, 2007. 25(9): p. 2363-2370.
106. Buzzai, M., et al., The glucose dependence of Akt-transformed cells can be reversed by pharmacologic activation of fatty acid beta-oxidation. *Oncogene*, 2005. 24(26): p. 4165-73.
107. Kalaany, N.Y., et al., Tumours with PI3K activation are resistant to dietary restriction. *Nature*, 2009. 458(7239): p. 725-731.
108. Leever, S.J., et al., Signalling through phosphoinositide 3-kinases: the lipids take centre stage. *Current opinion in cell biology*, 1999. 11(2): p. 219-225.
109. Engelman, J.A., et al., Effective use of PI3K and MEK inhibitors to treat mutant Kras G12D and PIK3CA H1047R murine lung cancers. *Nat Med*, 2008. 14(12): p. 1351-6.
110. Baysal, B.E., et al., Mutations in SDHD, a mitochondrial complex II gene, in hereditary paraganglioma. *science*, 2000. 287(5454): p. 848-51.

111. Thompson, C.B., et al., Metabolic enzymes as oncogenes or tumor suppressors. *N Engl J Med*, 2009. 360(8): p. 813-5.
112. Evans, J.M., et al., Metformin and reduced risk of cancer in diabetic patients. *BMJ*, 2005. 330(7503): p. 1304-5.
113. Hatlapatka, T., et al., Optimization of culture conditions for the expansion of umbilical cord-derived mesenchymal stem or stromal cell-like cells using xeno-free culture conditions. *Tissue Engineering Part C: Methods*, 2011. 17(4): p. 485-493.
114. Campisi, J., et al., Cellular senescence as a tumor-suppressor mechanism. *Trends in cell biology*, 2001. 11(11): p. S27-S31.
115. Chen, Z., et al., Crucial role of p53-dependent cellular senescence in suppression of Pten-deficient tumorigenesis. *Nature*, 2005. 436(7051): p. 725-730.
116. Pattappa, G., et al., The metabolism of human mesenchymal stem cells during proliferation and differentiation. *Journal of cellular physiology*, 2011. 226(10): p. 2562-2570.
117. Toyoda, M., et al., Ways for a mesenchymal stem cell to live on its own: maintaining an undifferentiated state ex vivo. *International journal of hematology*, 2007. 86(1): p. 1-4.
118. Schallmoser, K., et al., Rapid large-scale expansion of functional mesenchymal stem cells from unmanipulated bone marrow without animal serum. *Tissue Engineering Part C: Methods*, 2008. 14(3): p. 185-196.
119. Sensebé, L., et al., Clinical grade production of mesenchymal stem cells. *Bio-Medical Materials and Engineering*, 2008. 18: p. 3-10.
120. Heng, B.C., et al., Comparison of enzymatic and non-enzymatic means of dissociating adherent monolayers of mesenchymal stem cells. *Biological procedures online*, 2009. 11(1): p. 161-169.
121. Netter, F.H., et al., *Musculoskeletal System: A Compilation of Paintings*. Anatomy, Physiology, and Metabolic Disorders; Russell T. Woodburne, Edmund S. Crelin and Frederick S. Kaplan, Consulting Editors; Regina V. Dingle, Managing Editor. 1987: Ciba-Geigy Corporation.
122. Barrett, A.J., et al., Families and clans of serine peptidases. *Archives of biochemistry and biophysics*, 1995. 318(2): p. 247-250.

123. Crlscitelli, F., et al., Friedrich Wilhelm Kühne 1837–1900. *Vision research*, 1977. 17(11): p. 1317-1323.
124. Sklar, L.A., et al., Flow Cytometric Analysis of Ligand-Receptor Interactions and Molecular Assemblies*. *Annual review of biophysics and biomolecular structure*, 2002. 31(1): p. 97-119.
125. Dainiak, M.B., et al., Methods in cell separations, in *Cell Separation*. 2007, Springer. p. 1-18.
126. Dominici, M., et al., Minimal criteria for defining multipotent mesenchymal stromal cells. The International Society for Cellular Therapy position statement. *Cytotherapy*, 2006. 8(4): p. 315-317.
127. Bajpai, R., et al., Efficient propagation of single cells accutase-dissociated human embryonic stem cells. *Molecular reproduction and development*, 2008. 75(5): p. 818-827.
128. Madeira, A., et al., Human mesenchymal stem cell expression program upon extended ex-vivo cultivation, as revealed by 2-DE-based quantitative proteomics. *Plos one*, 2012. 7(8): p. e43523.
129. Fick, A., et al., Ueber diffusion. *Annalen der Physik*, 1855. 170(1): p. 59-86.
130. Hildner, F., et al., Human platelet lysate successfully promotes proliferation and subsequent chondrogenic differentiation of adipose-derived stem cells: a comparison with articular chondrocytes. *Journal of tissue engineering and regenerative medicine*, 2013.
131. Baraniak, P.R., et al., Scaffold-free culture of mesenchymal stem cell spheroids in suspension preserves multilineage potential. *Cell and Tissue Research*, 2012. 347(3): p. 701-711.
132. Sottile, J., et al., Fibronectin polymerization regulates the composition and stability of extracellular matrix fibrils and cell-matrix adhesions. *Molecular biology of the cell*, 2002. 13(10): p. 3546-3559.
133. Eguchi, K., et al., First results from KamLAND: Evidence for reactor antineutrino disappearance. *Physical Review Letters*, 2003. 90(2): p. 021802.
134. Hynes, R.O., et al., *Fibronectins*. 1990: Springer-Verlag New York:.

135. Date, G.C.K., et al., CERTIFICATE OF THE GUIDE. 2005.
136. Meloan, S.N., et al., Chemical Mechanisms of Staining Methods: Von Kossa's Technique: What von Kossa Really Wrote and a Modified Reaction for Selective Demonstration of Inorganic Phosphates. *Journal of Histotechnology*, 1985. 8(1): p. 11-13.
137. Baraniak, P.R., et al., Scaffold-free culture of mesenchymal stem cell spheroids in suspension preserves multilineage potential. *Cell Tissue Res*, 2012. 347(3): p. 701-11.

6.2 References (web)

- (1) <http://www.genome.jp/kegg/>; (20.8.2013; 11:36)
- (2) Nelson, D.L. and M.M. Cox, *Lehninger Biochemie*. 2001: Springer Berlin Heidelberg New York. (26.10.2013; 10:17)
- (3) <http://www.sciencemag.org/content/324/5930/1029.figures-only>; (20.8.2013; 12:04)
- (4) Immunobiology and Vascular Diseases; LV 881.004; Part III: Vascular Biology; ao. Univ. Prof. Dr. Christine Brostjan; SS2014. (20.8.2014; 16:25)
- (5) www.thermo.com/upcell; (21.08.13; 10:39)
- (6) http://www.tpp.ch/page/bilder/Produkte/TubeSpin/500/tubespin_50_incubator.jpg; (21.8.2013; 10:55)
- (7) Ninolab http://www.ninolab.se/fileadmin/Ninolab/pdf/innovatis/CuBiAn_XC.pdf; (22.08.13; 09:11)
- (8) <http://www.bioprocessonline.com/doc/cubian-xc-culture-biochemistry-analyzer-0002>; (22.8.2014; 16:08)
- (9) http://www.zellwerk.biz/prod_biostat.htm; 16:39; (19.08.2013)
- (10) http://www.zellwerk.biz/prod_11.jpg; (20.08.13; 10:06)
- (11) <http://www.bdbiosciences.com/ca/instruments/facsanto/index.jsp>; (22.8.14; 16:18)

- (12) <http://www.miltenyibiotec.com/en/products-and-services/macs-flow-cytometry/reagents/kits-and-assays/msc-phenotyping-kit-human.aspx>; (16.9.2013; 17:55)
- (13) <http://www.google.at/url?sa=i&rct=j&q=&esrc=s&source=images&cd=&cad=rja&uact=8&ved=0CAcQjRw&url=http%3A%2F%2Fwww.pharmaceuticalonline.com%2Fdoc%2Fbio-profile-analyzers-for-cell-culture-0001&ei=mj5BVJW9BIf7PLjOgcgC&psig=AFQjCNHy5O1qYqE0oNt9-BwoE0FJqvD4A&ust=1413648404373024>; (16.1.2014; 18:50)
- (14) http://www.google.at/url?sa=i&rct=j&q=&esrc=s&source=images&cd=&cad=rja&uact=8&ved=0CAcQjRw&url=http%3A%2F%2Fwww.tpp.ch%2Fpage%2Fprodukte%2F05_a_tubespinn.php&ei=BT9BVIZCC4GsPZ6vgYAI&psig=AFQjCNF-CpjkRZij_NqMc6rktcFvRvrB2g&ust=1413648499817875; (17.5.2014; 14:23)
- (15) http://alkalisci.com/media/catalog/product/cache/1/image/9df78eab33525d08d6e5fb8d27136e95/u/-/u-bottom-96-well-plate_2.png; (20.08.2013; 13:14)

7 Materials

7.1 Materials

Material	Manufacturer
Syringe filter, Minisart NY25, 0.25 µl	Sartorius AG, Gottingen
Pipette tips (20, 200, 1000 µl)	Brand GmbH & CO KG, Wertheim
Cell culture flasks (T25, T75, T175)	Sarstedt AG & Co, Numbrecht
Cell culture plates (6-, 12-, 24-, 96-Wells)	Sarstedt AG & Co, Numbrecht
Cell culture plates BD BioCoat, fibronectin	BD Bioscience, Bedford USA
Cell scraper, 13 mm	Klinge, Sarstedt AG & Co, Numbrecht
Conical tubes (15 ml, 50 ml)	Greiner Bio-One GmbH, Frickenhausen
Latex gloves, Diamond Grip Plus	Microflex, Reno, USA
Nitril gloves, Rotiprotect Nitril	Carl Roth GmbH & Co KG, Karlsruhe
Serologic Pipettes (5, 25, 50, 100 ml)	Sarstedt AG & Co, Numbrecht
Syringes	Becon Dickinson GmbH, Heidelberg
Needles	B. Braun Melsungen AG, Melsungen
Cryo Pure Tubes	Sarstedt AG & Co, Numbrecht
PCR Tubes, 0.2 ml	Kisker Biotech GmbH & Co KG, Steinfurt
Reaction tubes (1.5 ml, 2 ml)	Sarstedt AG & Co, Numbrecht
Lab flasks (100 ml, 250 ml, 1000 ml)	VWR International GmbH, Darmstadt
Nunc™ Dishes with UpCell™ Surface (174901)	Thermo Scientific GmbH, Langenselbold
Nunc™ Dishes with UpCell™ Surface (174904)	Thermo Scientific GmbH, Langenselbold
Nunc™ Dishes with UpCell™ Surface (174906)	Thermo Scientific GmbH, Langenselbold
Clear 96-well round bottom plate	BD-Bioscience, Bedford, USA (#353830)
Reaction tubes (1.5 ml, 2 ml)	Carl Roth GmbH, Karlsruhe, Germany (7080.1, 7083.1)
CELLSTAR® CELLreactor™ tubes	Greiner Bio-One GmbH, Frickenhausen, Germany (227245)

7.2 Equipment

Equipment	Manufacturer
Neubauer counting chamber	Brand GmbH, Wertheim, Germany
Centrifuge for conical tubes	Centrifuge 5702, Eppendorf AG, Hamburg
Centrifuge for conical tubes	Centrifuge 5424, Eppendorf AG, Hamburg

Ultra-pure water system	Arium 611, Sartorius AG, Gottingen
Mini-centrifuge	MiniSpin, Eppendorf AG, Hamburg
Lab rocker	Stuard mini-gryo-rocker SSM3, Bibby Scientific Limited, Stone, GB
Microscope Leica DMIL LED	Leica Camera AG, Solms
Incubator Heracell 150i	Thermo Scientific GmbH, Langenselbold
Vortex	VWR International GmbH, Darmstadt
Thermo Scientific Multiskan [®] FC Microplate	Thermo Scientific GmbH, Langenselbold
Photometer	Thermo Scientific GmbH, Langenselbold
Suction pump biovac 106 ILMVAC	ILMVAC GmbH, Ilmenau
Clean bench MSC-Advantage	Thermo Scientific GmbH, Langenselbold
Water bath	GFL GmbH, Burgwedel
Suction pump biovac 106 ILMVAC	ILMVAC GmbH, Ilmenau
Clean bench MSC-Advantage	Thermo Scientific GmbH, Langenselbold
Water bath	GFL GmbH, Burgwedel
Refrigerator -80 °C Hera freeze basic	Thermo Scientific GmbH, Langenselbold
Cryo tank -165 °C Cryotherm Biosafe MD	Cryotherm GmbH & Co. KG, Kirchen/Sieg
Microscope DM IL LED	Leica Camera AG, Solms
Microscope Kübler CODIX	Leica Camera AG, Solms
Flow cytometer BD FACSCanto II	BD Bioscience, USA
Centrifuge Beckman Coulter	Beckman Coulter GmbH, Krefeld
CuBiAn [®] XC Cultue Biochemistry Analyzer	Roche innovatis AG, Bielefeld
Bioprofile 100 Plus Analyzer	Nova Biomedical Corporation, USA
Autoclave Varioklav	Thermo Scientific GmbH, Langenselbold
Scale	Sartorius AG, Gottingen
Vortex	Aigner Unilab GesmbH, Innsbruck
Centrifuge Pico 17	Thermo Scientific GmbH, Langenselbold
Clean bench HERASAFE KS	Thermo Scientific GmbH, Langenselbold
Pressure container	Böhm, Steyr
Air-cushion inflator Parker	Greiner Bio-One GmbH, Frickenhausen
Cam Leica ICC50 HD	Leica Camera AG, Solms
Inkubator Heracell 240i	Thermo Scientific GmbH, Langenselbold
Inkubator Heracell 150i	Thermo Scientific GmbH, Langenselbold
Refrigerator HITECH ARTIS	AEG
Orbital shaker ELMI Sky Line Shaker DOS-10M	BioTech Quest, USA
Magnetic stirrer MSH Basic	IKA-Werke GmbH & Co KG, Staufen
Pipetting aid	Eppendorf AG, Hamburg

Pump	Laboport, Knf-Lab Trenton, USA
Pipette tips	VWR International GmbH, Darmstadt
Thermomixer	Thermomixer Comfort, Eppendorf AG, Hamburg
Cellreactor tubes	Greiner Bio-One GmbH, Frickenhausen

7.3 Chemicals

Chemicals	Manufacturer
Trypsin	Sigma Aldrich GmbH, München
Accutase	PAA Laboratories GmbH, Pasching
TrpLE™ Express	Gibco Invitrogen, Darmstadt
Accutase	GIBCO Invitrogen, Darmstadt
Trypsin	Polymun Scientific Immunobiologische Forschung GmbH, Klosterneuburg
Acetic acid	AppliChem GmbH, Darmstadt
A-Minimum Essential Medium (MEM)	GIBCO Invitrogen, Darmstadt
Alcian blue 8G Solution	Sigma Aldrich GmbH, München
BSA	Sigma Aldrich GmbH, München
Calcein	Sigma Aldrich GmbH, München
DAPI	Sigma Aldrich GmbH, München
DMSO	Sigma Aldrich GmbH, München
Ethanol	Carl Roth GmbH+Co. KG, Karlsruhe
EDTA	AppliChem GmbH, Darmstadt
Reaction tubes, 1.5 ml, 2 ml	Sarstedt AG & Co, Numbrecht
Gentamicin (10 mg/ml)	PAA Laboratories GmbH, Pasching
Human serum	Blutbank Linz
Isopropanol	Merck KGaA, Darmstadt
KCL	Honeywell Speciality Chemicals GmbH, Seelze
NaCl	Sigma Aldrich GmbH, München
Na ₂ HPO ₄ · 2 H ₂ O	Honeywell Speciality Chemicals GmbH, Seelze
Na ₂ S ₂ O ₃ -Solution	Sigma Aldrich GmbH, München
SDS	Sigma Aldrich GmbH, München
Nitrogen	Linde Gas Deutschland, Pullach
Formaldehyd	Sigma Aldrich GmbH, München

Trypan blue	Sigma Aldrich GmbH, München
Crystal violet	Sigma Aldrich GmbH, München
Oil Red O solution	Sigma Aldrich GmbH, München
AgNO ₃ solution	Sigma Aldrich GmbH, München

7.4 Differentiation Media

Differentiation Media	Manufacturer
Osteogenic Medium	Miltenyi Biotec GmbH, Bergisch Gladbach
Chondrogenic Medium	Miltenyi Biotec GmbH, Bergisch Gladbach
Adipogenic Medium	Miltenyi Biotec GmbH, Bergisch Gladbach

7.5 Solutions and buffers

Solutions	Formation
Calcein stock solution	200 µg/ml Calcein in ddH ₂ O (Sigma Aldrich GmbH, München)
Calcein working solution	Calcein-Stock solution and ddH ₂ O, 1:39)
Cryomedium	20% α -MEM Medium +70% HS + 10% DMSO
Von Kossa AgNO ₃ solution (5%)	5% AgNO ₃ in ddH ₂ O(Carl Roth GmbH & Co KG, Karlsruhe)
Von Kossa formaldehyd solution	5% Na ₂ CO ₃ + 0.2% formaldehyd
Fixation solution	4% formaldehyd in PBS
Alizarinrot S (C.I.58005)	Carl Roth GmbH & Co KG, Karlsruhe
PBS	137 mM NaCl, 2.7 mM KCl, 8.1 mM Na ₂ HPO ₄ · 2 H ₂ O, 1.8 mM KH ₂ PO ₄ pH 7.4

7.6 Kits

Kit	Manufacturer
MSC Phenotyping Kit, human	Miltenyi Biotec GmbH, Bergisch Gladbach

8 Methods

8.1 Biological material

AD-MSC were applied for all experimental approaches described below. AD-MSC were isolated from fat tissue, provided by division of plastic surgery of the Vienna General Hospital (AKH), approved by the ethics commission of Austria/Upper-Austria (request no.:200).

AD-MSC were tested negative for mycoplasma prior to experiments. Used passage 1(P1) cells [1×10^6 cells/ml] were conserved in basal-medium (α -MEM supplemented with +70% HS, from the blood bank Linz, Upper Austria and 10% DMSO in liquid nitrogen).

8.2 Isolation of AD-MSC

One day before the isolation of human mesenchymal stem cell from fat tissue, HANKS buffer I, HANKS buffer II, α -MEM culture medium, and α -MEM cell culture medium (+10% HS and 0.5% gentamicin) were prepared. All instruments were washed with ddH₂O, sterilized with ethanol (70%), and autoclaved to guarantee optimal sterility. The first step of the isolation started with carefully cutting fat tissue in pieces (approximately 0.5 cm³) by using a sterile scissor, followed by transferring the pieces (roughly 20 ml \approx 17-20 g of fat tissue) into 50 ml falcon tubes. In connection 10 ml collagenase solution (2 mg/ml) was added, vortexed, and incubated for exactly 1 hour at 37 °C. Afterwards the contents were vortexed homogenously and half of the volume (approximately 15 ml) was transferred to a new 50 ml falcon tube. The extant fat tissue was topped up with HANKS buffer I, followed by centrifugation at 300 x g for 5 min. By using a sterile spoon, the developed fatty supernatant was put in a new 50 ml tube and the middle layer was discarded by suctioning with a vacuum pump. In parallel, the fat pieces were re-suspended, flicked, and transferred to the fatty supernatant, followed by topping up with HANKS buffer II (up to 50 ml). The next centrifuge step at 300 x g for 10 min was performed, the produced fat with its supernatant was discarded, and the pellet was re-suspended in HANKS buffer II. The last centrifuge-step at 300 x g for 10 min was performed, the supernatant discarded, and the extant cell pellet flicked. Afterwards the cell suspension was added up to 30 ml cell culture medium. Finally, 15 ml of the cell suspension was submersed to a 75 cm² cell culture flask and incubated at 37 °C at either 5% CO₂ and 5% O₂, or 5% CO₂ and 21% O₂ in a humidified atmosphere. After 48 hours, the medium has to be changed. The isolation has been finished after the cryopreservation of the cells.

8.3 Cell thawing

Firstly, the cryopreservation vial was transferred from the liquid nitrogen tank (-180 °C) quickly into a 37 °C water bath and swivelled approximately for 2 min until the contents of the vial was thawed. All following steps were performed under a clean bench and started by

adding 1 ml cold α -MEM cell culture medium. After 2 min, the mixture was added with 7 ml α -MEM medium in a 15 ml conical tube and centrifuged for 5 min at 300 x g. The supernatant was carefully removed by using a suction pump and the extant cell pellet was flicked and then re-suspended in 1 ml α -MEM cell culture medium (+10% HS and 0.5% gentamicin). The cell suspension was transferred into a 175-cm² or 75-cm² culture flask and 30 ml or 15 ml of pre-warmed (37 °C) α -MEM cell culture medium (+10% HS and 0.5% gentamicin) was added. The flask was put in the incubator until the cells detached and reached a density of approximately 80% of confluence.

8.4 Enzymatic detachment

The cells were washed with 5 ml PBS, then detached by accutase attendance and pelleted by centrifugation for 5 min at 300 x g. The supernatant was discarded and the extant cell pellet was re-suspended in 1 ml of pre-warmed α -MEM cell culture medium (+10% HS and 0.5% gentamicin). Next, 20 μ l of trypan blue and 20 μ l of the cell suspension (dilution factor of 2) were mixed and the cells were counted by using a haemocytometer. This cell number was determined by trypan blue staining assay.

$$\frac{\sum \text{Cells of counted quadrates}}{\text{number of counted quadrates}} * \text{dilution factor} * 10^4 = \text{Cells/ml}$$

Formula 2: Calculation of the total cells/ml

$$\frac{\text{Cells}}{\text{ml}} \times V = \text{Total cell number}$$

Formula 3: Calculation of the total cell number.

8.5 Cumulative cell population doubling

The main idea of the long-term cultivation was to determine the total cell number (Cells/ml), population doublings (Nd) and the population doubling time (Td). During long-term cultivation, the cells were cultured over 20 passages. Every 3-4 days, when the cells reached a confluence of approximately 60-80%, the cell number, population doublings and population doubling time were assigned. At each passage, the cells were counted with a haemocytometer and according to the following formula, the population doublings were estimated:

$$Nd = \frac{\ln\left(\frac{x}{x_0}\right)}{\ln 2}$$

Formula 4: Calculation of the population doubling

Nd is the number of population doubling during a specific period of time (Δt).

x_0 is the initial number of viable cells at time $t = 0$; x is the number of viable cells at time t .

Population doubling time was calculated according to the following formula:

$$Td = \frac{\Delta t}{Nd}$$

Formula 5: Calculation of the population doubling time.

8.6 Population doubling level

The passage number applies to the number of times the cells in the cell culture have been subcultured. The population doubling level (PDL) refers to the total number of times the cells in the population have doubled since their first isolation *in vitro*. Population doubling level was calculated according to the following formula:

$$n = 3.32 (\log(x) - \log(x_0)) + Nd$$

Formula 6: Calculation of the population doubling level.

n is the final PDL number at end of a given subculture.

x is the cell yield at time = t .

x_0 is the cell number used as inoculum to begin that subculture.

Nd is the doubling level of the inoculum.

8.7 Proliferation: The exponential part of the cell growth curve

Cell growth is associated with cell development and cell division, which is known as reproduction. Cell division refers to growth of cell population, whereas one cell grows and divides to produce two new cells. By using cell growth in context of cell development, this means the increasing of cytoplasmic and volume, as well as increasing in genetic material before the replication takes place.

8.7.1 Examination of cell proliferation

Cells were expanded in standard TCPC (surface area 25 cm²) to 60-80% confluence and subsequent detached with accutase. For more details see section 8.5.

Cell numbers were estimated by counting in a haemocytometer (see section 8.4). A specific amount of cell suspension according to a seeding density of 4000 or 3000 cells/cm² was transferred in new cell culture ware (9.6 cm², 25 cm², 75 cm² or 175 cm²) with a specific amount of α -MEM cell culture medium (+10% HS and 50 μ g/ml gentamicin) and incubated at 37 °C at either 5% CO₂/5% O₂ (hypoxic) or 5% CO₂/21% O₂ (normoxic) conditions. Cells from the same donor were used for both oxygen concentration (5% O₂ and 21% O₂).

8.7.2 The CuBiAn[®] XC biochemistry analyser

The CuBiAN[®] XC is a compact version of a bench top, random access biochemistry analyser, and based on photometric measurement principle (figure 41).



Figure 41: CuBiAN[®] XC photometric measurement analyser. (taken from (7)).

A broad range of interesting substances can be detected, in this study, including the measurement of glucose and lactate concentration. The CuBiAN[®] XC is equipped with a photometric measurement unit that allows for automatic selection from 340-800 nm. The end point and rate analysis are possible from 0.1-3.0 absorbance. The CuBiAN[®] XC analyser was started by following the instructions in the instrumental user manual. The procedure and measurement was executed according to the standard protocol of Roche innovatis AG (taken from (8)).

The metabolic activity of AD-MSC under different oxygen tensions was investigated via the CuBiAN[®] XC photometer analyser (see section 4.1.2).

The glucose consumption during long-term cell expansion in the static cell culture system was determined with formula 7.

$$\begin{aligned} & \text{Initial glucose concentration } \left(\frac{g}{l}\right) - \text{measured glucose concentration} \left(\frac{g}{l}\right) \\ & = \text{Glucose consumption} \end{aligned}$$

Formula 7: Calculation of the glucose consumption. Measurement was performed with the CuBiAN[®] XC photometer analyser.

8.8 Cell differentiation

To get the information of cell differentiation capacities, AD-MSC were plated on a fibronectin-coated 12-well cell culture plates with a density of 4000 cells/cm². Afterwards, the cells were cultivated for approximately 72 hours until full confluence of 60-80% was achieved in α -MEM cell culture medium (+10% HS and 50 μ g/ml gentamicin) at 37 °C at either 5% CO₂/5% O₂ (hypoxic) or 5% CO₂/21% O₂ (normoxic) conditions. After this cultivation, the cell culture medium was exchanged with specific osteogenic, chondrogenic, and adipogenic differentiation medium (supplemented with 0.5% GM, Miltenyi Biotec

GmbH). During the differentiation, all media were exchanged every third day. The total differentiation time was in total 21 days.

8.8.1 Fibronectin coated plates

Fibronectin is a protein of the extracellular Matrix (ECM) which procures the attachment of AD-MSC on collagen fibers and heparin side chains of proteoglycans because such cells attach to collagen very strongly [132].

Fibronectin binds to integrines (a cell adhesion molecule, create cell-matrix contact), which are located on the cell surface and establish transmembrane contact with cell's cytoskeletons. MSCs express fibronectin at a very high rate [133].

The Biocoat cell ware used for the differentiation is coated with human fibronectin (HFN). HFN is a broad range cell adhesion factor that can be used as a thin coating on tissue culture surface to promote adhesion of MSC. HFN exists as a soluble proteins in plasma and as an insoluble multimer in the extracellular matrix and on cell surfaces [132, 134].

Fibronectin coated cell culture ware provides the ability to control *in vitro* cellular environments for differentiation under physiologically conditions. ECM is secreted by MSCs to form intestinal matrix and basement membrane which constitutes the framework to which cells are anchored. Basement membrane separates cells from mesenchymal connective tissue and provides the orientation and stability required for the organization and development of the characteristics of a specific tissue. ECM has been recognized for its dynamic role in the regulation of differentiation [135].

8.8.2 Fixation of the cell layer

The cell layer was fixed for 45 min in the dark by 4 °C with the fixation solution for all planned staining. In this fixing procedure, the old cell culture media was removed, each well was washed thrice with 1 ml pre-warmed PBS (37 °C), PBS was removed and 1 ml of the fixation solution (4% formaldehyde in PBS) was added to each well. The fixed fibronectin coated plates were incubated at 4 °C for 40 min. All wells were then washed thrice with cold PBS and sealed with parafilm and stored at 4 °C as far as the staining procedures started.

8.8.3 Staining procedures

8.8.3.1 Alcian Blue staining

Proteoglycans which are located in the ECM of AD-MSC were visible by the application of Alcian blue staining. The fixed cells were washed thrice with 1 ml PBS and then incubated for 3 min in 3% acetic acid (1 ml/each well) at room temperature. The samples were then incubated with 1 ml of Alcian Blue solution (1% Alcian Blue 8GX in 3% acetic acid) for 30 min at room temperature. After the incubation, the cell layer was washed thrice with 1 ml 3% acetic acid and then several times with 1 ml distilled water. The availability of proteoglycans was detected with a light microscope.

8.8.3.2 Alizarin Red staining

Alizarin or 1, 2-dihydroxyanthraquinone (also known as Turkey Red) is an organic compound that has been used throughout as a red dye. It is composed to calcium so called EDTA-metal-ion-chelate complex. Alizarin Red stain detected calcium-inclusions in the extracellular matrix. The cell layer was washed thrice with 1 ml PBS and then incubated with 1 ml Alizarin Red solution (0.5% Alizarin Red in ddH₂O) for 15 min at room temperature. The cells were then washed thrice with 1 ml PBS. The existence of these inclusions was visualized by a light microscope.

8.8.3.3 Calcein staining

Calcein fluorescent staining has a high affinity to Ca-ions (Ca²⁺), which is accumulated in the ECM. The fixed cells were washed thrice with 1 ml distilled water and afterwards incubated with 1 ml of calcein solution (5 µg/ml in H₂O) in the dark at 4 °C over night. After the incubation time the cell layer was washed thrice with 1 ml PBS and subsequently covered with 1 ml PBS. The fluorescence of the calcein was detected at an emission wavelength of 530 nm and at an excitation wavelength of 480 nm.

8.8.3.4 DAPI staining

4', 6-diamidino-2-phenylindole dihydrochloride (DAPI) is a fluorescent stain and binds to regions in the DNA. As a result, the cell nucleus of AD-MSK can be visualized. The cell layer was washed thrice with 1 ml PBS and then incubated with 1 ml DAPI solution (2 µl stem-solution/ dye buffer; stem-solution: 500 µg/ml DAPI in H₂O; dye buffer: 100 mM Tris pH 7 (12.11 g/l), 150 mM NaCl (8.76 g/l), 1 mM CaCl₂ (water free: 0.11 g/l), 0.5 mM MgCl₂ (hexahydrat: 0.1 g/l), 0.1% Nonidet-P40), for 15 min at 37 °C. Afterwards the cells were washed thrice with 1 ml PBS. The fluorescence of DAPI was detected at an emission wavelength of 460 nm and at an excitation wavelength of 360 nm.

8.8.3.5 Oil Red O staining

Adipocytes are detected with Oil Red O staining, which is a diazo-dye and binds directly to fatty acid and triacylglyceride. These adipocyte vesicles, which are full of triacylglyceride, were visualised by Oil Red O staining as red vacuoles. The fixed cell layer was washed twice with 1 ml ethanol (50% w/v) for 2 min and afterwards was incubated with 1 ml Oil Red O solution (0.5% in propylene glycol) for 20 min at room temperature. After incubation, the cells were washed twice with 1 ml ethanol (50% w/w) for 2 min and were washed with 1 ml PBS for 5 min. The availability of red vacuoles was detected with a light microscope.

8.8.3.6 Von Kossa staining

The Von Kossa stain is used to quantify mineralization in cells. The stain principle is a precipitation reaction in which silver ions react with phosphate in the presence of an acidic

material as a result photochemical degradation of silver phosphate to silver that occurs under light illumination [136].

Therefore the Von Kossa stain aids the visualisation of targets of interest, namely intracellular and extracellular cellular components such as DNA and proteins by the deposition of metallic silver particles on the targets of interest. Fixed cells were washed thrice with 1 ml distilled H₂O, followed by incubating with 1 ml AgNO₃-solution (5% in ddH₂O) for 30 min in the dark at room temperature. Afterwards, the cell layer was washed thrice with 1 ml ddH₂O, followed by irradiation with UV-light (wavelength of 365 nm) for 2 min at room temperature. Eventually the background was decolorized with 1 ml 5% Na₂S₂O₃ in ddH₂O for 2 min. The subsistence of calcium inclusions in the extracellular matrix were detected with a light microscope.

8.8.4 Metabolites measurement during cell differentiation

During the long-term cell differentiation, on day 3, 7, 14, and 21, glucose and lactate measurements were performed. All analyses were tested with the specific differentiation media (Miltenyi) to a reference media (α -MEM +10% HS +0.5% GM). Especially for glucose plotting the g/l values in the supernatant (explicit from the CuBIAN[®]XC photometric measurement analyzer, see section 8.7.2) does not make a lot of sense, since the media already have different glucose concentrations to begin with. As mentioned in section 8.7.2 the glucose consumption is calculated according to formula 7. All indications of the initial glucose and lactate concentrations in the fresh media are seen in table 5, section 4.1.4.

8.9 Comparison of different enzymatic means of dissociation adherent monolayers of AD-MS

The dissociation of adherent AD-MS with Trypsin S, Trypsin P, Accutase and TrypLE[™] Express under normoxic conditions (21% O₂) were compared.

8.9.1 Cell viability assessment

Frozen AD-MS were first revitalized, cultivated over 3 passages and seeded at a cell density of exactly 4000 cells/cm² (total cell number was 3.84 x 10⁴ cells in a 25 m² cell culture flask) in α -MEM cell culture medium (+10% human serum and 0.5% gentamicin) for 72 hours. The cells were plated on 2 tissue culture 6-well plates (surface area = 9.6 cm², n=3/enzyme). After 3 days of incubation, the α -MEM cell culture medium was aspirated with a suction pump. Immediately, the extant cell layer was washed with pre-warmed PBS (600 μ l) and removed. 600 μ l enzyme per well was transferred with caution and the exact time was noted (the first measuring point was after 5, the second after 15 and the third after 45 minutes) while the cells were incubating at 37 °C in a humidified atmosphere of 5% CO₂ and 21% O₂. The detached cells were homogenised by carefully pipetting and 100 μ l cell suspension sample was taken and mixed with 100 μ l pre-warmed α -MEM cell culture medium (+10% HS and 0.5%

gentamicin). 20 µl of trypan blue and 20 µl of the mixed cell suspension was immingle (1:2 dilution) and the living and dead cell numbers were estimated by counting in a haemocytometer.

The cell viability was estimated according to the following formula:

$$\frac{\text{viable cells}}{\sum \text{viable} + \text{dead cells}} * 100 = \text{viable cells (\%)}$$

Formula 8: Cell viability (%).

8.9.2 Preparation of compensation samples of the flow cytometer

Compensation is required for flow cytometry and refers to the manufacturer's instructions and software manual for a more detailed compensation procedure for the instrument which is used. All fluorochromes have excitation and emission spectra. The excitation spectrum is a range of light wavelengths that add energy to a fluorochrome, causing it to emit light in another range of wavelengths, the emission spectrum. Within a flow cytometer, the appropriate ranges of excitation and emission wavelengths are selected by band pass filters. However, when emission spectra overlap, fluorescence from more than one fluorochrome may be detected. To correct for this spectral overlap, a process of fluorescence compensation is used, seen in table 13. This ensures that the fluorescence detected in a particular detector derives is solely from the fluorochrome that is being measured. An optimal compensation (see section 4.3.2) for the flow cytometer analysis is therefore indispensable and extremely important before starting the immune-fluorescent staining.

Table 13: Used parameters of the flow cytometer compensation.

Fluorochrome	% Fluorochrome	Spectral overlap
FITC	APC	0.02
PE	APC	0.01
PerCP-Cy5.5	APC	1.01
APC	FITC	1.36
PE	FITC	34.87
PerCP-Cy5.5	FITC	3.00
APC	PE	0.05
FITC	PE	0.54
PerCP-Cy5.5	PE	8.23
APC	PerCP-Cy5.5	7.22
FITC	PerCP-Cy5.5	0.11
PE	PerCP-Cy5.5	0.05

The cell number after harvesting with Accutase, TrpLE™ Express and Trypsin was determined and five aliquots (PerCP, PE, APC, FITC, blank), each with 5 x 10⁵ AD-MS, was

were taken. The cell suspensions were then centrifuged at 300 x g for 10 min. Each supernatant was completely aspirated and the samples for PerCP, PE, APC and FITC were re-suspended in 100 µl of buffer (buffer solution containing: phosphate-buffered saline (PBS), pH 7.2, 0.5% bovine serum albumin (BSA) and 2 mM EDTA). The aliquot blank was re-suspended in 500 µl of buffer. 10 µl of CD73-Biotin was added in aliquot PerCP, CD105-PE in aliquot PE, 10 µl of CD73-APC in aliquot APC and 10 µL of CD90-FITC was put in aliquot FITC. Each mixed aliquot was promptly incubated for 10 min in the dark at 4 °C. All aliquots were then washed by adding 2 ml of buffer and centrifuged at 300 x g for 10 min, followed by aspirating the supernatant completely. 10 µl of Anti-Biotin-PerCP was added to aliquot PerCP, mixed and incubated for 10 min in the dark at 4 °C. Afterwards, the cells were washed with 2 ml of the buffer and centrifuged at 300 x g for 10 min, followed by aspirating the supernatant completely. Finally, each cell pellet was separately re-suspended in 600 µl of buffer and the compensation (table 13) of the flow cytometer was started according to the standard protocol provided (BD FACSCanto II flow cytometer) (taken from (8)).

8.9.3 Immuno-fluorescent staining

The immuno-fluorescent staining of AD-MSK was performed according to the standard protocol of MSC Phenotyping Kit, Human-Miltenyi Biotec (taken from (9)). The used Flow cytometer (BD FACSCantoll) was adjusted with different parameters, seen in table 14.

Table 14: Used parameters of BD FACSCantoll.

Filter	Voltage	Log
FSC	200	
SSC	360	
APC	550	✓
FITC	450	✓
PE	500	✓
PerCP-Cy5.5	480	✓

All except FSC (forward scatter) and SSC (side scatter) represented the intensity in a logarithmical scale. In contrast, FSC and SSC worked in a linear range (table 14). In brief, AD-MSK were harvested using different digestive enzymes. In this study Accutase, TrpLE™ Express and Trypsin (Sigma) were used, followed by determining the cell number with a haemocytometer. Two aliquots (1 and 2) were taken and each was set up to a concentration of 1×10^6 cells. Afterwards the two separate cell suspensions were centrifuged at 300 x g for 10 min, followed by aspirating the supernatant completely. Each aliquot was re-suspended in 100 µl of buffer (buffer solution containing: phosphate-buffered saline (PBS), pH 7.2, 0.5% bovine serum albumin (BSA) and 2 mM EDTA). 10 µl of the MSC Phenotyping Cocktail (table 14) was added into aliquot 1 and 100 µl of the Isotype Control Cocktail was taken into aliquot 2. Both were mixed well and incubated for 10 min in the dark at 4 °C. The cells were

then washed by adding 2 ml of the buffer and centrifuged again at 300 x g for 10 min, followed by aspirating supernatant completely. Each cell pellet was then re-suspended in a suitable amount of buffer (1 ml) for an analysis by flow cytometry. At least, 1×10^5 gated events were acquired on a logarithmical fluorescence scale.

Table 15: Cocktail of fluorochrome-conjugated monoclonal antibodies.

Antibody	Manufacturer	Cocktail
CD14-PerCP	Miltenyi Biotech GmbH	MSC Phenotyping Cocktail, human
CD20-PerCP	Miltenyi Biotech GmbH	MSC Phenotyping Cocktail, human
CD34-PerCP	Miltenyi Biotech GmbH	MSC Phenotyping Cocktail, human
CD45-PerCP	Miltenyi Biotech GmbH	MSC Phenotyping Cocktail, human
CD73-APC	Miltenyi Biotech GmbH	MSC Phenotyping Cocktail, human
CD90-FITC	Miltenyi Biotech GmbH	MSC Phenotyping Cocktail, human
CD105-PE	Miltenyi Biotech GmbH	MSC Phenotyping Cocktail, human
CD90-FITC	Miltenyi Biotech GmbH	MSC Isotype Control Cocktail, human
CD105-PE	Miltenyi Biotech GmbH	MSC Isotype Control Cocktail, human
CD73-APC	Miltenyi Biotech GmbH	MSC Isotype Control Cocktail, human
CD73-Biotin	Miltenyi Biotech GmbH	MSC Isotype Control Cocktail, human
Anti-Biotin-PerCP	Miltenyi Biotech GmbH	MSC Isotype Control Cocktail, human

8.10 Short-term cell expansion with alternative surfaces

AD-MSC which are problematic to detach from traditional culture-ware (in this case T-25 flask and 6 well plate, Starstedt) by enzymatic methods, may benefit from alternative culture ware, (culture ware with UpCell™ Surface). This technology is based on temperature reducing processes and as a consequence, cell detachment will be guaranteed.

This study compared the absolute yield of AD-MSC harvested from different UpCell™ Surface formats using temperature reduction with those which were harvested from so called traditional culture-ware (T-25 flask and 6 well plate) by using accutase as the digestive enzyme under normoxic (21% O₂) and hypoxic (5% O₂) conditions. Cell growth was inspected in both types of surfaces.

8.10.1 Thermo Scientific Nunc UpCell™ surfaces under normoxic condition

***In vitro* cell culture**

For the expansion in the Thermo Scientific NuncUpCell™ surfaces, frozen AD-MSC were first revitalized. Then, during seeding with 4000 cells/cm², pre-warmed (37 °C) α -MEM cell culture medium (+10% HS and 0.5% gentamicin) was used to ease attachment of the cells. The most important step was avoiding scratching the surface with pipette tips because this may destroy the whole temperature responsible surface. The minimum attachment time range of AD-MSC was 12 to 24 hours. The cells were cultured at 37 °C in a humidified atmosphere

of 5% CO₂ and 21% O₂ for 5 days in 4 different culture wares (Thermo Scientific Nunc UpCell™ 3.5 cm Dish (174904), Thermo Scientific Nunc UpCell™ 6.0 cm Dish, Sarstedt T-25 cell culture flask and Sarstedt 6 well plate, one of six was used). At days 3, 4 and 5, light microscope pictures for qualitative and the total cell numbers for quantitative conclusions were estimated by counting in a haemocytometer. The NuncUpCell™ surfaces became hydrophobic below 32 °C, followed by cell detachment from the surface. To avoid inspected cell detachment during an observation under a light microscope, it was necessary to keep short in order to prevent cooling and undesired cell detachment (see figure 19, section 4.2.1).

8.10.2 Detachment of cells by using temperature reduction

AD-MSK on the Thermo Scientific NuncUpCell™ surface with a density of approximately 60-80% confluence, without cell-cell junctions are ready to detach. The surfaces were moved from a 37 °C incubator on a rotary orbital shaker (79 rpm) at room temperature (approximately around 20-23 °C) in order to detach the cells under hydrophobic condition with mechanical forces as aid for an optimal detachment (figure 42).

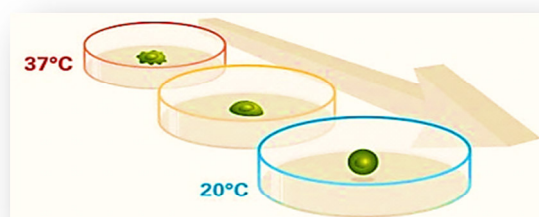


Figure 42: Detachment of AD-MSK. The covalently immobilized polymer poly (N-isopropyl acrylamide), or PIPAAm layer is hydrophobic at 37 °C, allowing cells to attach and grow. When the temperature is reduced to below 32 °C, the PIPAAm layer becomes hydrophilic, binds water and swells, resulting in the release of adherent cells (taken from (5)).

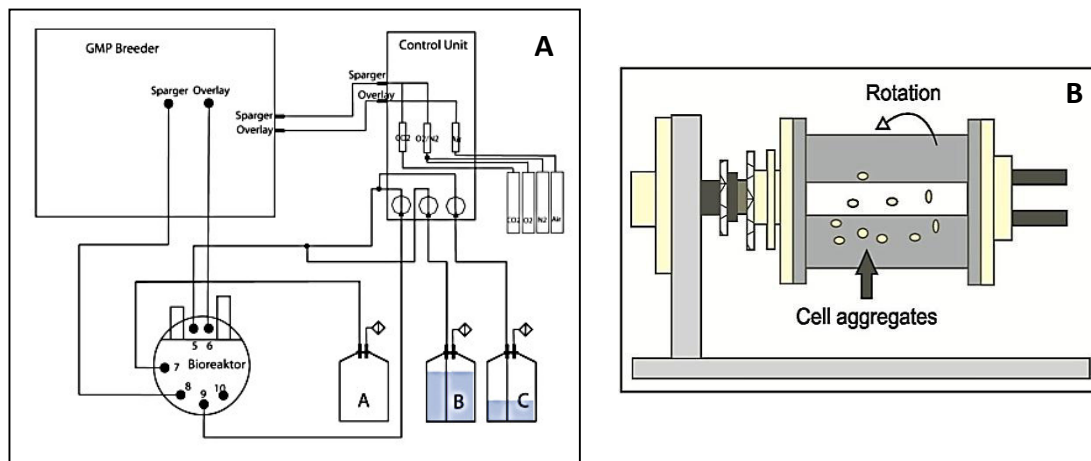
After a detachment time of 45 min, the cells were observed under the light microscope to determine whether they are optimally detached from the surface or not. The detached cells were promptly washed with a specific amount of pre-warmed (37 °C) PBS (2 ml) for 2 min under sterile conditions. Non-adherent cells were removed by this washing step and transferred in 50 ml falcon tubes, followed by centrifuging at 300 x g for 5 min. After aspirating the supernatant the harvest cells were carefully flicked and then added with 430 µl α-MEM cell culture medium (+10% HS and 0.5% gentamicin). Then, cell numbers were estimated by counting in a haemocytometer (see section 8.4).

8.10.3 Thermo Scientific NuncUpCell™ surface under hypoxic condition

The cell expansion as well as the cell harvest of AD-MSK in a humidified atmosphere of 5% CO₂ and 5% O₂ was executed according to the standard protocol of Thermo Scientific NuncUpCell™ Surface. For more details see section 8.10.1 and 8.10.2. The types of the culture ware (Thermo Scientific Nunc UpCell™ 6.0 cm Dish (174906), Sarstedt 6 well plate) and the humidified atmosphere (5% CO₂ and 5% O₂) were different during this experiment.

8.11 Cell expansion in the Z[®]RP 2000 H bioreactor

The tubing system, all sensors, and the bioreactor were sterilized in 70% ethanol, then further sterilized in an autoclave according to the standard protocol of Z[®]RP cell-cultivating-system of Zellwerk GmbH (9) and finally, via UV-sterilization in the breeder. The bioreactor was sterilized in ethanol for approximately 1 hour. After the sterilization, the feed-flask, waste-flask, and the tubing system was connected to the reactor and all sensors were installed according to the manufacturer's piping and instrumentation diagram of the Z[®]RP 2000 H bioreactor (figure 43). In addition to the installation, the entire system was filled up with 120 ml of pre-warmed α -MEM cell culture medium (+10% HS and 0.5% gentamicin) for 24 hours and the sterile run was performed. After 24 hours, 5 ml of cell culture media sample was taken from the reactor, followed by transferring to a 25 cm² cell culture flask and incubating at 37 °C in an atmosphere of 5% CO₂ and 5% O₂ for 72 hours (hypoxic condition). This was done to check the sterility of the system and afterwards glucose and lactate concentrations were measured via the Nova BioProfile analyser. The sense of this working step was in order to get the right information of metabolic consumption as well as production.



- A: Waste flask
- B: Feed flask
- C: Gas flask

Figure 43: A-Instrumentation and piping diagram of the Z[®]RP 2000 H bioreactor. B-Principle of cell attachment on polycarbonate cell carrier slides (taken from (10)).

The expansion of AD-MSK in the Z[®]RP 2000 H bioreactor started with the revitalization of deep-frozen AD-MSK (stored at -180 °C), following by cultivation over 2 passages. The

seeding in the bioreactor was at a cell density of 1500 cells/cm². AD-MSC were seeded on both sides of the polycarbonate cell carrier slides (figure 43-B) with an attaching time of 24 hours for each side of the slide. This step was referred to as first and second attachment of the AD-MSC, and in parallel, a static control flask with 75 cm² surface area was made with a cell density of 1500 cells/cm² under hypoxic condition (5% O₂ tension) for a cultivation time of 5 days (Cell expansion in the Z[®]RP 2000 H bioreactor was performed over 5 days). After the first attachment, the rotation bed was activated for a quarter turn, followed by stopping the rotation and then filling the reactor with 1.5 x 10⁶ cells in 130 ml pre-warmed α -MEM cell culture medium (+10% HS and 0.5% gentamicin). The total cell count was actually 3 x 10⁶ cells in the rotating-bed-system. After attachment on both sides of the polycarbonate cell carrier slides, bed rotation and medium circulation were induced. The medium circulation and the bed rotation were set on 0.1 ml/min and 0.3 U/min. Once per day, always at the same time, cell culture media from the rotating bioreactor was sampled by using a syringe via a membrane located on the bioreactor, for metabolic analysis with the Bioprofile 100 Plus analyser (see section 8.11.1). This instrument observed the consumption of glucose as well as the production of lactate and the weight of the feed and waste flask were noted for gravimetric analysis.



Figure 44: Z[®]RP 2000 H bioreactor system with control unit and breeder (taken from (11)).

Moreover the breeder as well as the reactor temperature was set at 37 °C. The atmosphere was set on 5% CO₂ and 5% O₂ for cultivated AD-MSC (hypoxia). Therefore, this cultivation was performed under hypoxic condition (5% O₂). After 5 days of the expansion, the cells were harvested. The cell-harvest started by emptying the reactor's cell culture medium using the pump, then filling with 130 ml pre-warmed PBS (37 °C) and washing the attached cells for 5 min at a rotation speed of 1 U/min. Afterward, the reactor's PBS was also purged, followed by filling with 80 ml of pre-warmed accutase (37 °C). This enzymatic reaction had an incubation time of exactly 20 min with a rotation speed of 0.3 U/min. After this incubation with accutase, the harvested cells were collected in 50 ml falcon-tubes. The next step was a centrifugation for 5 min at 300 x g, followed by aspirating the supernatant carefully with a suction pump. The originated cell-pellets were then softly flicked and re-suspended in 30 ml α -MEM cell culture medium (+10% HS and 0.5% gentamicin). At the end of this dynamic cultivation, three analyses were performed. First the cell count was determined by counting in

a haemocytometer, second a MTT test was performed and last but not least flow cytometric analysis was done.

8.11.1 Nova BioProfile analyser

Nova BioProfile analysers (figure 45) include four models of fully automated cell culture analysers with test menus of two to ten tests, including chemistry, gases, and electrolytes. Each model offers automatic calibration, one-button operation, and 40 position batch processing capability. The analyser measures glucose, lactate, acetate, ammonium, pH, sodium, potassium and a choice of either phosphate or glycerol. The measurement principle is on the one hand based on potentiometric electrodes (pH, CO₂, NH₄⁺, Na⁺, K⁺, acetate), which measure charged ions and also has a membrane that is selective to the ion being measured.

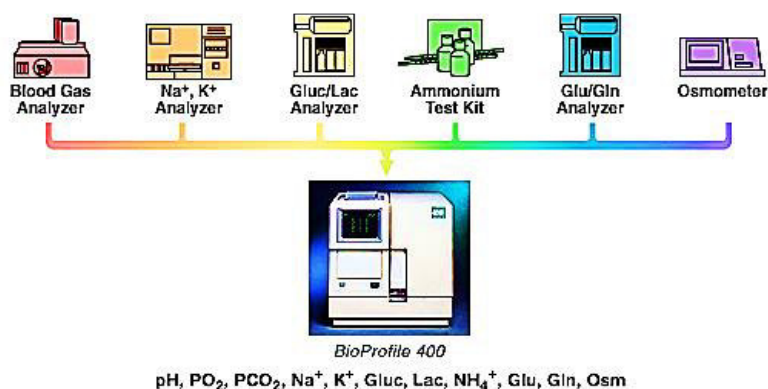


Figure 45: Principle of the Nova BioProfile analyser 100 plus (taken from (12)).

On the other hand this analyser uses an amperometric electrode, which consists of an oxygen permeable membrane covering a platinum cathode and voltage proportional to the concentration of the measured glutamate, glucose, lactate and glutamine biosensors are amperometric electrodes. These electrodes have immobilized enzymes incorporated into their membranes and as a result, they develop a current proportional to the substrate being measured. The first described measurement principle was used for the glucose and lactate measurements during the dynamic cell expansion in the Z[®]RP 2000 H bioreactor system.

The glucose consumption was calculated according to formula 7 (see section 8.7.2).

The Nova BioProfile analyser was started by following the instructions in the instrumental user manual. The procedure and measurement were executed according to the standard protocol of Nova biomedical Bioprofile automated 100 plus analyser (13).

8.11.2 Metabolic activity assessment (MTT assay)

The MTT assay is a photometric method that enables the determination metabolic activity of AD-MS, which successfully measures the viability of the cells. Production of the yellow colorant MTT (3-(4, 5-Dimethylthiazol-2-yl)-2, 5-diphenyltetrazolium bromide) relies on enzymatic reduction by NADH in mitochondria where purple formazan is obtained and

formazan crystals grow inside the cell. These crystals are then dissolved by addition of the detergent SDS (sodium dodecyl sulfate) in diluted hydrochloric acid (figure 46).

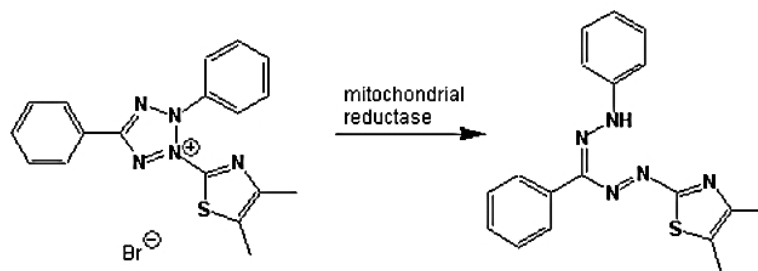


Figure 46: The reduction of MTT.

The maximum absorbance of the colored solution was measured at 570 nm and as a reference at 630 nm to determine the effect of the media for the measurement. A sample with all reagents but without cells were measured as blank for further calculations. The final optical density was determined by calculating the difference of the absorbance maximum at 570 nm and 630 nm.

The photometric method started by removing old cell culture medium via a suction pump, followed by washing the cells with 1 ml pre-warmed PBS. In the meantime, a solution of 10% MTT (1.2 ml MTT stock solution and PBS) was prepared. Afterwards, the PBS was removed and the total cell number of expanded AD-MSC in the Z[®]RP 2000 H was calculated (see section 8.4). Afterwards the counted cells were centrifuged at 300 x g for 5 min. In addition the supernatant was removed and the cell pellet was re-suspended in 1 ml α -MEM stock solution. 7.3×10^4 AD-MSC were mixed with 110 μ l of the MTT working solution and added in each well of a 96-well cell culture plate. In addition, the cells were incubated at 37 °C in a humidified atmosphere of 5% CO₂ and 5 or 21% O₂ for 4 hours (the oxygen tension of 5 or 21% O₂ depends on the experiment). Cultivated AD-MSC under hypoxic conditions were put in an incubator with 5% O₂ tension and cells which were expanded under normoxic condition were incubated with 21% O₂. 90 μ l of the SDS solution was then added in each well and the plates were scanned via 800 dpi resolutions, followed by incubating the cells over night at 37 °C/5% CO₂ and 5 or 21% O₂. Next, the plates were taken out of the incubator and the cell viability with a photometric method was started according to the instructions in the instrumental user manual. The procedure and measurement was executed according to the standard protocol of Thermo Scientific Multiskan[®]FC Microplate Photometer. Besides, the samples of the 75 cm² control flask were performed in the same way as mentioned before. Based on the raw data from the Thermo Scientific Multiskan[®]FC Microplate Photometer, calculations were carried out by subtracting each reference value from its maximum absorption value. This was performed for all samples and blanks. These values were then used to calculate averages, standard deviations, and standard errors of the mean (SEM). Blank values (average of all eight medium measurements) were subtracted from the sample values.

8.12 Dynamic cell expansion in the TubeSpin[®] bioreactor

The current opinion in the field of stem cell cultivation and tissue engineering implies attempts to create *in vitro* conditions which mimic the physiological and biochemical environment of the cells within the body. In course of these attempts, efforts were taken to cultivate stem cells in a 3-dimensional (3D) environment. One method to achieve this is to generate so called cell-spheroids which are composed of a defined number of cells. The size of these spheroids can be a few μm (e.g. by using hanging drop technologies) up to $500\mu\text{m}$. The challenge in cultivation of relative large spheroids is the need of nutrition and a correct gas composition in the core. Whereas the vascular system of the body provides oxygen and glucose to all tissues and also arrange disposal of metabolites, such system is not available in artificial formed cell clusters.

To ensure such supply, various bioreactor systems were designed to establish an artificial environment which promotes diffusion processes and on the other hand minimize mechanical sheer stress. One of these systems can be found in the disposable TubeSpin[®] bioreactor (Greiner-Bio-One) provided with filter tops made of polypropylene. To ensure gas exchange, the filter caps exhibit several holes covered with a PTFE coated capillary pore filter membrane with a pore size of $0.2\ \mu\text{m}$. The TubeSpin[®] bioreactor is also known as (described in literature as synonyms mostly according to brand designations) Tube-Spin[®] bioreactors, CultiFlask or CELLSTAR[®] CELLreactor).

The actual aim of this project was to generate spheroid aggregates from AD-MSC and elucidate the proliferation of AD-MSC during dynamic cultivation in 3D structures without carriers or scaffolds. This was accomplished in the TubeSpin[®] bioreactor. Additional, cells were analysed in regard to cell metabolic activity via MTT assay.

In this work AD-MSC spheroids were formed by using an aggregation technique in U-bottom plates, followed by transferring to the TubeSpin[®] bioreactor, which has the advantage that this 3D cell-culture system does not has his own agitator, which would be responsible for the moving, but instead works by using an orbital shaker, which is controlled extraneous and produces the optimal dynamic in the whole suspension-bioreactor without any shear forces (figure 47).



Figure 47: Tube Spin bioreactor (taken from (14)).

Creation of 3D-cell-aggregates

8.12.1 Prior-cultivation (static) in TCPS

For the expansion in the TubeSpin[®] bioreactor, frozen AD-MSC were first revitalized and then cultivated over 4 passages (P1 to P4) in cell culture flask with 175 cm² or 75 cm² surface areas at a cell density of 4000 cells/cm² according to established SOP 0401 (AG Kasper), see section 8.3 under static conditions (37°C; 5% CO₂ and 21% O₂).

8.12.2 Spheroid generation

After the first cultivation, the cells were transferred to a 1.5 ml reaction tubes according to protocols published by Hildner et.al. [130] with an initial total cell number of 3×10^5 cells, followed by centrifuging at 350 x g for 5 min. During this step 3D-cell aggregates were generated. A total of 40 3D-cell spheroids were generated and were put in the incubator at 37 °C and 21% O₂ tension for 157 min under constant shaking on a shaking platform (mini gyro rocker at 13 rpm). Additionally cells were seeded with a density of 3000 cells/cm² in 4 T-75 flasks as a static control for later analysis (static reference).

8.12.3 Second cultivation in U-bottom 96 well plates

After the aspiration, the second-cultivation started and each created spheroid (3×10^5 cells/spheroid) was transferred in the U-bottom plate (figure 48) and added with 200 µl pre-warmed α -MEM cell culture medium (+10% HS and 0.5% gentamicin) for 24 hours at 37 °C and 21% oxygen concentration on an orbital shaker (13 rpm).

After incubation in 1.5 ml tubes, cell aggregates (spheroids) appear detached from tube wall and could be easily transferred into separate wells of a silicon coated round U-bottom 96 well plate via micropipette and covered with 200 µl pre-warmed α -MEM cell culture medium (+10% HS and 0.5% gentamicin). For this purpose micropipette tips were cut with a sterile scissor for extension of the tip orifice to guarantee a contactless transfer of the spheroids.

As recently shown by Baraniak et. al. [137] spheroids could also be generated without centrifugation as mentioned above (section 8.12.2). To elucidate the influence of mechanical stress through the centrifugation procedure, alternative spheroids were created directly in U-bottom 96 well plates (figure 49). Therefore, 4 wells of the U-bottom plate were seeded with 3×10^5 cells in 200 µl pre-warmed α -MEM cell culture medium (+10% HS and 0.5% gentamicin) each. Cells, unable to adhere on siliconized surfaces concentrated in the centre of the U-shaped wells through gravitational forces.

Spheroids formed without the application of a centrifuge as well as spheroids formed by the application of a centrifuge were incubated in U-bottom plates for additional 24 hours on a shaking platform (13 rpm, 37°C) under normoxic condition.

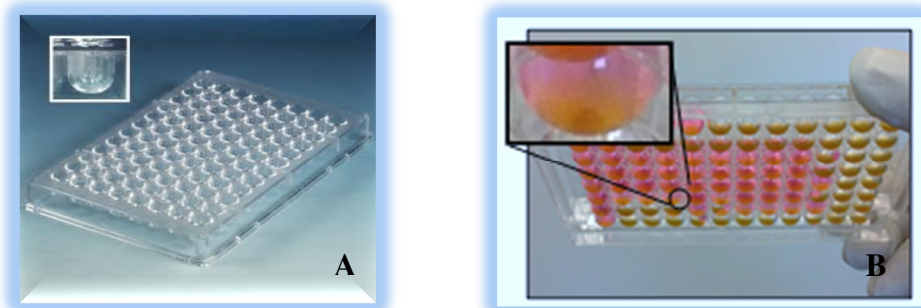


Figure 48: A-U-bottom 96 well plate (taken from (15)). B-Original picture of the used U-bottom 96 well plate.

8.12.4 Morphological examination of created 3D-cell-aggregates

In addition, phase contrast images of the spheroids created by AD-MSC were obtained after the second cultivation in U-bottom 96 well plates, before seeding in the TubeSpin[®] bioreactor. Different spheroids were assessed visually for differences in the cell dimension and morphology and the cross-section area of spheroids was measured by using a light microscope (40 x lens) to get the suitable information of the cell-clusters.

8.12.5 Expansion in the TubeSpin[®] bioreactor

Prior to transfer of the spheroids into TubeSpin[®] bioreactor, 4 spheroids were transferred into separate 1.5 ml tubes, lysed and analysed for of total single nuclei (see section 8.12.3). Subsequently, 60 spheroids with an average of 1.1×10^5 cells/spheroid were transferred into 15 TubeSpin[®] bioreactors containing 10 ml pre-warmed α -MEM cell culture medium (+10% HS and 0.5% GM) each. In total, 4 spheroids were seeded in 1 TubeSpin[®] bioreactor resulting in a cell count of 4.4×10^5 cells/TubeSpin[®] bioreactor. The transfer of the spheroids from U-bottom plates to the TubeSpin[®] bioreactor was carried out via micropipette and tips modified as described above. 3D-cell-spheroids were cultivated for 7 days in TubeSpin[®] bioreactor (n=3) on a shaking platform (mini gyro rocker). α -MEM cell culture medium (+10% HS and 0.5% GM) was exchanged after 3 days of cultivation. Through anticipated increase of spheroid mass (weight) and the fact that the Tube Spin[®] bioreactor's surface is not coated with re-pallets, an increase of the rocking speed from 13 rpm to 60 rpm was carried out to avoid adherence and aggregation of single spheroids on centre of the conical TubeSpin[®] bioreactor bottom. Total volume and rocking speed accord to protocols, recently published by Baraniak et.al. [137] and were modified to actual spheroid diameters. The cell proliferation capacity was determined after each time point (24, 48, 72 and 168 hours) by using crystal violet staining assay (see section 8.12.6).

8.12.6 Cell proliferation assay of AD-MSC in the suspension TubeSpin® bioreactor

Cell count of single spheroids was accomplished by simultaneously lysis and nuclei staining through incubation of whole spheroids or cell aggregates deriving from spheroids in a staining solution composed of citric acid [0.1M] and crystal violet [0.1%] in ddH₂O by using crystal violet cell colony staining assay. Obviously loss of nuclei during the lysis/staining procedure necessitated an ongoing modification of the protocol. Protocol adjustments include initial incubation of spheroids in 1ml trypsin (37°C, 8 min), subsequent vigorous vortexing and several up-and-down pipetting to separate single cells from the main aggregate. Although modifications result in satisfactory cell counts in later approaches, it should be noted that first cell counts may not reflect the actual cell number. Spheroids derived from U-bottom plates were transferred in 200 µl α-MEM cell culture medium (+10% HS and 0.5% gentamicin) to 1.5 ml centrifuge tubes and mixed with 600 µl staining solution. After an incubation time of 2 hours at room temperature (RT), spheroids were disrupted through gently up-and-down pipetting. Subsequently 2 x 15µl of the suspension were transferred to a Neubauer counting chamber and counted (8 squares/sample). Calculation of the cell number was accomplished using the following formula:

$$\frac{\text{Cells}}{\text{ml}} = \frac{\sum \text{cells}}{\text{squares}} \times \text{dilution factor} \times 10^4 \text{ cells}$$

Formula 9: Calculation of the cell number.

After dynamic cultivation of spheroids in the TubeSpin® bioreactor (4 Spheroids/bioreactor) for 24 hours, α-MEM cell culture medium (+10% HS and 0.5% GM) was removed and 400 µl staining solution (crystal violet) was added directly into the TubeSpin® bioreactor. The 3D structure of the spheroids was disrupted through gently vortexing for 10 seconds followed by an incubation step for 2 hours at RT. Subsequently, samples were vortexed again for 10 seconds and remaining aggregates finally disrupted through up-and-down pipetting. Following cell counts were realized as described above. Spheroids deriving from the TubeSpin® bioreactor after dynamic cultivation for 48 hours, were centrifuged direct in the TubeSpin® bioreactor (n = 4 spheroids/TubeSpin® bioreactor) at 300 x g for 5 minutes. After one washing step with 1 X PBS, spheroids were initial disrupted through addition of trypsin (1ml/TubeSpin® bioreactor) and incubated for 8 minutes at 37 °C. After vigorous vortexing, the cell suspension was again centrifuged at 300 x g for 5 minutes. Remaining trypsin was removed via suction device and 800 µl staining solution was directly added to the pellets. Cells were re-suspended in the staining solution via vigorous vortexing and the samples were incubated for a minimum of 2 hours at RT. Subsequent cell counting was carried out as described above. Further cell counts (after 72 h and 96 h) were carried out using the modified protocol which was applied on spheroids cultivated for 48 hours (described above). The

arithmetic mean of cells per spheroid was accomplished by division of the total cell number from the TubeSpin[®] bioreactor (n=3) through factor 12 (4 spheroids/TubeSpin[®] bioreactor). The results over a cultivation period of 96 hours are displayed in figure 49.

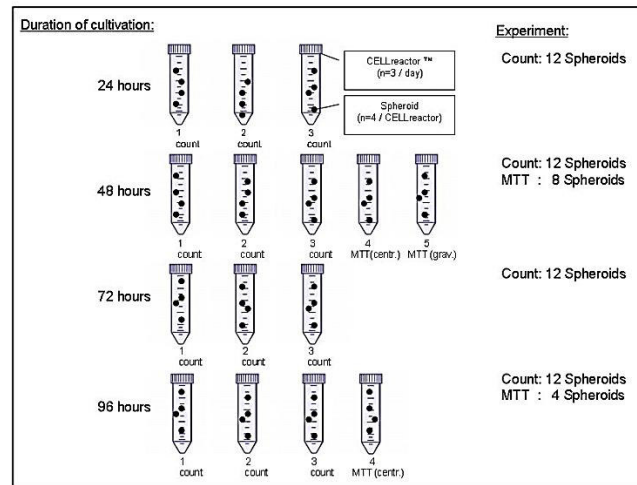


Figure 49: Experimental set-up- Dynamic 3D-cell cultivation in the TubeSpin[®] bioreactor.

According to figure 49 the 3D-cell-spheroids were either analysed by cell counting (count) to determine the proliferation rate or by MTT assay (MTT centr.) to determine the metabolic activity of AD-MSC after cultivating in the bioreactor. To compare the metabolic activity of the previous mentioned two cell-aggregate formation methods (see section 4.5.2), the cells used for MTT assay were either generated by centrifugation or by gravitational force.

8.12.7 Metabolic activity assessment (MTT assay)

The viability of spheroid derived cells was determined via MTT assay after 3 and 7 days of dynamic spheroid cultivation (see section 8.11.2). Cells (4 Spheroids/TubeSpin[®] bioreactor) were washed one time with 2 ml 1 X PBS followed by centrifugation at 300 x g for 5 minutes. The supernatant was discarded and the pellet was re-suspended via flicking of the tube. After further re-suspension in 1.5 ml basal medium, cell suspension was aliquoted to separate wells of a 96 well plate (99 µl each) and supplemented with 10% 3-(4,5-Dimethylthiazol-2-yl)-2,5-diphenyltetrazoliumbromid (MTT) solution (=11 µl MTT in PBS [5µg/µl]). MTT assay was carried out according to established protocols (SOP 0202, AG Kasper); see also section 8.11.2.

8.13 Statistical analysis

Experimental results were represented as mean (MN) ± standard deviation (SD) of the trials. Statistical significance was accepted at p-value < 0.05 by using one-sample Student's t-tests.

9 Supplementary materials

Flow cytometric analysis of different digestive enzymes

Flow cytometric analysis was performed at passage 6 and passage 9 of AD-MSC to investigate the influence of surface markers via flow cytometric analysis of surface antigen expression. Cultured AD-MSC were stained with the phenotype (red) and isotype cocktail (grey) against CD14, CD20, CD34, CD45, CD73, CD90, CD105 and isotype control IgG-conjugated fluorophores, as seen in figure 50-52.

According to figure 50-52 (below), flow cytometric analysis of AD-MSC demonstrated that AD-MSC were negative for hematopoietic (CD34, CD45, CD20) and endothelial (CD14) markers and that they were positive for specific immune-phenotypic MSC markers (CD73, CD90, CD105) after passage 6 and 9 by using Accutase, Trypsin S and TrpLE™ Express, see also section 4.3.2.

These histograms showed that after using different digestive enzymes the adipose-derived cells still have an MSC-like immuno-phenotype, as defined by ISCT (International Society of Cellular Therapy) standards [126].

In conclusion, by using Accutase, TrpLE™ Express and Trypsin S, the MSC population expressed CD105, CD73 and CD90 and lacked expression of CD45, CD34 and CD14.

9.1 Accutase

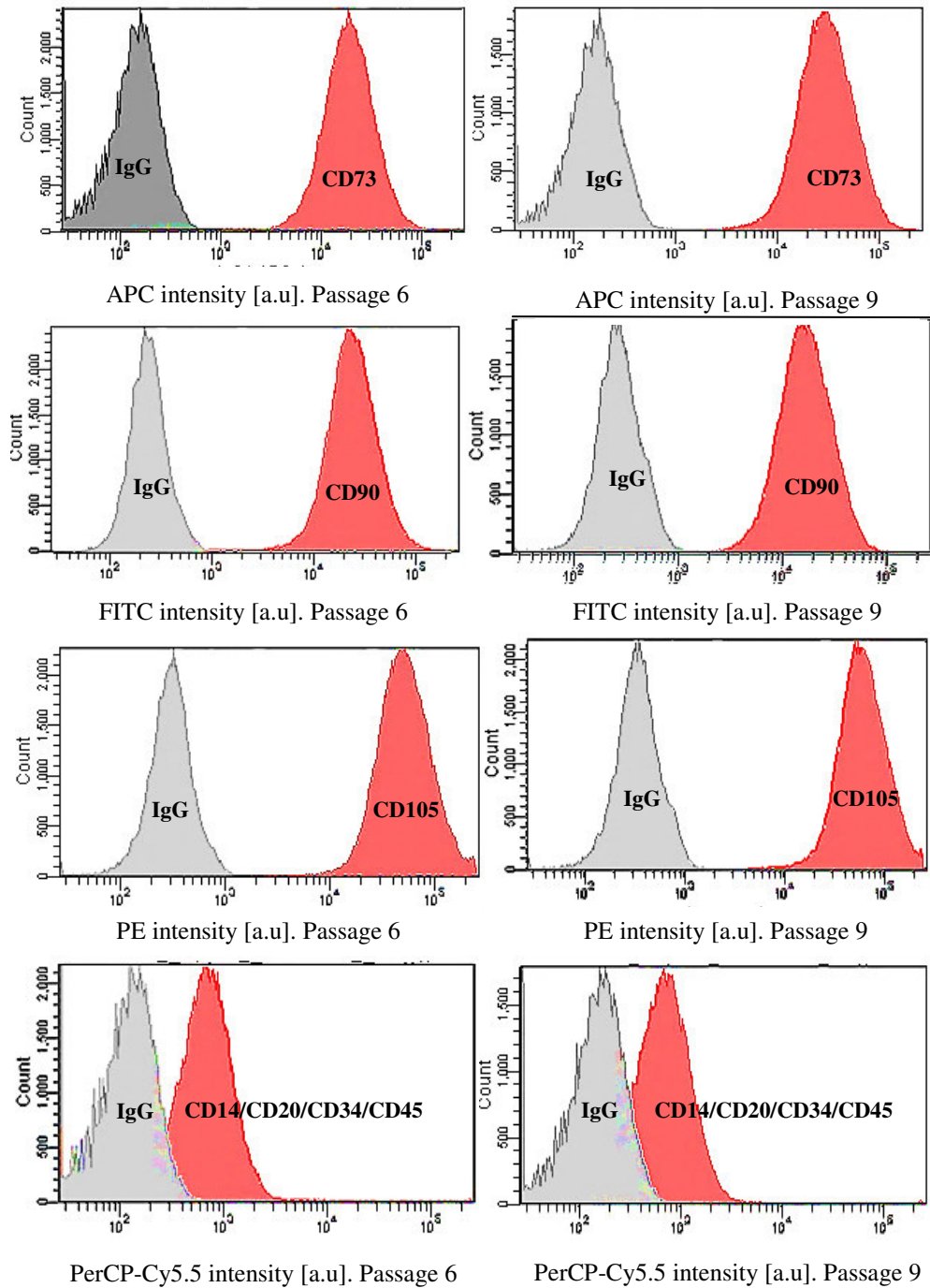


Figure 50: Flow cytometric analysis of cultured AD-MSC after passage 6 and 9, detached with Accutase. Data represent APC, FITC, PE and PerCP-Cy5.5 intensity after passage 6 and 9 of AD-MSC.

9.2 Trypsin S

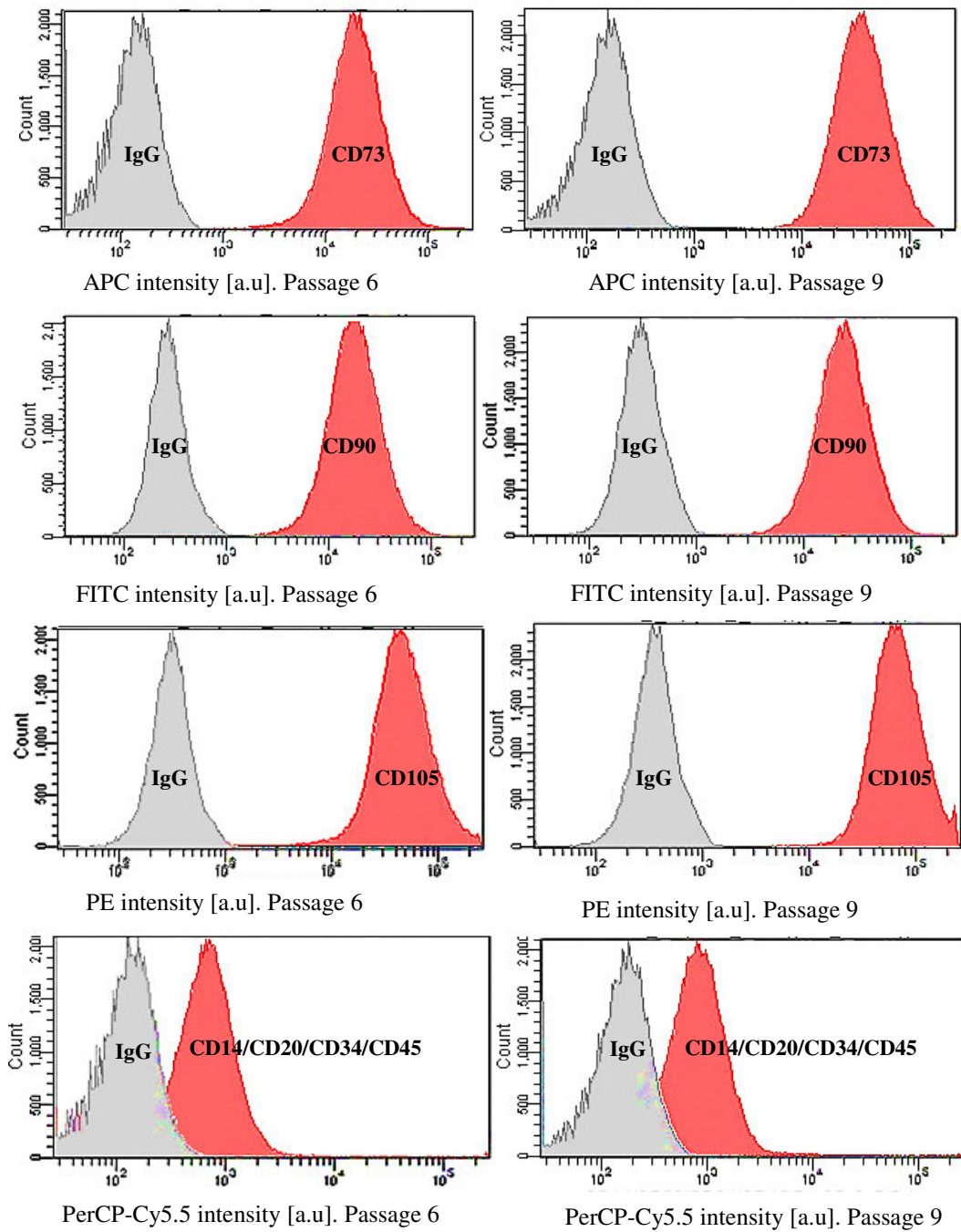


Figure 51: Flow cytometric analysis of cultured AD-MSC after passage 6 and 9, detached with Trypsin S. Data represent APC, FITC, PE and PerCP-Cy5.5 intensity after passage 6 and 9 of AD-MSC.

9.3 TrpLE™ Express

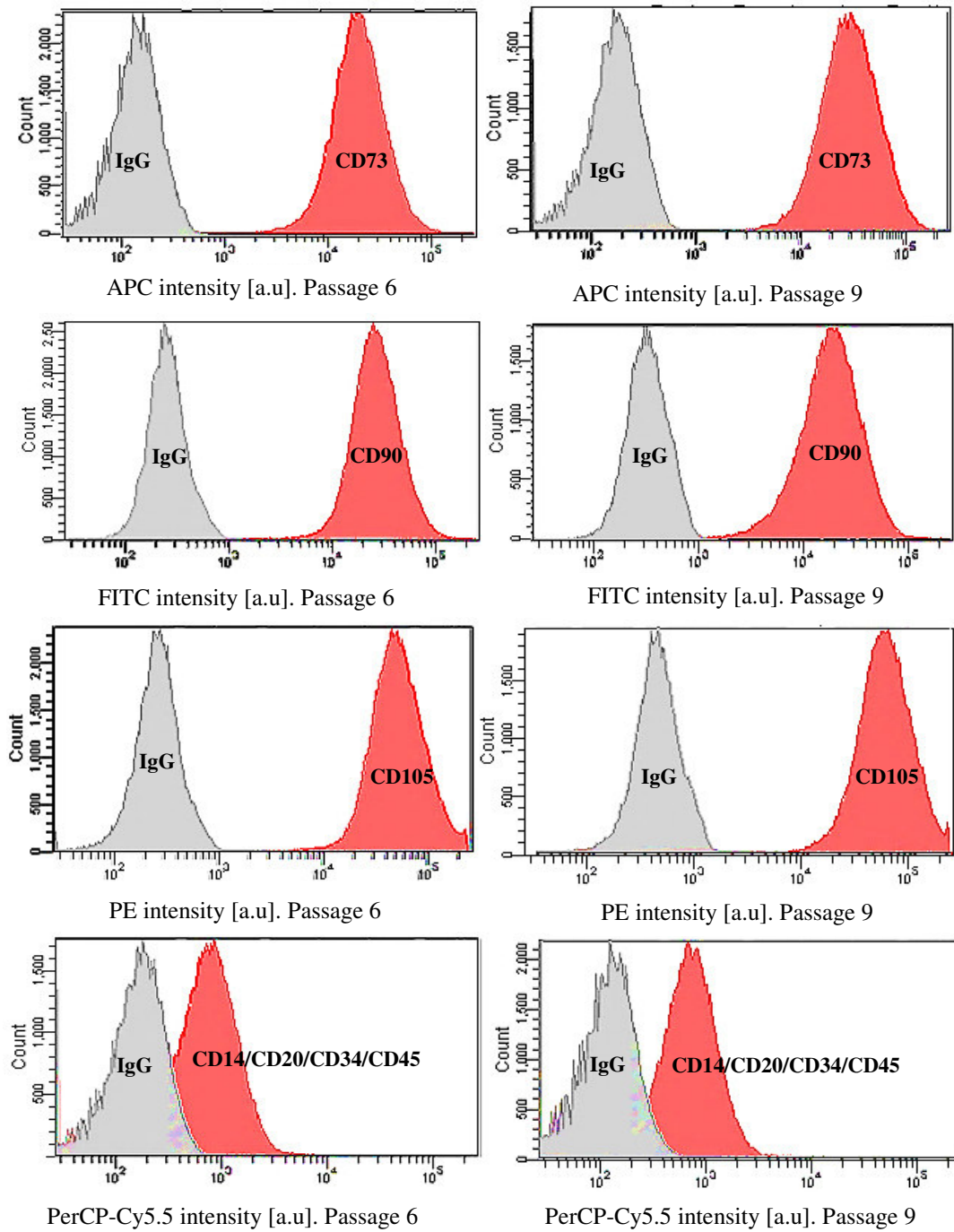


Figure 52: Flow cytometric analysis of cultured AD-MSC after passage 6 and 9, detached with TrpLE™Express. Data represent APC, FITC, PE and PerCP-Cy5.5 intensity after passage 6 and 9 of AD-MSC.

10 Acknowledgements

Finally I want to thank all the people who attended and supported me during the informative, interesting, and especially cheerful time during the six months I spent with my master thesis. This was a very important and teachable phase for me as a student.

First of all I owe Univ. Prof. Dr. Cornelia Kasper a debt of gratitude for having the chance to get an insight into her scientific institution, for her explanations of the theoretical background, her support, and for her guidance throughout this endeavour.

Secondly I am honoured to have had the opportunity to work with Dr. Anne Neumann and I am especially grateful for her help, scientific advice, and theoretical and practical support.

Furthermore I want to thank Mag. Gregor Kollwig for his help by all daily routines in the laboratories.

In addition thank you Dominik Egger M.Sc., Urzula Puc M.Sc., Simon Suchocki B.Sc., Daniel Remmers B.Sc., Christine Strauß, Luigia Muto, Philipp Nold M.Sc., Karoline Gutkas B.Sc., and especially Dr. Verena Charwat for her support and helpful tips. Verena you are such a great and wonderful person, thank you so much.

Thank you Paul for your love, support and especially for your proofreading (I know that you hate this lab-jargon). Thank you for encouraging me to do what I believe in.

Thank you Kathi also for your proofreading, thank you so much.

Thank you Chrisi for helping me with the horrible word-formatting.

Last but not least, I thank my family: Mika, Sidi, my mum and my dad. Thank you for being here for me.

Quae legeris, memento !

[Cato major]

11 Curriculum Vitae

Persönliche Daten

Name	Monira Awad
Geburtsdatum	03.10.1990
Geburtsort	Linz, Österreich
Staatsangehörigkeit	Österreich

Schulbildung

2005-2009	Bundesoberstufenrealgymnasium, Linz
2001-2005	Bundesrealgymnasium, Linz
1997-2001	Volksschule, Linz

Studium

2009 - 2013	Bachelor Studiengang „Biotechnologie und Lebensmittelwissenschaften“, Universität für Bodenkultur Wien, Österreich
2013-2015	Master Studiengang „Medizinische Biotechnologie“, Universität für Bodenkultur Wien, Österreich MedUni Wien, Österreich

Förderungen

2010/ 2014	Leistungsstipendium der Universität für Bodenkultur, Wien
2013	Femtech Stipendium, AIT (Austrian Institute of Technology), Wien

